SENSING AND DECODING BRAIN STATES FOR PREDICTING AND ENHANCING HUMAN BEHAVIOR, HEALTH, AND SECURITY

Garima Bajwa, B.Tech., M.Eng.

Dissertation Prepared for the Degree of

DOCTOR OF PHILOSOPHY

UNIVERSITY OF NORTH TEXAS

August 2016

APPROVED:

Ram Dantu, Major Professor
Rajiv M. Joseph, Committee Member
Cornelia Caragea, Committee Member
Hyunsook Do, Committee Member
Barrett R. Bryant, Chair of the Department of Computer Science and Engineering
Coastas Tsatsoulis, Dean of the College of Engineering
Victor Prybutok, Vice Provost of the Toulouse Graduate School

Bajwa, Garima. *Sensing and Decoding Brain States for Predicting and Enhancing Human Behavior, Health, and Security*. Doctor of Philosophy (Computer Science and Engineering), August 2016, 140 pp., 20 tables, 59 figures, 153 numbered references.

The human brain acts as an intelligent sensor by helping in effective signal communication and execution of logical functions and instructions, thus, coordinating all functions of the human body. More importantly, it shows the potential to combine prior knowledge with adaptive learning, thus ensuring constant improvement. These qualities help the brain to interact efficiently with both, the body (brain-body) as well as the environment (brain-environment). This dissertation attempts to apply the brain-body-environment interactions (BBEI) to elevate human existence and enhance our day-to-day experiences. For instance, when one stepped out of the house in the past, one had to carry keys (for unlocking), money (for purchasing), and a phone (for communication). With the advent of smartphones, this scenario changed completely and today, it is often enough to carry just one's smartphone because all the above activities can be performed with a single device. In the future, with advanced research and progress in BBEI interactions, one will be able to perform many activities by dictating it in one's mind without any physical involvement. This dissertation aims to shift the paradigm of existing brain-computer-interfaces from just 'control' to 'monitor, control, enhance, and restore' in three main areas - healthcare, transportation safety, and cryptography. In healthcare, measures were developed for understanding brain-body interactions by correlating cerebral autoregulation with brain signals. The variation in estimated blood flow of brain (obtained through EEG) was detected with evoked change in blood pressure, thus, enabling EEG metrics to be used as a first hand screening tool to check impaired cerebral autoregulation. To enhance road safety, distracted drivers' behavior in various multitasking scenarios while driving was identified by significant

changes in the time-frequency spectrum of the EEG signals. A distraction metric was calculated to rank the severity of a distraction task that can be used as an intuitive measure for distraction in people - analogous to the Richter scale for earthquakes. In cryptography, brain-environment interactions (BBEI) were qualitatively and quantitatively modeled to obtain cancelable biometrics and cryptographic keys using brain signals. Two different datasets were used to analyze the key generation process and it was observed that neurokeys established for every subject-task combination were unique, consistent, and can be revoked and re-issued in case of a breach. This dissertation envisions a future where humans and technology are intuitively connected by a seamless flow of information through ‘the most intelligent sensor’, the brain.

ACKNOWLEDGMENTS

Pursuing my PhD degree has been one of the most fruitful endeavors of my life. For this, I would like to thank my advisor Dr. Ram Dantu, who gave me the opportunity to work on a myriad of research projects including my dissertation on brain research. I am grateful for his full confidence in me to independently develop and shape my research ideas. I am thankful to my committee members - Dr. Rajiv M. Joseph, Dr. Caragea Cornelia, and Dr. Hyunsook Do - for serving on my committee and their valuable suggestions to improve the quality of research and the dissertation. I experienced an excellent support system at UNT, ranging from my advisor Dr. Dantu to the Professors and staff members in the department.

This dissertation is a dedication to my parents, Dr. Iqbal Singh Bajwa and Dr. Usha Bajwa. They were my role models, and I always aspired to emulate them by adopting research and teaching to be an important part of my life. They instilled in me a dream of becoming a scientist to improve the lives of people and make a valuable contribution to the society. There have been ups and downs, moments of distress, but I have never regretted being where I am or the research I have pursued. I am extremely lucky to have the support of Anjan, Jasmeen and Shubhra, who played a major role in keeping me grounded and motivated. I am also thankful to my wonderful grandparents, whose philosophies guided me to think about the bigger picture in life.

I have been very fortunate to cherish the company of Phalgun Nelaturu. Our relentless discussions helped me learn and grow, and develop a bond of unconditional love.

I would also like to thank Harpreet Singh Rekhi, for his support in all my endeavours.

Special thanks to Shamiparna Das for her continuous love, concern, and affection, and to Stephanie Deacon, who took care of many unexpected roadblocks at difficult times.

Finally, I would also like to thank my lab mates - Shanti, Ambareesh, Rajasekhar, Enkh, Fazeen, Chaitra, and my friends, especially Harpreet, Amit, and Mageshwari, whose presence and company made life at Denton feel like home away from home.

My PhD journey has been an extremely motivating and satisfying experience, both emotionally as well as professionally.

TABLE OF CONTENTS

LIST OF TABLES

LIST OF FIGURES

CHAPTER 1

INTRODUCTION

1.1. Background

The human brain is often called 'the most complex object in the known universe' [132]. It is fascinating to explore the engineering behind this bewildering complexity. The brain is responsible for the body's physical and mental health, response to external stimuli, and a person's behavior/nature. It is the brain, which gives a person a sense of identity and a unique personality [99]. The brain sits at the head of the human body, both literally and figuratively, controlling and regulating all bodily processes. It achieves this by sending electric signals through neurons (nerve cells) to all parts of the body, and in turn receiving signals from them through the same route [43]. The unique patterns of this electrical activity form the language of the brain.

The electrical activity gives rise to electric pulses which can be most easily detected on the scalp as changes in electric potentials due to currents flowing through scalp tissue, arising from synchronous activity/firing of neurons. This process of measuring electric potentials on the scalp is called electroencephalography (EEG) [134]. EEG measurements vary depending on a persons state of mind, the activity being performed, and his/her mood. A set of measurements made during a particular activity represent a person's brain state for that activity. Brain state not only varies from activity to activity, but also from person to person. Thus, a person's brain state is their unique signature, just like their fingerprints or DNA [99].

1.2. Motivation

Our lives today, are very comfortable due to technology. Be it the automatic lighting up of a room on entering or the automatic collision avoidance of self-driving cars, sensors not only provide convenience (sensors in lights), but also safety (car sensors) and security (burglar alarms). Similarly, the human brain is responsible for all functions of the human body. It acts as an intelligent sensor by helping in effective signal communication and execution of logical functions and instructions. More importantly, it shows the potential to combine prior knowledge with adaptive

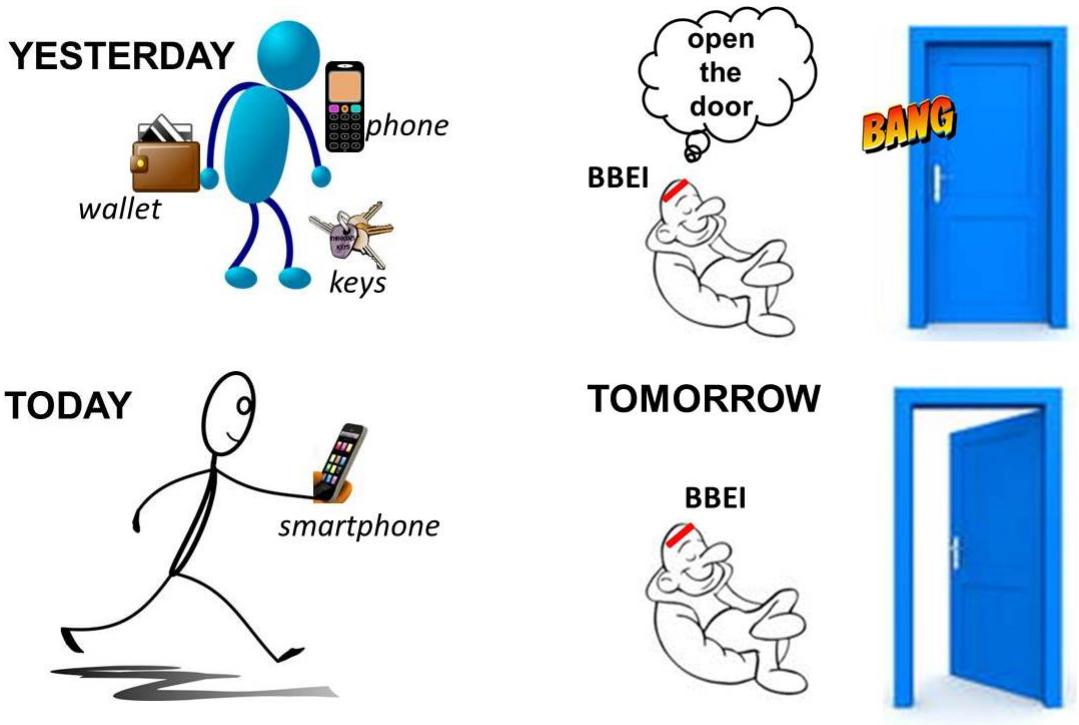

FIGURE 1.1. An example to illustrate a futuristic scenario of brain-body-environment interaction.

learning, thus ensuring constant improvement. These qualities help the brain to interact efficiently with both, the body (brain-body) as well as the environment (brain-environment).

The grand challenge is to apply brain-body-environment interactions (BBEI) to elevate human existence and enhance our day-to-day experiences. For instance, when one stepped out of the house in the past, one had to carry keys (for unlocking), money (for purchasing) and a phone (for communication). With the advent of smartphones, this scenario changed completely and today, it is often enough to carry just one's smartphone because all the above activities can be performed with a single device. In the future, with advanced research and progress in BBEI interactions, one will be able to perform many activities by dictating it in one's mind without any physical involvement. This study envisions a future where humans and technology are intuitively connected by seamless flow of information through 'the most intelligent sensor', the brain.

1.3. Objective

The primary goal of this dissertation is to realize the brain as a super sensing entity that facilitates any and all interactions of the body with the environment. Whenever a human being

interacts with his/her surroundings, the unique signature of his/her brain state is invariably found in the way he/she responds to external factors, his/her state of mind during this interaction, etc. The multisensory experience originates from merging all the information together parallelly from all senses.

It is my aim to use this ubiquitous nature of the human brain signals to decode the brain-state information. My work is interdisciplinary to Computer Science, Neuroscience and Digital Signal Processing, with a focus on recording, analyzing, and decrypting brain signals through EEG measurements. This information can be used to enhance the above mentioned interactions by making them better, faster, safer, and more convenient to improve the quality of life.

1.4. Dissertation Roadmap

To capture the ubiquitous nature of the human brain as a super sensing entity that facilitates brain-body-environment (BBE) interaction. To validate this hypothesis, I am focusing my efforts in three broad, varied fields - healthcare, transportation safety, and cryptography. The most important criteria that binds them together is the idea of using brain signals to elevate human experience and improve lives of people. My research focusses on shifting the paradigm of existing brain-computer-interfaces from just control to monitor, control, enhance, and restore by developing qualitative and quantitative measures for more accurate and in-depth understanding of brain-body interactions.

My work is organized around these goals as specified below (Figure 1.2):

- *Biometric Application*: Introducing a new paradigm of cancelable biometrics based cryptographic key generation: *brain-environment-interaction (BEI)*
- *Public Safety*: Sensing of driving behavior and distractions for safe driving: *(BEI)*
- *Health support system*: Quantifying cerebral blood flow regulation process for monitoring autoregulation - introduce it as a brain vital sign for routine use by physicians and general public (considered as a grand challenge): *brain-body-interaction (BDI)*
- *Assisted living / Rehabilitation tools*: Mental activities classification for brain-computer-interface applications: *brain-computer-interface (BCI)*
- *Software Platform*: facilitate EEG knowledge discovery applications on mobile platform

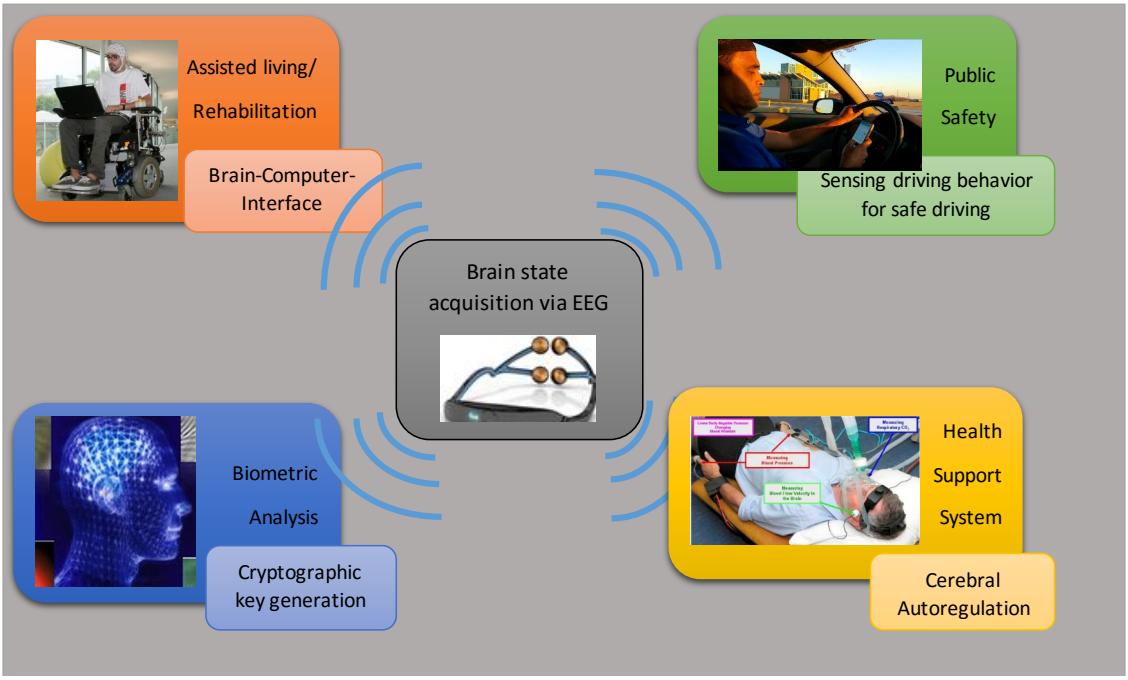

FIGURE 1.2. An overview of the brain body interactions evaluated in the thesis.

1.5. Contributions

In this section, I will highlight the significance and impact of each project in the three areas - cryptography, transportation safety, and healthcare.

1.5.1. Neurokey: Cancelable Biometric based Key Generation

For an individual, the number of biometric features are limited - ten finger prints, a single set of face features, and two iris images. Though it is hard to replicate these biometrics, the problem is that once they are compromised, there are not many alternatives. Thus, the present biometric key generation (BKG) systems suffer from the problem of permanent loss of one's biometric feature in case of a compromise by an adversary. Under such circumstances, a user may run out of their limited unique identity features. The advantage of using other forms of cryptographic generators such as password based or thermal noise etc. is that they can be revoked and re-issued in case of a breach. This is not a natural advantage in biometric based crypto-systems. If someone's DNA is compromised in the database, it is impossible to create a different cryptographic key.

Through my research, I am analyzing a biometric key generation approach using the human brain waves as a solution to this problem. In this novel approach the number of ways in which the

biometric key can be changed is limited only by one's imagination. The feasibility of deriving this Neurokey was studied by using the online EEG data of various mental tasks.

1.5.2. Drive Safe - Save Lives: Sensing Distracted Driving Behavior

Driver distraction is one of the primary factors of accidents, followed by drunk driving, and speeding. It has become a big concern in road safety and health measures are being taken by National Highway Traffic Safety Administration [117]. The number of people killed in distraction-affected crashes totaled 3,328 in 2012 [41, 117, 67]. The underlying problem is that humans cannot multitask efficiently. The brain switches between one task and another resulting in slower response times to the events on the road [3].

The simple fact is that drivers don't realize or understand how cellphones and other distractions take away focus from driving. The only way to identify cognitive distraction is through detecting cognitive overload using an individual's brain waves. This can be used to create an intuitive measure for distraction in people analogous to the Richter scale for earthquakes.

In my work, a clear indication of distracted behavior was identified using the EEG signals in a real world scenario in contrast to a virtual simulated driving environment. One of the biggest challenges in EEG analysis was to reduce the number of electrodes. This was overcome by isolating one electrode (FC5) from 14 electrode locations with a mean accuracy of $91.54 \pm 5.23\%$

1.5.3. Neurosign- A Sixth Vital Sign

The brain requires an adequate continuous supply of blood for its proper functioning. It has an intrinsic ability to maintain a constant blood flow despite changes in systemic blood pressure. Cerebral blood flow is the measure of blood supply to the brain in a given time and is typically around 50 ml/100g/min (100g of brain tissue) [104]. It is as fundamental to our body as any other vital sign (heartbeat, respiratory rate, temperature, blood pressure and oxygen saturation). A major limitation in measuring the regulation of cerebral blood flow is the lack of a gold standard for its assessment.

Scientists have been able to measure blood flow in the brain since 1948 with help of various expensive techniques such as MRI (magnetic resonance imaging), TCD (trans cranial doppler) and

NIRS (near-infrared spectroscopy). They provide snapshots of blood flow at defined intervals and are inadequate for continuous monitoring. Hence, there is a significant delay between monitoring the onset of brain disorders (e.g. migraine, ischemia and stroke) and their subsequent treatments [148].

In my experimental observations, changes in blood pressure affected the estimated cerebral blood flow and the underlying EEG signals. Using this information I developed an index of dynamic blood flow regulation by correlating the blood flow in the brain and blood pressure variation with EEG signals.

CHAPTER 2

UNDERSTANDING ELECTROENCEPHALOGRAPHY (EEG)

2.1. Introduction

Our brain has hundreds of billions of neurons. When large number of neurons fire at the same time, they produce voltage fluctuations resulting from the ionic current flows. Electroencephalography (EEG) is the recording of this electrical activity along the scalp that is detectable to an electrode placed on the head. EEG are also commonly known as the brain waves [133]. Richard Caton in 1875 was the first to observe the electrical activity with monkeys and rabbits and Hans Berger (considered as the father of modern EEG) was the first to observe EEG from humans. [78]. EEG signals are typically described as rhythmic oscillations in certain frequency ranges (Figure 2.1). The basic groups include [134]:

- *Delta*: Rhythmic activity between 0.5-4 Hz.
- *Theta*: Rhythmic activity between 4-8 Hz.
- *Alpha*: Rhythmic activity between 8-13 Hz.
- *Beta*: Rhythmic activity between 13-30 Hz.
- *Gamma*: Rhythmic activity between $>$30 Hz.

2.2. EEG Measurement

Most of the EEG studies use an electrode cap to record the electric pulses from the scalp. EEG acquisition is a non-invasive procedure, presents no known risks or limitations and be repeatedly used with patients, normal adults, and children [134]. There is a special cap that contains electrodes at certain locations over different areas of the brain. The brain is mainly divided into cerebrum (containing cerebral cortex) and cerebellum (Figure 2.2.

The cerebrum consists of mainly four lobes [42] described as follows:

- *Frontal lobe* is involved in working memory, emotions and actions.
- *Parietal lobe* helps to integrate various sensory modalities from the environment and visual-spatial processing.

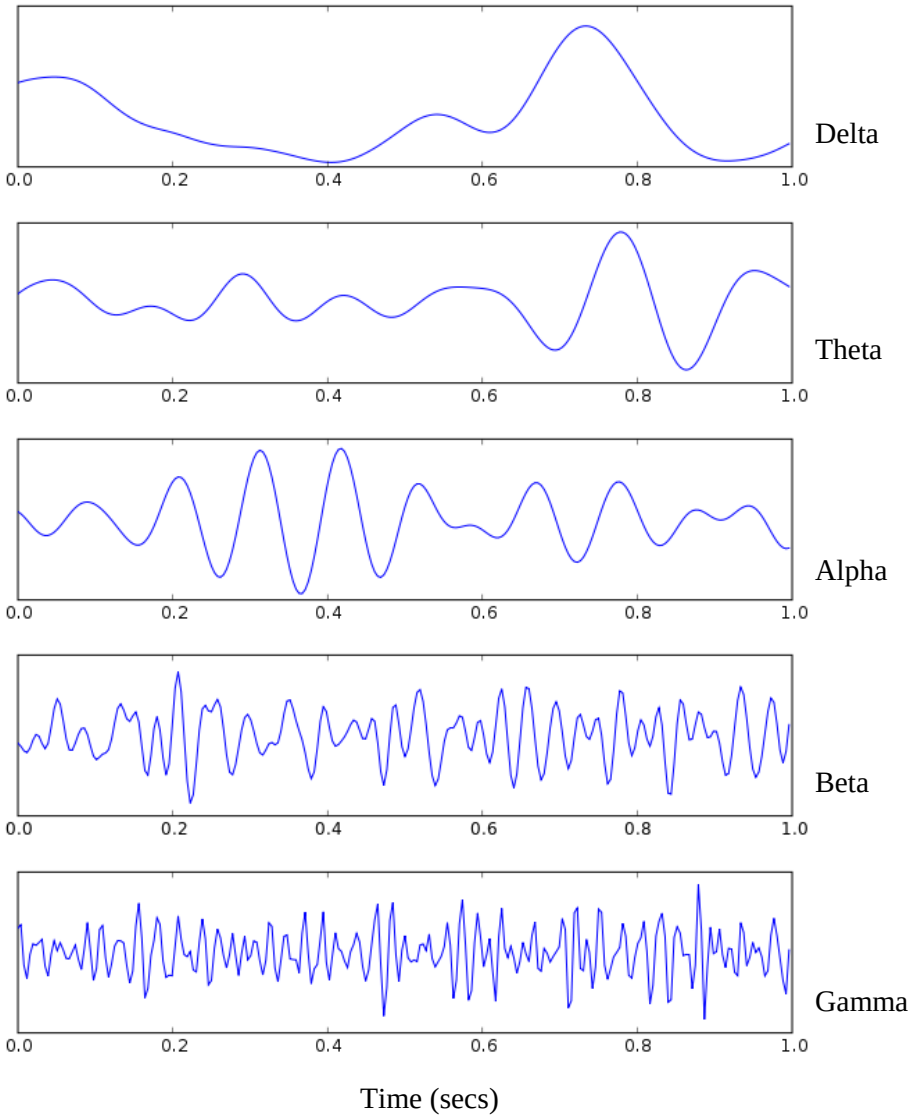

FIGURE 2.1. Various types of EEG bands filtered from one second of an EEG sample. (Uploaded in Wikipedia By Hugo Gamboa. Free License. Used under Creative Commons Attribution-ShareAlike 3.0 Unported (CC BY-SA 3.0).)

- *Occipital lobe* is the visual processing centre of the human brain.
- *Temporal lobe* is associated with memory, language and auditory processing.

Many laboratories use between 16 and 64 electrodes, but the caps with more number of electrodes have been used in scientific and medical studies. International 1020 system (Figure 3.2) is an internationally recognized method to describe and apply the location of scalp electrodes in the context of an EEG test or experiment. Figures 2.3 and 2.4 show an example of the clinical and

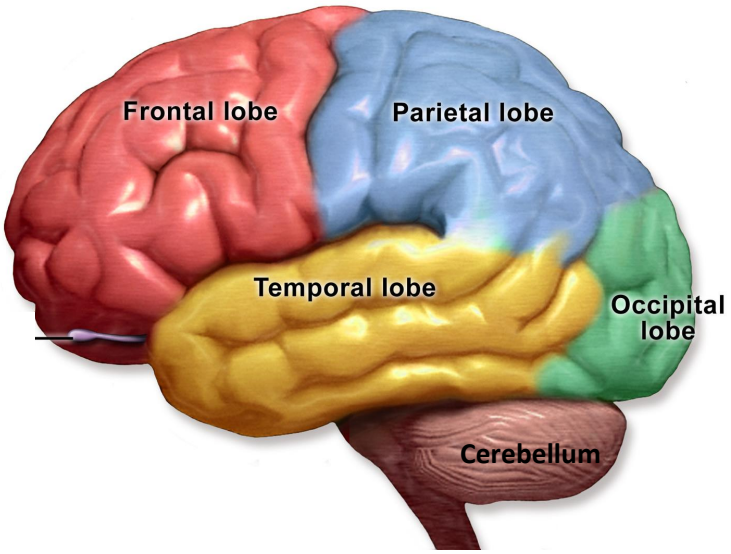

FIGURE 2.2. Major parts of the brain. (Uploaded in Wikipedia By Bruce Blaus. Free License ("Blausen gallery 2014". Wikiversity Journal of Medicine. DOI:10.15347/wjm/2014.010. ISSN 20018762). Used under Creative Commons Attribution 3.0 Unported (CC BY 3.0).)

consumer EEG recording devices.

2.3. Discussion

EEG was traditionally limited to neuroscience applications, and clinical treatments and research. Quantitative EEG (QEEG) describes a procedure of recording, pre-processing, quantifying, analyzing, and interpreting electrical impulses from the human brain. QEEG applications are gradually extending into areas such as effective human computer interfaces, gaming training, entertainment, and other ubiquitous computer applications in addition to the cerebro-vascular disorders, epilepsy, ADHD and other clinical applications.

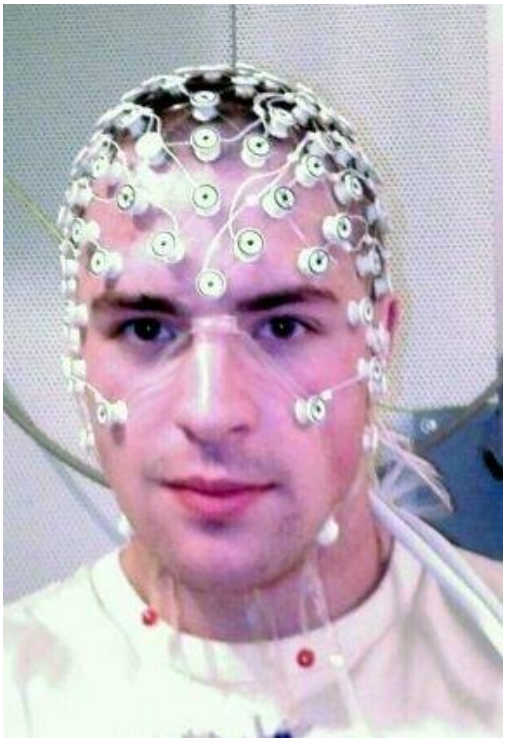

FIGURE 2.3. Example of a multi-electrode system that may be used for recording in clinical circumstances. (Uploaded in Wikipedia by Thuglas at English Wikipedia [Public domain], via Wikimedia Commons Free.)

FIGURE 2.4. Example of a single electrode consumer device used for EEG recording [96].

CHAPTER 3

NEUROKEY: TOWARDS A NEW PARADIGM OF CANCELABLE BIOMETRICS-BASED KEY GENERATION USING EEG

3.1. Structured Abstract

Background: Brain waves (Electroencephalograms, EEG) can provide conscious, continuous human authentication for the proposed system. The advantage of brainwave biometry is that it is nearly impossible to forge or duplicate as the neuronal activity of each person is unique even when they think about the same thing.

Aim: We propose exploiting the brain as a biometric physical unclonable function (PUF). A user's EEG signals can be used to generate a unique and repeatable key that is resistant to cryptanalysis and eavesdropping, even against an adversary who obtains all the information regarding the system. Another objective is to implement a simplistic approach of cancelable biometrics by altering one's thoughts.

Method: Features for the first step, Subject Authentication, are obtained from each task using the energy bands obtained from Discrete Fourier Transform and Discrete Wavelet Transform. The second step constituting the Neurokey generation involves feature selection using normalized thresholds and segmentation window protocol.

Results: We applied our methods to two datasets, the first based on five mental activities by seven subjects (325 samples) and the second based on three visually evoked tasks by 120 subjects (10,861 samples). These datasets were used to analyze the key generation process because they varied in the nature of data acquisition, environment, and activities. We determined the feasibility of our system using a smaller dataset first. We obtained a mean subject classification of 98.46% and 91.05% for Dataset I and Dataset II respectively. After an appropriate choice of features, the mean half total error rate for generating Neurokeys was 3.05% for Dataset I and 4.53% for Dataset

This chapter is presented in its entirety from Garima Bajwa and Ram Dantu, "Neurokey: Towards a New Paradigm of Cancelable Biometrics-based Key Generation using Electroencephalograms." *Computers and Security*, 62 (2016),95-113, with permission from Elsevier (http://dx.doi.org/10.1016/j.cose.2016.06.001) [9].

II, averaged over the subjects, tasks, and electrodes. A unique key was established for each subject and task, and the error rates were analyzed for the Neurokey generation protocol. NIST statistical suite of randomness tests were applied on all the sequences obtained from the Neurokey generation process.

Conclusion: A consistent, unique key for each subject can be obtained using EEG signals by collecting data from distinguishable cognitive activities. Moreover, the Neurokey can be changed easily by performing a different cognitive task, providing a means to change the biometrics in case of a compromise (cancelable).

3.2. Introduction

The design of cryptographic systems has two parts; a cryptographic algorithm (complex mathematical function) and a cryptographic key. According to Kerckhoffs' principle, a cryptosystem should be secure even if everything about the system, except the key, is public knowledge [114]. Hence, the strength of the cryptographic systems depends on the secrecy of the weakest link, i.e., cryptographic keys (crypto keys). The majority of encryption algorithms desire long, random keys that are difficult to memorize. Alternately, these crypto keys are stored in a database and released upon presentation of an authentication token (password). Such a scenario increases the likelihood of tokens being compromised by sharing (willfully or coercively), losing or stealing.

Generating truly random numbers to be used as cryptographic keys has been an age old problem. Biometrics alleviates the problem of remembering passwords or PINs, providing a stronger defense against repudiation. It is significantly harder to forge, copy, share, and distribute biometrics compared to passwords or PINs [57]. The authors believe that strong cryptographically secure keys can be obtained from biometric-dependent key generation systems given the appropriate selection of enrollment schemes, feature descriptors/vectors, and entropy mixers as surveyed by Rathgeb et al. [119]. Advancements in biometrics-based cryptographic systems provide a better solution to the key management practices that address the security weakness of conventional key release systems using passcodes, tokens or pattern recognition [153]. Biometrics such as iris recognition, fingerprints, voice, hand geometry, and facial recognition are being employed at present to derive cryptographic keys [56, 136]. The immutability and non-repudiability of these biometrics

make them a strong tool for biometric-dependent key generation systems [27, 14].

For an individual, the number of biometric features is limited. We only have ten fingerprints, a single set of face features, and two iris images. Though it is hard to replicate these biometrics, the key problem is that once they are compromised, there are not many alternatives. Thus, the present biometric key generation (BKG) systems suffer from the problem of permanent loss of one's biometric feature in case of a compromise by an adversary, and a user may run out of their limited unique identity features. The advantage of using other forms of cryptographic generators such as password-based or thermal noise is that they can be revoked and re-issued in the case of a breach. This is not a natural advantage in biometrics-based cryptosystems. If a person's DNA is compromised in the database, it is impossible to create a different cryptographic key. To overcome this, the system of cancelable biometrics has emerged.

Ratha et al. [118] first introduced the system of cancelable biometrics where distortions on the biometric features are varied to provide various versions of a biometric template. As a result, it can be revoked or changed like generic passwords and yet remain unique for intended applications. The catch here is that the 'evil eve' can still plan a feasible attack based on the auxiliary or helper distortion data. Hence, it is extremely challenging for cancelable biometrics to scale up to both performance and non-invertibility of transformed features [20, 59].

We propose a biometric key generation approach using the human brain waves (Electroencephalograms - EEG signals) as a solution to this problem. The brain is what gives a sense of identity and a unique personality to a person. The brain sits at the head of the human body, both literally and figuratively, controlling and regulating all bodily processes. It achieves this by sending electric signals through neurons (nerve cells) to all parts of the body, and in turn receiving signals from them through the same route. The unique patterns of the electrical activity form the language of the brain. These electric pulses can be most easily detected on the scalp as changes in electric potentials due to currents flowing through scalp tissue, arising from synchronous activity/firing of neurons. This process of measuring electric potentials at the scalp is called Electroencephalography (EEG). EEG measurements vary depending on a person's state of mind, the activity being performed, and his/her mood. A set of measurements made during a particular activity represents

an individual's brain state for that activity. Brain state not only varies from activity to activity, but also from person to person. Thus, an individual's brain state is their unique signature, just like their fingerprints or DNA.

3.2.1. Motivation

Noninvasive brain-computer interfaces (BCI) have enhanced our capabilities to study the neural circuits and utilize them for applications ranging from those in the medical field like neuroprosthetics to entertainment like neurogaming. In this paper, we propose a new modality for generating crypto keys (Neurokeys) from an individual's EEG signals while a subject performs certain mental tasks. As the tasks can be easily substituted by altering the passthoughts [135], these EEG signals extend a simplistic approach to implementing cancelable biometrics-based crypto key generation.

Empirical reasons to exploit EEG for a plausible Neurokey are as follows:

- *Physical unclonable function (PUF)*: EEGs are nearly impossible to forge because the neuronal wiring of each person is unique and will result in a different pattern of EEG between subjects while performing similar mental activities [152] analogous to PUFs.
- *Cancelable*: EEG readings enable us to develop cancelable biometric keys since taking a reading requires having the user engage in a specific cognitive task that can be changed if the user's biometric information is compromised.
- *Entropy*: The measured EEG biometrics have a high entropy across populations i.e. the amount of uncertainty in the key from an adversary's point of view is large.
- *Coercion Attack*: Biometric keys from EEG signals could possibly provide prevention under coercion attacks as the brain responses change under threat [23, 102]. Gupta et al. [46] showed that detecting changes in a user's skin conductance provided good resistance against coercion attacks when the keys were generated using both voice and skin conductance.

We believe our breakthrough idea will interest a diverse research community including machine learning, cryptography, and computer security.

3.2.2. Problem Definition

The goal of this research initiative is to provide portable, on-the-go, cognitive keys with a possibility of regeneration even on mobile devices. This eliminates the problem of key management for encryption of user-specific data which can now be protected by the Neurokey obtained from one's EEG signals. The solution to the following research question is intended: *Can we consistently generate a Neurokey in any environment to differentiate between individuals based on their cognitive activity?* We aim to validate how the existing challenges affect the usefulness of EEG signals as a key generation scheme.

3.3. Related Work

There are four fundamental requirements to use a biometric as a cryptographic key generation system [57]. *Universality*: it should be possible to generate keys from the biometric features of all individuals. *Uniqueness*: the system should be able to separate keys of different persons with a reasonably low failure probability. *Consistency*: biometric characteristics of the individuals should remain fairly constant for a reasonable time. *Collectable*: biometric values should be easy to obtain, easy to quantify, and cause no discomfort.

EEG signals can be easily recorded using a headband containing dry or wet electrodes on a desktop or mobile device. Early works by Poulos et al. [116] and Paranjape et al. [110] studied the possibility of using the brain signals as a means for a new biometric authentication system. The theory of neurologists that the EEG carries genetic information of an individual [139, 87, 7] influenced their studies. Since then, several researchers have contributed towards establishing the feasibility of using EEG for biometric authentication systems, with a focus on improving the accuracy [115, 105, 18, 108, 91, 52, 94, 121, 2, 66].

On similar lines, Thorpe et al. [135] describe a system that uses pass-thoughts as opposed to a conventional text-based password for user authentication, making it resistant to dictionary and shoulder-surfing attacks. Chuang et al. [21] performed usability studies to advance the idea that consumer grade single electrodes in a non-clinical setting are sufficient to fulfill the requirements of accuracy for classification. Also, various mental tasks based on difficulty, enjoyability and recall ability were evaluated for the performance of the system. Another interesting work by Yeom

et al. [147] was based on the paradigm that unique subject-specific brain wave patterns exist in response to the visual stimuli of self and non-self face images. The validation of the stability of the EEG waves over time was established by comparing the inter-individual variation in spectral observations to the intra-individual stability over more than a year [95].

Only a few research studies have explored the possibility of employing the brain signals to generate keys for cryptographic applications. Palaniappan et al. [107] present one of the early ideas about the use of EEG for PIN generation. Their system was based on P300 based BCI design incorporating an external visual stimulus paradigm. They identified Cz electrode to be appropriate considering a limited number of trials. Lokeshwari et al. [86] proposed data encryption using a genetic algorithm with EEG. Their system intends to feed a pseudorandom number generator with a seed obtained from EEG feature extraction. Their system represents a theoretical idea with a lack of implementation analysis.

3.3.1. Contributions of the Paper

To our knowledge, no one has extensively studied the performance of a biometric system using EEG for both authentication and cryptographic key generation, utilizing different types of online EEG datasets varying in the nature of data collection, the number of electrodes, and the types of activities.

Our EEG key generation is based on a cascade system of EEG authentication followed by key generation. It is similar to a key binding system that binds a random key with a user's biometric data at the time of enrollment and releases the key upon successful authentication [128, 136]. The difference is that our system derives the random key also by using the subject's EEG biometrics itself. The inherent property of authentication ensures that the subject whose EEG signals are being used to generate his/her cryptographic key is the one whom he/she claims to be. An adversary also has to obtain access to both the authentic features and the feature vectors (of keys) to attack the system. It helps increase the overall resistance of the system to forgery as the key is never retrieved if the authentication fails.

The key generation scheme does not require original biometrics data to be stored. The feasibility of changing Neurokeys for the same subject by switching to a different mental activity

is also studied, thus, providing a usable and comparable alternative to cancelable biometrics-based key generation schemes. In summary, the paper explores the following:

- Empirical evaluation of using EEG for Neurokey generation
- Experimental feasibility of using EEG for Neurokey generation
- Potential as a cancelable biometrics-based key generation

3.4. System Overview

Our proposed cancelable Neurokey generation scheme, shown in Figure 3.1, has three phases:

Enrollment: In this phase, an individual establishes the authentic regions of his EEG features for a chosen activity using his training samples. These regions are stored as a template to authenticate later and generate the cryptographic keys. We shall not dig into the biometric template security in this paper [13, 56].

Authentication: The second part of the system will authenticate a subject using the classic biometric approach. The key is generated directly from the EEG features of an individual after the person has been authenticated using those same signals.

Key Generation: The key generation scheme does not require original biometrics data to be stored. It accepts the EEG signals of the established mental activity and generates the feature vectors after the appropriate feature selection. The feature vectors are binarized using the authentic regions of an individual in the template to generate the key. Though authentication phase is a screening process itself, the generated key is matched to the stored hash value of the genuine key to be accepted or rejected.

Lastly, the feasibility of changing a Neurokey for the same subject by switching to a different mental activity is also studied, thus, providing a usable and comparable alternative to other distortion-based cancelable biometric key generation schemes.

3.5. Experimental Data

Currently, the approaches to obtain biometrics from EEG data are derived from brain responses to either visually evoked stimuli or mental tasks. Our goal was to study the key generation

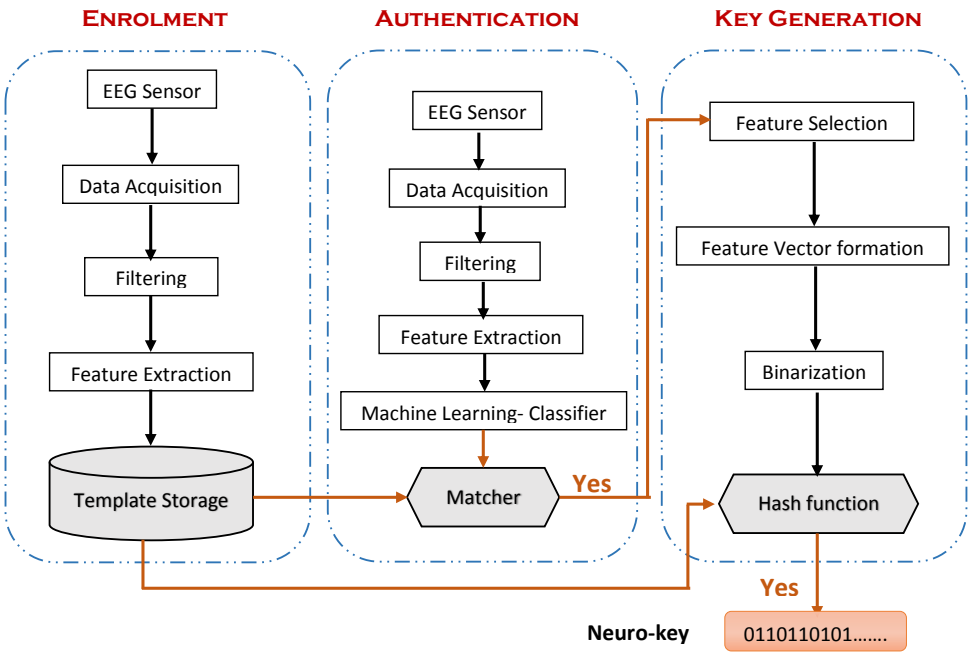

FIGURE 3.1. The flow of key generation from EEG of the subjects.

process from such EEG datasets, varying in nature of data collection equipment, environment and activities, and their subsequent impact on the generation of keys.

In our investigation, we applied our methodology to two public EEG datasets to determine:

- *Dataset 1:* Experimental feasibility using seven subjects dataset (mental task activations)
- *Dataset 2:* System's general applicability using 120 subjects dataset (visually evoked stimuli)

3.5.1. Dataset I

This dataset has been obtained previously by Keirn and Aunon [69, 62, 61]. It consists of EEG signals from seven subjects performing five mental tasks. The tasks were chosen in a way to invoke hemispheric brainwave asymmetry.

3.5.1.1. Task Description

The five mental tasks are described as follows:

- Baseline Task: This task was considered as a reference or a base that was used to control and measure EEG signal activity. The subjects were asked not to engage in any specific

mental task and relax as much as possible with very few movements, and to think of nothing in particular.

- Letter Task: In this task the subjects were instructed to mentally compose a letter to a friend or relative without vocalizing it.
- Math Task: The subjects were shown images consisting of some multiplication problems, such as 49 times 78, and were asked to solve them, again without vocalizing or making any physical movements.
- Geometric Figure Rotation: The subjects were instructed to visualize a particular three-dimensional block figure being rotated about an axis.
- Visual Counting: The subjects were asked to imagine a blackboard and to visualize numbers being written on the board sequentially.

3.5.1.2. Data Collection

Signals were recorded from six channel placements C3, C4, P3, P4, O1, and O2 specified by 10-20 electrode placement via an Electro-Cap elastic electrode cap. The standard electrodes placement is shown in Figure 3.2.

The subjects were asked to sit in a sound controlled booth with dim lighting and noiseless fans for ventilation. The electrodes were connected through a bank of Grass 7P511 amplifiers and band pass filters (0.1–100 Hz). Data recording was done at a sampling rate of 250 Hz with a Lab Master 12 bit A/D converter mounted in an IBM-AT computer. Eye blinks were detected using a separate channel of data recorded from two electrodes placed above and below the subject's left eye.

All tasks were performed with the subjects eyes open. Subject 1, left handed, aged 48, and Subject 2, right-handed, aged 39, were employees of a university. Subjects 3-7 were right-handed college students between the ages of 20 and 30. All were male subjects except Subject 5. They performed five trials of each task in one day. Each task lasted for 10 seconds, and they returned to do another five-trial session on a different day. Subjects 2 and 7 completed only one five-trial session. Subject 5 completed three such sessions and the rest completed only two sessions.

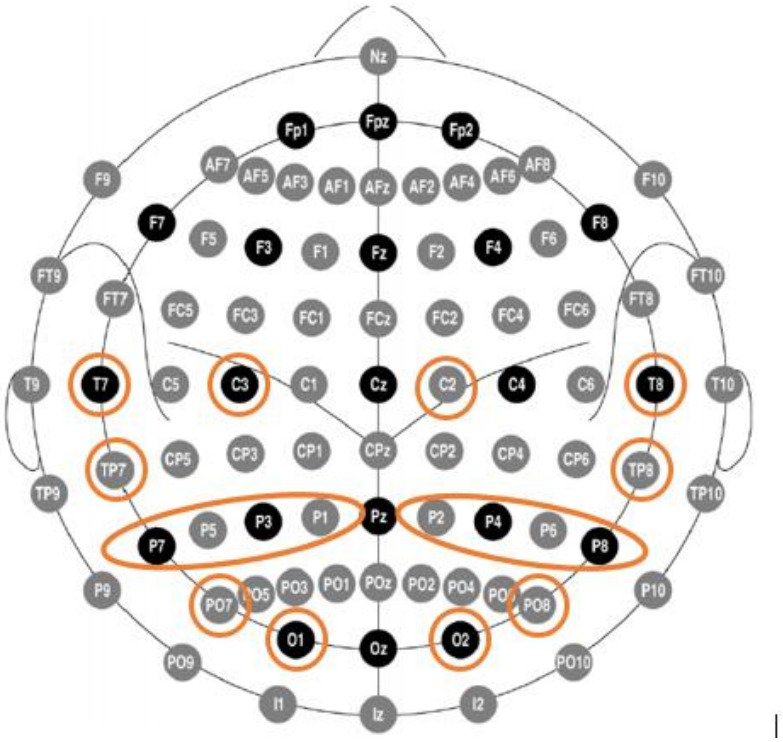

FIGURE 3.2. Black circles indicate positions of the original 10-20 system [58], gray circles indicate additional positions introduced in the 10-10 extension [103]. The occipitotemporal region of interest is marked in color.

3.5.2. Dataset II

This dataset was taken from UC Irvine Machine Learning Repository [55]. It was collected to examine EEG correlates of genetic predisposition to alcoholism. The dataset is described below [151].

3.5.2.1. Task Description

There were two groups of subjects: alcoholic and control. Each subject was exposed to either a single visual stimulus (S1) or to two stimuli (S1 and S2). These stimuli were composed of pictures of objects obtained from the 1980 Snodgrass and Vanderwart picture set [127]. In the case of second stimuli (S2), it was presented in either a matched condition where S1 was identical to S2 or in a non-matched condition where S2 differed from S1. The duration of each picture stimulus in each test trial was 300 ms. The interval between each trial was fixed to 3.2 s. The occurrence of matching and non-matching stimuli were randomized.

TABLE 3.1. Comparisons of the datasets

Datasets	Dataset I	Dataset II
Subjects	7	120
Electrodes	6	64
Activities	5	3
Frequency	250 Hz	256 Hz
Total trials	325	10,861
Recording duration per trial per activity	10 sec	1 sec

So, we divided the data into three sub-tasks; S1_task, S2_NoMatch, and S2_Match to study the generation of keys in these three scenarios. An important consideration is that we will generate the keys from 1 s of EEG data as compared to 10 s in the previous dataset. The comparison of datasets is given in Table 3.1.

3.5.2.2. Data Collection

The dataset contains EEG measurements from 64 electrodes placed on a subject's scalp at a sampling rate of 256 Hz for 1 second duration. There were 122 subjects and each subject completed 120 trials of the three visually evoked stimulus presented in a random fashion. We removed the data of two subjects as the EEG signals were noisy and contained many error trials. The data was recorded in a sound attenuated RF shielded room with the subject seated in a reclining chair. The signals were amplified with a gain of 10,000 by EpA2 amplifiers (Sensorium, Inc) with a bandpass between 0.02 and 50 Hz. Data readings involving eye and body movements ($>$ 73.3 uV) were rejected as noise.

3.6. Feature Extraction Process

Several methods can be used to extract features from the EEG signals. Different methods produce different size of feature vectors. We take advantage of both Discrete Fourier Transform (DFT) and Discrete Wavelet Transform (DWT) to extract the relevant features from the EEG signals. DFT breaks down the signal into its constituent sinusoids of different frequencies whereas the DWT breaks the signal into its wavelets, using scaled and shifted versions of a mother wavelet. Wavelet properties of temporal localization and Fourier's frequency localization make them an ideal combination for extracting properties of non-stationary signals such as EEG.

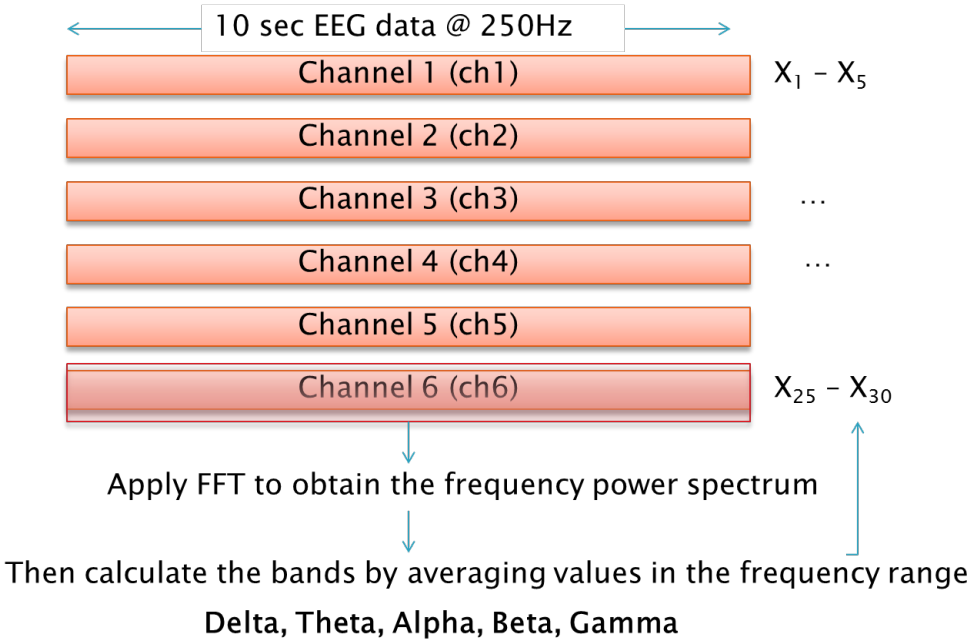

FIGURE 3.3. Process of FFT feature extraction from frequency distribution of different channels.

3.6.1. Discrete Fourier Transform

Time domain signal of each channel was converted into the frequency domain using Fast Fourier Transform (FFT), an efficient algorithm for computing the DFT of a sequence. The standard EEG frequency bands obtained are:

- *Delta (δ)*- rhythmic activity between 1-4 Hz
- *Theta (θ)*- rhythmic activity between 4-8 Hz
- *Alpha (α)*- rhythmic activity between 8-12 Hz
- Beta *(β)*- rhythmic activity between 13-30 Hz
- Gamma *(γ)*- rhythmic activity between 30-44 Hz

These bands were calculated for each channel. Therefore, the FFT feature vector consisted of five features for an electrode. Figure 3.3 shows the process of obtaining FFT features of subject classification for the authentication process.

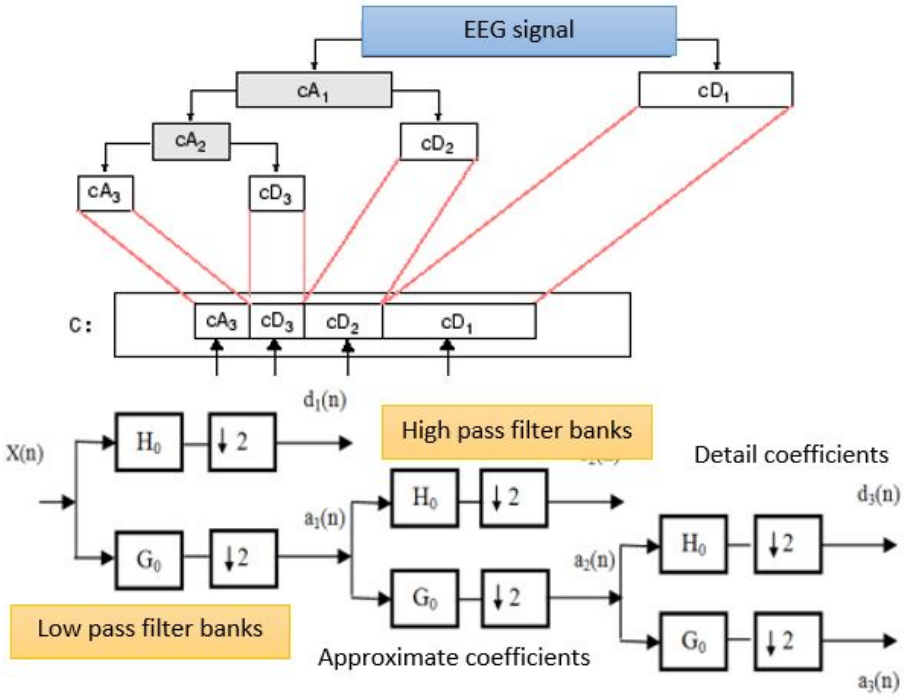

FIGURE 3.4. Decomposition structure of the Discrete Wavelet Transform.

3.6.2. Discrete Wavelet Transform

We used the Daubechies family of wavelets to create robust features for the subject classification. The general decomposition of the signal into its detail and approximate coefficients was achieved by applying a series of high and low pass filters to the signal. Figure 3.4 shows the sequential application of the filters. Unlike FFT, DWT provides a time-frequency representation of the signal and the Daubechies wavelet's irregular shape and compact nature help in analyzing signals with discontinuities or sharp changes. Each wavelet characterized by the vanishing moments is used to represent the polynomial information in a signal. We compared 'db4', 'db6' and 'db8' and found 'db8' to be the most appropriate for capturing the underlying changes in the EEG signals. The decomposed coefficients at DWT levels have been approximated to the nearest standard EEG frequency bands as shown in Table 3.2.

Instead of using all the coefficients at each decomposition level, we extracted the following statistical information from the wavelet coefficients at every level.

- Mean of the absolute values of the coefficients in each level (both high and low sub-band)
- Average power of the wavelet coefficients in each sub-band

TABLE 3.2. Wavelet-decomposition level and EEG sub-bands relationship (A - approximate coefficients, D - detail coefficients)

Energy band	Frequency Range	Decomposition Level
Delta	0 - 4 Hz	A5
Theta	4 - 8 Hz	D5
Alpha	8 - 16 Hz	D4
Beta	16 - 32 Hz	D3
Low Gamma	32 - 64 Hz	D2
High Gamma	64 - 128 Hz	D1

- Standard deviation of the coefficients in each sub-band

The DWT feature vector was composed of 18 features for an electrode (six energy bands * 3 statistical features per band). Thus, the combined DWT-FFT feature vector for a subject had 23 features per electrode.

3.7. Authentication

3.7.1. Repeatability

Measurement of an individual's EEG samples taken at multiple time frames are almost never identical. *We studied the problem of repeatability of the EEG biometrics for the identification process by using various sessions of EEG recordings, obtained at different time intervals (different days and times) for training and testing in the classifier.* Random samples were chosen from the datasets, 66% as train set and rest as a test set, and classification was carried out using 10-fold cross validation. The mean of 10 such sampling processes were used to calculate the results. Similarly, the Neurokeys were tested by splitting the dataset into genuine and imposter users for each subject.

3.7.2. Classification

We performed discretization of feature vectors as another preprocessing step before the classification. Supervised discretization transforms numeric attributes to nominal attributes and takes into account the class labels as compared to unsupervised discretization like equal binning or frequency. WEKA (Waikato Environment for Knowledge Analysis) tool was used to analyze the dataset [49]. The tool accepts ARFF (Attribute Relationship File Format) file format. Our MATLAB data set in a cell array format was converted into appropriate ARFF file for each of the

feature extraction methods. For each of the ARFF file two types of classification models, Support Vector Machine and Bayesian Network, were used.

Support vector machine (SVM) was used as a classifier because of its accuracy and ability to separate the classes using the concept of hyperplane separation to the data, mapping the predictors onto a new, higher-dimensional space in which they can be separated linearly. The performance metrics were compared with Bayesian network classifier. Neural networks including Multilayer perceptron took a considerably long time to build and classify and hence, not included in comparisons.

The extracted features from each record were corresponding to the task performed by the subjects. Once the classification was performed, the results were analyzed, and the performances were compared using the following metrics.

(1) $$Accuracy = \frac{T_p + T_n}{T_p + T_n + F_p + F_n}$$

(2) $$Precision = \frac{Tp}{Tp + Fp}$$

(3) $$Recall = \frac{Tp}{Tp + Fn}$$

(4) $$F - measure = \frac{2 \cdot Precision \cdot Recall}{Precision + Recall}$$

where T_p = True positive, T_n = True negative, F_p = False positive and F_n = False negative.

We based our results on the datasets described in the previous section that consists of 325 records from Dataset I and 10,861 records from Dataset II. For Dataset II, the initial feature extraction was carried out with 61 electrodes (excluding the reference electrodes). Our aim was to empirically derive a subset of electrodes (features) in such a manner that it does not affect the subject classification significantly. In the dataset the topographical distribution of the event-related

TABLE 3.3. Subject classification for each classifier across various tasks for Dataset I.

	Support Vector Machine			Bayesian Network		
	Accuracy	F-measure	ROC area	Accuracy	F-measure	ROC area
Baseline	96.92%	0.969	0.982	98.45%	0.985	1
Count	98.46%	0.985	1	100%	1	1
Letter	96.92%	0.968	1	95.38%	0.953	0.999
Multiply	100%	1	1	100%	1	1
Rotation	100%	1	1	100%	1	1

potentials to picture stimuli were mainly located in the occipitotemporal area of the brain [151] as shown in Figure 3.2 (marked in color). We achieved a higher distinguishability in the activities using occipital, temporal and central lobes of the brain, compared to the other electrode positions. We were able to isolate a subset of 18 electrodes from 61 electrodes (T7, T8, O1, O2, PO7, PO8, TP8, TP7, P3, P4, P5, P6, C3, C4, P8, P7, P1 and P2).

Table 3.3 shows the classification performance of Dataset I. Table 3.4 displays the classification accuracies and F-measures for successive empirical combination of electrodes for S1_task in Dataset II. Having empirically established the 18 best electrodes from this activity, the classification metrics for other activities of Dataset II were obtained only using these electrodes in Table 3.5. Measures were derived from the confusion matrix to evaluate the performance of the models using the metrics in equations 1-4. Bayesian Network performed better for the smaller dataset (Dataset I) while SVM provided improved measures as the dataset became bigger (Dataset II).

3.8. Neurokey Generation

The authentication ensures that the subject whose EEG signals are being used to generate his personal cryptographic key is the one who he claims to be. As stated before, the feature extraction process here should be different because the classifier used for subject authentication can handle variations in the values of the feature set. Contrary to this, even a small variation will change the key by a significant number of bits. The following subsections describe the feature selection and binary feature vectorization processes.

TABLE 3.4. Subject classification with SVM for S1_task in Dataset II using successive empirical combination of electrodes.

Electrode combinations for classification	Accuracy	F-measure	ROC area
T7 T8 O1 O2 PO7 PO8	80.81%	0.803	0.803
T7 T8 O1 O2 PO7 PO8 P8 P7	82.63%	0.822	0.912
T7 T8 O1 O2 PO7 PO8 PO1 PO2	82.20%	0.817	0.91
T7 T8 O1 O2 PO7 PO8 TP8 TP7	85.61%	0.852	0.927
T7 T8 O1 O2 PO7 PO8 TP8 TP7 P3 P4	86.81%	0.865	0.933
T7 T8 O1 O2 PO7 PO8 TP8 TP7 P5 P6	88.97%	0.887	0.944
T7 T8 O1 O2 PO7 PO8 TP8 TP7 P3 P4 P5 P6	89.70%	0.895	0.948
T7 T8 O1 O2 PO7 PO8 TP8 TP7 P3 P4 P5 P6 C3 C4	90.91%	0.907	0.954
T7 T8 O1 O2 PO7 PO8 TP8 TP7 P3 P4 P5 P6 C3 C4 P8 P7	91.22%	0.911	0.956
T7 T8 O1 O2 PO7 PO8 TP8 TP7 P3 P4 P5 P6 C3 C4 POZ OZ	90.94%	0.907	0.961
T7 T8 O1 O2 PO7 PO8 TP8 TP7 P3 P4 P5 P6 C3 C4 P8 P7 PO1 PO2	90.96%	0.908	0.954
T7 T8 O1 O2 PO7 PO8 TP8 TP7 P3 P4 P5 P6 C3 C4 P8 P7 P1 P2	92.28%	0.921	0.954
FP1 FP2 F7 F8 AF1 AF2 FZ F4 F3 FC6 FC5 FC2 FC1 T8 T7 CZ C3 C4	79.56%	0.794	0.813
F7 F8 AF1 AF2 FZ F4 F3 FC6 FC5 FC2 FC1 T8 T7 CZ C3 C4 CP5 CP6	75.27%	0.7515	0.787
AF1 AF2 FZ F4 F3 FC6 FC5 FC2 FC1 T8 T7 CZ C3 C4 CP5 CP6 CP1 CP2	74.14%	0.741	0.752
FZ F4 F3 FC6 FC5 FC2 FC1 T8 T7 CZ C3 C4 CP5 CP6 CP1 CP2 P3 P4	82.70%	0.8235	0.844
All Electrodes	96.17%	0.961	0.981

TABLE 3.5. Subject classification for each classifier across various tasks for Dataset II.

	Support Vector Machine			Bayesian Network		
	Accuracy	F-measure	ROC area	Accuracy	F-measure	ROC area
S1_task	92.28%	0.921	0.954	87.46%	0.875	0.993
S2_NoMatch	90.45%	0.899	0.952	87.54%	0.876	0.995
S2_Match	90.43%	0.898	0.952	88.22%	0.882	0.995

3.8.1. Feature Selection

We used a similar approach of Chuang et al. [21] to study the self-similarity within the subjects and cross-similarity amongst different subjects' EEG feature vectors across multiple trials. Self-similarity refers to similarity of the feature vectors arising from multiple trials of the same task within a subject. Cross-similarity measures similarity of the feature vectors arising from every combination of the trials of the same task between different subjects. The following equation represents a general case to determine similarity between feature vectors based on the cosine distance.

$$similarity = cos(\Theta) = \frac{A \cdot B}{||A||||B||} = \frac{\sum_{i=1}^{n} A_i * B_i}{\sqrt{\sum_{i=1}^{n} A_i^2} * \sqrt{\sum_{i=1}^{n} B_i^2}} \tag{5}$$

$if A == B : self - similarity, A \neq B : cross - similarity$

Figures 3.5(a) and 3.5(b) show the self-similarity and cross-similarity scores for both the Datasets averaged over the tasks. The self-similarity scores were higher than the cross-similarity across all the subjects. The relative percentage difference between the two scores was used to determine the distinguishability between the feature vectors. The subjects that scored low on self-similarity also showed less relative percentage difference to cross similarity. This is a probable contributing factor to false acceptance rates in the system. As observed by Chuang et al., there was a good variation between the subjects for the relative difference scores. This difference was useful in deriving a unique key for a person's authenticated feature region.

The distribution of feature vectors for every subject was obtained from the training samples of each mental activity. We assumed that these distributions would also be distinguishable if the feature vectors of the subjects could be differentiated based on the variations in relative percentage difference of the similarity scores. The global feature segmentation protocol used to generate the Neurokeys was adopted from Chang et al. [18] who extended the original Monrose et al. [93] scheme of stable key generation. The procedure for the approach is as follows:

- First, the features were calculated from the time domain EEG signals using FFT and DWT across all electrodes, activities and subjects. Feature vectors for key generation from each electrode were formed by

(6) $$Feature\_vector = \frac{(\delta)^3 + (\theta)^3 + (\alpha)^3 + (\beta)^3 + (\gamma)^3}{(\delta) + (\theta) + (\alpha) + (\beta) + (\gamma)}$$

- The distribution of feature vectors for each electrode and activity was obtained from the training samples of a subject and parameters such as mean and standard deviation were calculated for each distribution.
- The width of the global distribution was defined using the global mean and standard deviation via a segmentation parameter, k_seg.

  $Window\_start = \mu_{global} - k\_seg * \sigma_{global}$

  $Window\_end = \mu_{global} + k\_seg * \sigma_{global}$

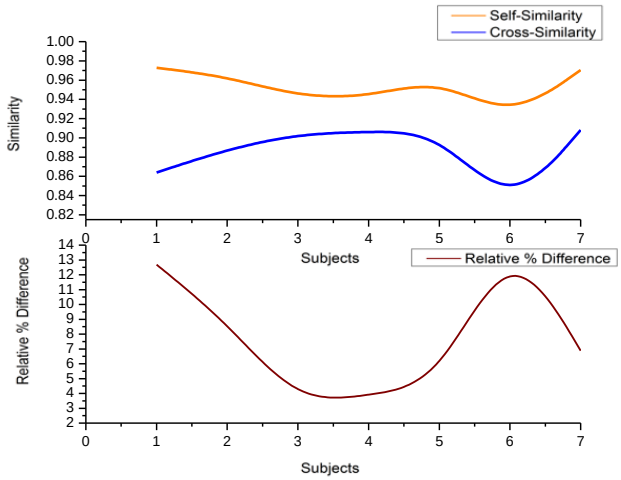

(a)

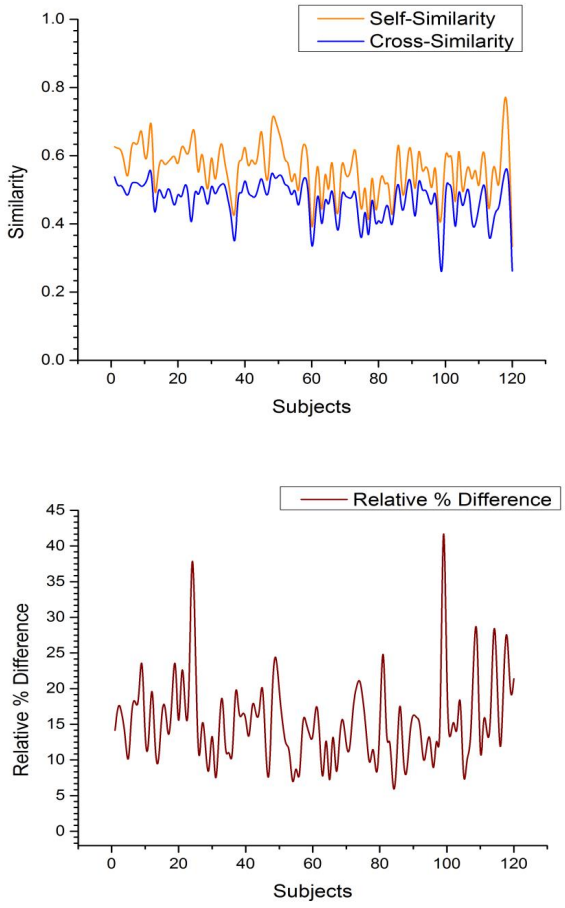

(b)

FIGURE 3.5. Similarity scores obtained across each subject of the Dataset I (a) and Dataset II (b).

- Equiprobable interval bins were derived in the global distribution using the authentication region of each subject's feature vector.

  $Auth\_region_{(sub,feature)} = [\mu_{sub,feature} - k_{sub,feature} * \sigma_{sub,feature}, \mu_{sub,feature} + k_{sub,feature} * \sigma_{sub,feature}]$

  The maximum value of $k_{sub,feature}$ parameter was calculated using the distinguishability criterion [18] as

  $k_{sub,feature} = (\mu_{global,feature} - \mu_{sub,feature})/\sigma_{sub,feature}$

- Each feature vector from the training samples was mapped to an appropriate bin in the global distribution. The bin containing the maximum feature vector samples of the subject was used to represent that feature.

  $if(feature\_vector \geq (Window\_start + increment * step\_size) \&\& feature\_vector \leq (Window\_start + (increment + 1) * step\_size))$

  The step size was proportional to the authentication region of a subject's feature vector, thus, varying the number of equiprobable bins in the global distribution with each subject, electrode, and activity. Figure 3.6 shows an example of key generation region using a feature of a subject in the global distribution.

- The key bits were computed from the feature vector using the binary feature quantization explained in the next subsection.

- This process was repeated for the six electrodes of Dataset I and the chosen 18 electrodes of Dataset II across all the subjects to generate the keys. The length of keys can be changed by combining different electrodes as required by the user conditioned to a particular application.

3.8.2. Binary Feature Quantization

To use the keys for any cryptographic application, the feature vectors have to be binarized appropriately without compromising the inherent security properties of the biometrics. The statistical evaluation of the Neurokeys is detailed in next section. The basic idea to extract the bits was to use the binary value of the feature vectors and perform the mixing function using the authentication regions of each subject's electrode. We can also use the SHA-1 hash function to spread the

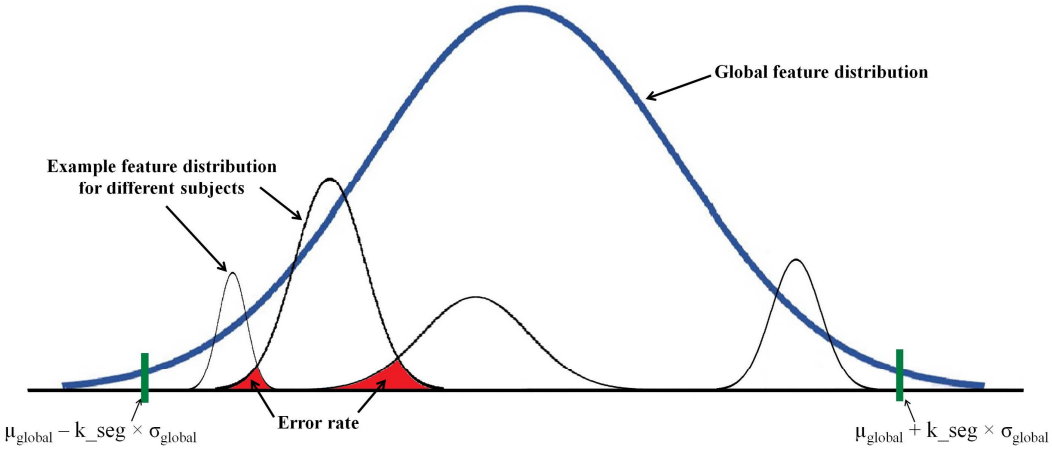

FIGURE 3.6. Example key generation process from the global feature distribution of an electrode for a subject [18].

bits more uniformly in the keys. The index of the circular shift was obtained using the number of segments in the global feature window. After all the concatenation rounds for the desired number of electrodes (18 in this case), the average key length of 230 bits was derived from each subject and activity. The pseudo code for the quantization is shown in Algorithm 1.

Algorithm 1 Binary feature vector quantization

Require: Biometric feature vector Fv , number of segments *N*, Authentic region Ar
Ensure: Neurokey N_key
  for $i \leftarrow 1$ to N_sub **do** ▷ Number of subjects
    for $j \leftarrow 1$ to N_elec **do** ▷ Number of electrodes
      $temp\_key[0] \leftarrow dec$ to $bin(F_v[i][j])$ ▷ Binary quantization
      $seed \leftarrow F_v[i][j]$ mod $Ar[i][j]$ ▷ Determine seed for temporary key
      $temp\_key[k] \leftarrow XOR(temp\_key[k-1], seed)$
      $key[k] \leftarrow circularshift(temp\_key[k], N[i][j])$ ▷ Use the number of segments to perform the circular shift
      $N\_key[i] \leftarrow (N\_key[i]||key[k])$ ▷ Concatenate the bits from each round to form the key
    end for
  end for
  return N_key

3.8.3. Key Evaluation

The amount of data with various parameters can restrict the ability to derive a unique and repeatable key from the entire data set for each subject as outlined in Table 3.6. The number of possible combinations of electrodes to determine an optimal combination given by $\sum_{k=0}^{n-1} \binom{n}{k}$ is

TABLE 3.6. Complexity of deriving the key.

Parameters (n)	Frequency
No. of electrodes (Ne)	1 to 61
Frequency windowing (Fw)	5
Time-Frequency windowing (Tw)	18
Distribution of Data (Dd)	1
Segmentation parameter (Sk)	1
Number of subjects (Sub)	7 to 120
Complexity	(Ne x Fw x Tw) ++ (Dd x Sk x Sub) = O(n^3)

significantly large. Therefore, a subset of electrodes derived during the subject classification will be used in key generation.

The following metrics were considered to evaluate the keys generated from the subjects.

False Acceptance Rate (FAR) is the measure of the likelihood that the Neurokey system will incorrectly accept the derived key from an unauthorized user. As there is only one legitimate user, keys of all other subjects in the dataset apart from the authorized user were used to assess this error rate.

False Rejection Rate (FRR) is the ratio of the number of times the Neurokey system will incorrectly reject the derived key of a genuine user to the total attempts. The dataset of the subjects was randomly split into 40% train and 60% test sets to assess this error rate.

Half Total Error rate (HTER) is an average of the FAR and FRR, defined as:

$$HTER = \frac{FAR + FRR}{2} \tag{7}$$

K_seg, the number of segments in the global window, was a crucial parameter in determining the width of the global window for the feature key and the initialization of the seed in Neurokey binarization. Figure 3.7 shows the variation of HTER with the segmentation parameter averaged across subjects and electrodes. The graph is an exponential variation and K_seg =10 was chosen to be an optimal number for the window segmentation.

We also wanted to study the error rates corresponding to the number of trials needed to enroll a user in the key generation process. Figure 3.8 shows the HTER versus the number of trials

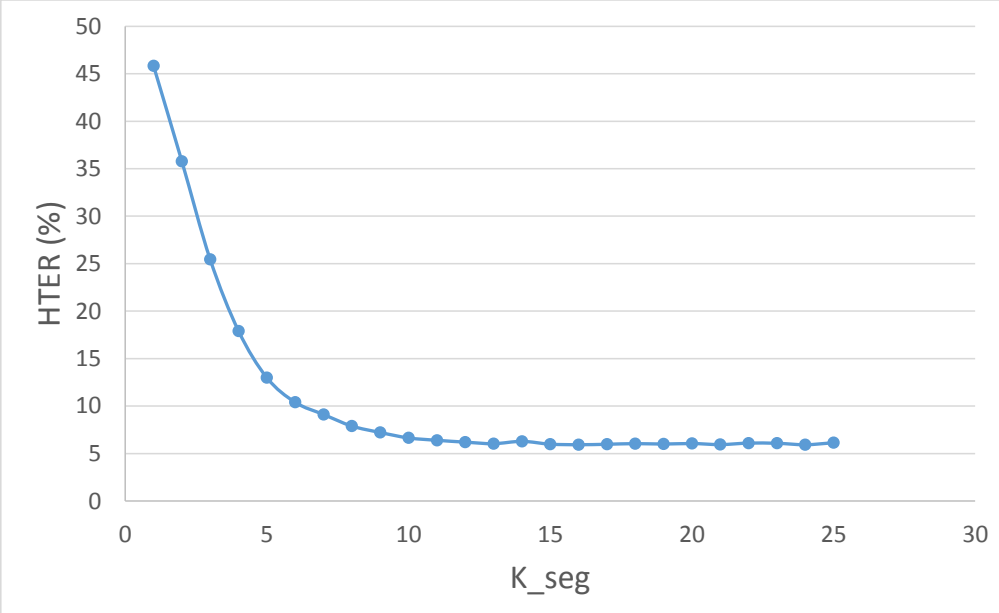

FIGURE 3.7. HTERs for varying the segmentation parameter values averaged across electrodes and subjects.

for both the datasets. In each dataset, the subjects did not perform an equal number of trials. So, the curves in this figure are plotted up to thirteen trials for Dataset I and five trials for Dataset II. These were the minimum of the number of trials performed by the subjects in each dataset. Thus, it gave a measure of the average number of trials required to enroll a user.

Figure 3.9 shows the HTERs for Dataset I, averaged over the electrodes. The mean HTERs for Dataset II (4.53%) were slightly higher compared to Dataset I (3.05%). Since Dataset II represents a larger population, we shall analyze it in greater detail than Dataset I. We compared the FAR's and FRR's of the Neurokeys obtained using FFT, DWT and combined FFT-DWT feature vectors in Figures 3.10(a), 3.10(b) and 3.10(c) for the S1_task. The error rates for other two tasks of Dataset II using DWT-FFT feature vectors are shown in Figures 3.11(a) and 3.11(b). We also studied an alternate view of the error rates for the subjects averaged across all electrodes in Figure 3.12. It shows the fraction of users versus the probability of failure of generating their own genuine Neurokey.

FFT features were more suited for the key generation as both average FAR and FRR were less compared to DWT features. Combining the two features, FAR further reduced to nearly zero in many electrodes. This could be an excellent feature to keep away adversaries. However, the

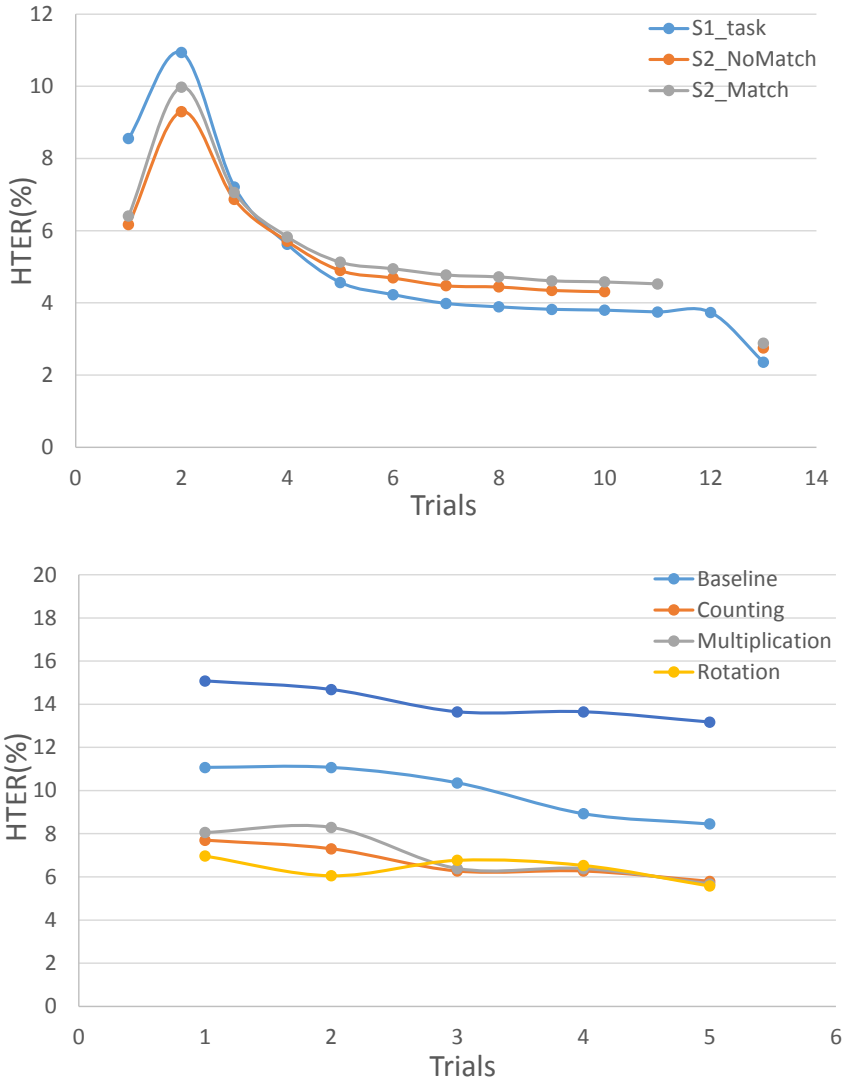

FIGURE 3.8. HTERs variation with number of trials for Dataset I (top) and Dataset II.

increased FRR would comparatively degrade the overall performance of the system.

3.8.4. Randomness Measures - NIST Statistical Test Suite

We utilized the guidelines of the statistical test suite for random number generators by NIST to evaluate the output of our biometric key generator [122]. These tests are helpful in determining the suitability of a generator for the cryptographic application. We tested our sequences with nine out of the fifteen tests that applied to our system (Table 3.7). It is difficult to include the details of all NIST tests in this paper. We briefly list the parameters that help to understand the evaluation of

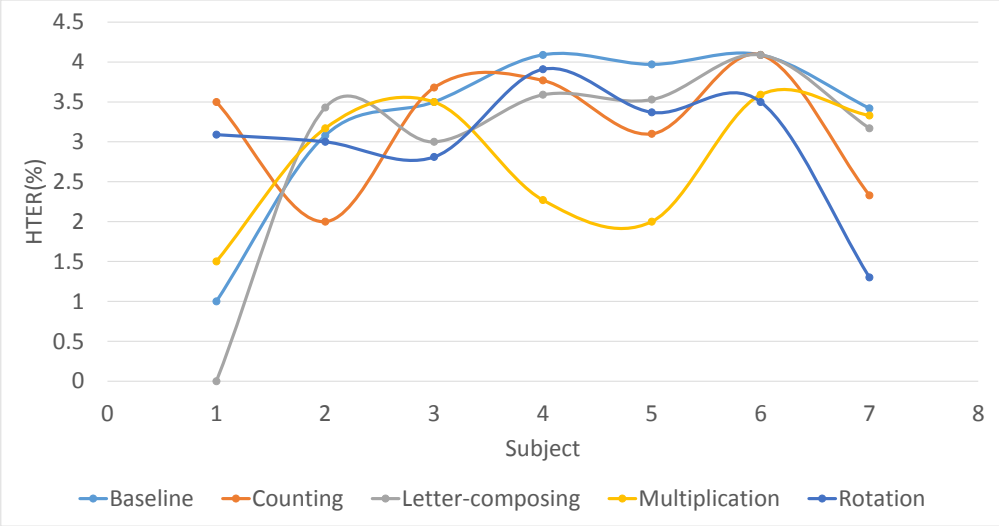

FIGURE 3.9. HTERs variation for Dataset I for each subject and activity averaged over the electrodes.

each test.

Ho:: The null hypothesis that the sequence being tested is random.

Ha:: The alternative hypothesis that the sequence is not random.

α**::** The level of significance of the test. It is the probability that a test will indicate that the sequence is not random when it really is random. The default value of significance is 0.01.

: A p-value $>= \alpha$ would mean that the sequence would be considered to be random with a confidence of 99%. A p-value $< \alpha$ would mean that the sequence is non-random with a confidence of 99%.

Each test was carried out for Dataset II for a sample size = 360 sequences resulting from 120 subjects, and 3 activities combined for 18 electrodes. A useful interpretation of the 3240 results (120*3*9 tests) is necessary. Two approaches outlined by NIST include (1) Examine the proportion of sequences that pass a statistical test and (2) Verify the distribution of p-values from a test for uniformity.

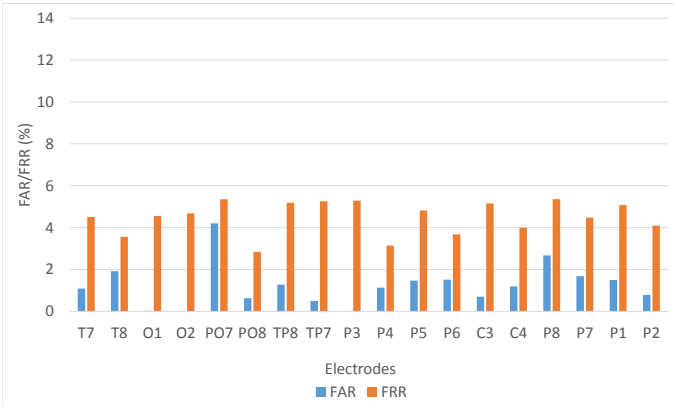

(a)

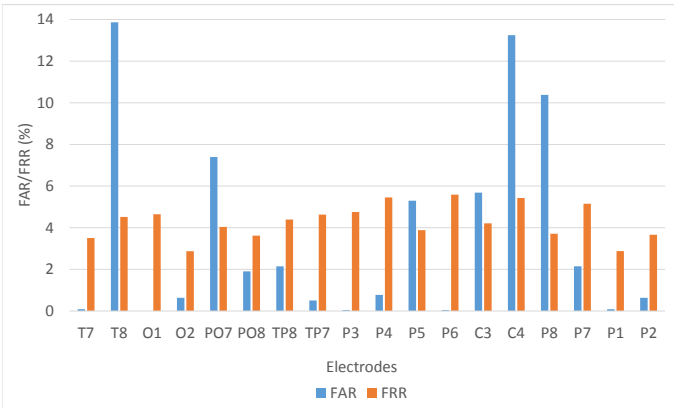

(b)

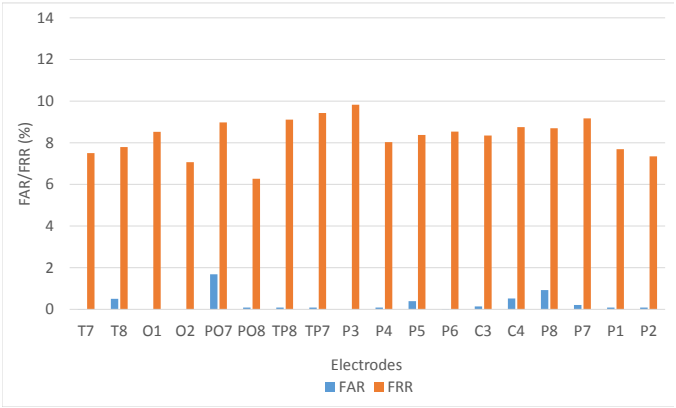

(c)

FIGURE 3.10. False acceptance and rejection rates for each electrode averaged across the subjects for S1_task (Dataset II) using different feature vectors (FFT feature vectors (a), DWT feature vectors (b), DWT-FFT feature vectors (c)).

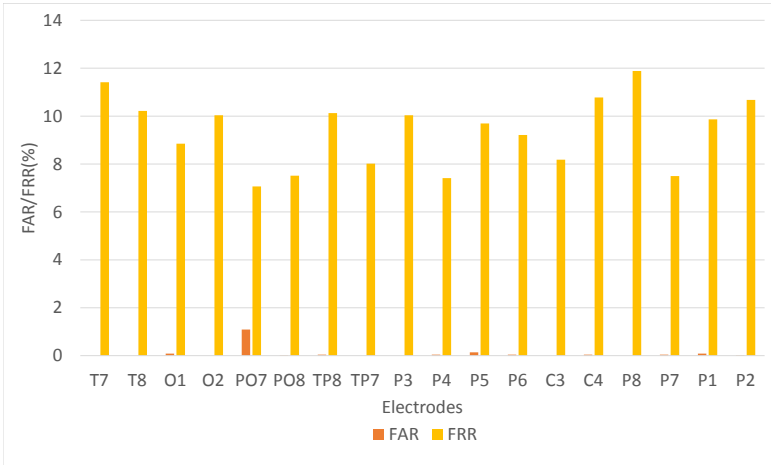

(a)

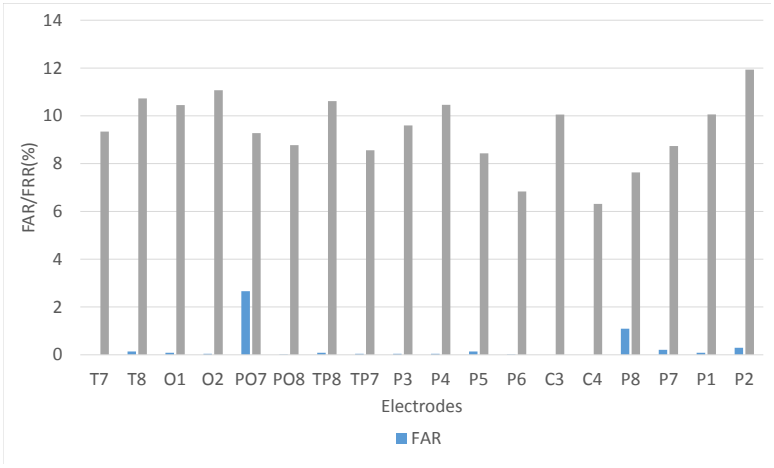

(b)

FIGURE 3.11. False acceptance and rejection rates for each electrode averaged across the subjects for S2_NoMatch (a) and S2_Match tasks (b), using DWT-FFT feature vectors for Dataset II.

3.8.4.1. Proportion

The acceptable range of proportions that pass the test is given using α, the level of significance, and m, the sample size.

(8) $$Range = \tilde{p} \pm 3\sqrt{\frac{\tilde{p}(1-\tilde{p})}{m}}$$

where $\tilde{p}$ = 1-α, α = 0.01 and m = 360 sequences, we get range = 0.99 $\pm$ 0.01573213272 (i.e. proportions should lie above 0.97426786).

TABLE 3.7. Results for the proportion of sequences passing the tests and the uniformity of p-values.

Statistical test	Proportion	Decision	P-value of p-values	Decision
Frequency (Monobit) Test	0.975222	Pass	0.983235	Uniform
Frequency Test within a Block	0.988889	Pass	0.985372	Uniform
Runs Test	0.997222	Pass	0.989165	Uniform
Longest Run of Ones in a Block	0.979444	Pass	2.82E-19	Non-Uniform
Spectral Test	0.172222	Fail	1.49E-06	Non-Uniform
Non-overlapping Template	0.979889	Pass	8.46E-06	Non-Uniform
Serial Test a	0.983333	Pass	0.978447	Uniform
Serial Test b	0.983333	Pass	0.882427	Uniform
Approximate Entropy Test	0.975	Pass	0.982684	Uniform
Cumulative Sums Test	0.727778	Fail	0.996361	Uniform

3.8.4.2. Distribution

The distribution of p-values of a test is evaluated by dividing the interval between 0 and 1 into 10 sub-intervals. The frequency of p-values that lie within each sub-interval is calculated. Uniformity is statistically determined by χ^2 test and finding the P-value of all p-values for a test [64]. If P-value $>= 0.0001$, then the sequences can be considered to be uniformly distributed.

$$\chi^2 = \sum_{1}^{10} \frac{(F_i - m * S_i)^2}{m * S_i} \tag{9}$$

$$P\text{-}value = igamc(9/2, \chi^2/2) \tag{10}$$

where F_i gives the frequency of p-values in the i*th* sub-interval, m is the sample size, S_i denotes the rate of each i*th* bin which is computed from the histogram of p-values and *igamc* is the incomplete gamma function.

3.9. Discussion

The accuracies and F-measures of the subject classification using Support Vector Machine and Bayesian Network are shown in Tables 3.3 and 3.4. Dataset I (using six electrodes) had a mean accuracy of 98.46% whereas Dataset II (using selected 18 electrodes) had a mean accuracy of 91.05%, averaged over the activities. It is due to the vast difference in the number of subjects in the two datasets. The F-measures and ROC areas were reasonable given that the EEG signals were

recorded over multiple sessions separated in time. From the observations, we can conclude that Bayesian Network can be used to classify small datasets, and SVM can be used for large datasets. Dataset II will be analyzed and discussed more as it represents a larger population set.

Our system faces the trade-offs such as entropy vs practicality and number of features vs accuracy. All subsets of electrodes shown in Table 3.4 showed lower classification accuracies compared to using 61 electrodes together (96.17%). But, clearly some subsets obtained better classification than the rest (mainly frontal electrodes). For instance, using a subset of 18 electrodes (bold in Table 3.4) achieved an accuracy of 92.28% whereas the subset of 18 electrodes containing FP1 through C4 (italics in Table 3.4) showed an accuracy of 79.56%. The reasons for this could be:

- Feature reduction is sensitive to type of electrode because its characteristics are dependent upon underlying brain activations. Zhang et al. [151] showed that the topographical distribution of event-related potentials to picture stimuli were mainly located in the occipito-temporal areas of the brain, and these regions play a key role in high level visual information processing. We also observed that using occipital, temporal and central brain areas of the brain (P3, P4, O1, O2, C3, C4), resulted in higher distinguishability of the activities compared to other electrode positions.
- The features from biometrics such as fingerprints [90] are well established but feature extraction from EEG is still an active area of research. Hence, estimating the entropy contribution of each electrode to the system is a challenging endeavor. Using all the 61 electrodes increases the total number of features that may account for accommodating the variations in EEG among the trials.

For key generation process, we observed that using the same feature vectors of authentication for key generation indeed caused avalanche effect in error rates. The mean HTERs were nearly nine to 10 times lower using the global feature segmentation [18] feature selection process for key generation. It is not feasible to detail all these comparisons currently in this paper. The activities that provided better classification among subjects also produced lower error rates for the Neurokey generation process. For example, the rotation and multiplication activities had F-measures of 1

for subject classification. They also had low mean HTER values in the range of 2-3% (averaged over the subjects and electrodes). Similarly, S1_task of Dataset II with 0.961 F-measure provided a better subject distinguishability compared to other visually evoked stimulus tasks. It had a mean HTER of 4.28% (FAR 0.27%, FRR 8.30%). Thus, combining the activity with certain electrodes will help to generate strong cryptographic keys. The flexibility to change an activity upon compromise is an attribute not yet offered by most of the existing biometrics. The mean HTERs of Neurokeys from other activities were also low (S2_NoMatch 4.78%, S2_Match 4.8%). It has been shown that brain responses change during threat [23], providing a resilient solution to coercion attacks. Another possible solution could be to think of a different activity than the enrollment activity when forced to reveal one's authentic biometric key. However, it requires further work to test the performance of our scheme to key generation under a threat/coercion attack model.

As observed previously in Figure 3.10, Neurokeys from the DWT (FAR 3.60%, FRR 4.27%) and FFT (FAR 1.23%, FRR 4.50%) feature vectors had lower mean error rates compared to the combined DWT-FFT feature vectors (FAR 0.27%, FRR 8.30%). Failure rate of our system has similar implications as other biometrics-based cryptographic systems. The UK Biometrics Working Group has suggested a scheme for understanding relative biometric strengths - FAR of 1.0% as basic security strength, 0.01% as medium and 0.0001% as high security strength [45, 111]. Our Neurokey system fulfills this criterion of basic strength with a best FAR of 0.27%. However, the current FRR of 8.30% implies that a user will be falsely denied permission to his/her encrypted content in one out of nearly 12 access requests (when used as a private key). This leads to user annoyance while also rendering the system undeployable in large settings. False acceptance rate (FAR) is the most critical accuracy metric in a cryptographic system because an imposter break-in is certainly a more critical event than other failures of a biometric key system. Therefore, the keys generated from DWT-FFT features were accepted to be tested against the NIST randomness tests. We are currently working towards improving the FRR metrics to make it a more usable system.

With any biometric data, there will be changes in a user's characteristics - fingerprints change with time, scarring, aging and general wear, voice-scan system is influenced by sore throats, and facial-scan is affected by changes in weight. There will be a need to update the EEG feature

vectors of the subjects whenever there is a biological or emotional change in the brain so that the EEG signals can effectively authenticate a genuine user and reject an imposter. Five to seven trials were needed to establish a key for the user (Figure 3.8), which is relatively small. We also studied the probability of failure to generate a genuine key for the users from their biometric samples collected over different sessions in time, shown in Figures 3.12(a), 3.12(b) and 3.12(c). For S1_task, 19 users failed to generate their genuine keys with a maximum failure probability of 6%. For S2_NoMatch task, 18 users failed to generate their genuine keys with a 9% maximum failure probability. For S2_Match task, 16 users did not generate their genuine keys with a 9% failure probability. This shows that some tasks are better for certain group of users to generate their Neurokeys. Nonetheless, there is an alternative task to switch one's Neurokey in the case of a compromise.

We performed the NIST tests on the sequences obtained from the tasks of Dataset II. The average length of key bits generated from each activity using 18 electrodes was 230 bits. Most of the sequences passed these tests. However, Spectral Test and Cumulative Sums Tests were not able to produce the proportion of the sequences that should pass the threshold of 0.9742. Majority of the NIST tests recommend a minimum input size of 100 bits. The recommended input size for Spectral Test is 1000 bits and our system was tested with an average length of 230 bits. This could be a possible reason for the test failure by a big margin. This test is based on the Discrete Fourier Transform to detect periodic features in the bit strings. These features play an important role in cryptanalysis [50]. Also, the proportion of sequences passing the Cumulative Sums test was below the threshold. It implies that some of the sequences had too many zeros or ones in the beginning or at the end, which can be easily detected by an adversary by cryptanalysis of a few sequences. For a sequence to have good random properties, the cumulative sum of the partial sequences should be near zero. For the uniform distribution test, Longest-Run-of-Ones in a Block and Non-overlapping Template Test showed non-uniform distribution of p-values. This is because the variety of p-values in these tests were limited even though the sequences passed the tests.

Using the results of Datasets I and II, we prove the feasibility of deriving random bits from the EEG biometrics of a person. Irrespective of the differences in activities, electrodes, and

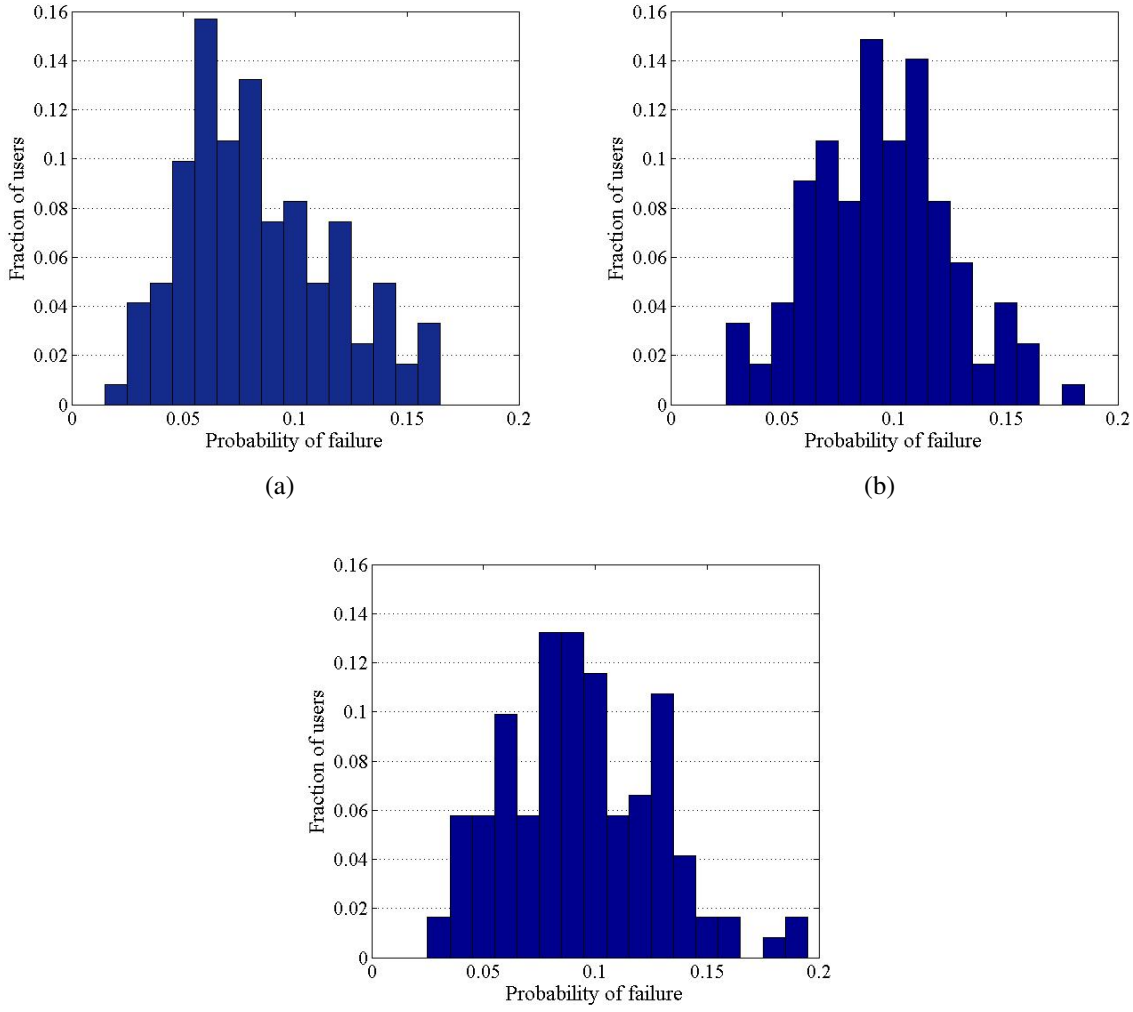

(a) (b)

(c)

FIGURE 3.12. The fraction of users versus the probability of failure of generating their own genuine Neurokey for Dataset II (S1_task (a), S2_NoMatch task (b), S2_Match task (c)).

recording conditions, a key can be derived with a low error rate. A smaller dataset provides better authentication capability and lower error rates for the Neurokeys. For a larger data set, despite having acceptable mean HTERs for the keys, we need better feature vectorization for subject authentication.

3.10. Security Analysis

Template Security: The information regarding the global feature segmentation protocol and an individual's authentic region needs to be stored. The authentic region windows of all subjects

and feature vectors are equiprobable in the global window. However, the authentic window widths are not equal for any subject or feature i.e. equiprobable ! = equal interval. Hence, an imposter gains no information regarding the feature vector or EEG biometric sample from the equiprobable authentic regions. The template can be secured using techniques suggested by Lucas et al. [13] and Jain et al. [56].

Key Space: It is a crucial factor of a cryptographic system and refers to the set of all possible keys (2^n combinations for n bits key). Average key space for the Neurokey generation is 230 bits per activity. Combining different activities will change the maximum length of keys for subjects. Thus, the range theoretically is 230 to 690 (230*3) bits. However, the effective key space is given by 1/False Acceptance Rate (FAR) [44]. Comparing with other biometrics, we see that Token (10^{12}) > Password (10^{14} - 10^6) > Iris (10^6) > Fingerprint, PIN (10^4) > Neurokeys (1/0.0027 $\sim$ 370) > Face (6.25) [44]. Our current effective key space performs better than face biometrics only and is comparable to basic the key sizes of standards such as AES and DES. A reasonable defense against guessing and search attacks would be similar to the conventional systems that restrict the number of failed attempts by a user. We hope to increase the Neurokey space in future by exploring better entropy mixers for our system.

Entropy: It is the amount of uncertainty to guess the key from an adversary's perspective. The maximum is n bits for a truly randomized key and zero for a guessable key.

$$Entropy = \sum_{i}^{n} p(x) log_2 p(x) \tag{11}$$

where n = the total number of possible locations for a feature vector in the global window and p(x) = the probability of a feature vector occurring at each location in the global window. The overall entropy is less than n, i.e. 230 bits as stated above, since we accommodate variations among the genuine EEG samples of the subjects using the mean and standard deviation of the EEG features. The average entropy for the subjects, averaged over the tasks and electrodes, was 82 bits for our system.

3.11. Practical Considerations

Brain-computer interface (BCI) applications were considered impractical just two decades ago. In the last 6 years, with the advent of affordable, comfortable, more sensitive, and dry EEG headsets possessing high resolutions (up to 512 Hz) [131, 150], BCI is now used routinely to control prosthetics [72], wheelchairs [131, 53] and gaming applications [101].

Not very far in the future, we will be using EEG for cryptographic purposes similar to today's commonplace biometrics like fingerprinting. This study is a step in that direction and was aimed to explore the challenges and study the outcomes of a system using EEG as a cancelable biometric identifier for key generation.

Social engineering attacks, dictionary attacks, and phishing attacks have not been studied in a systematic fashion for the EEG-derived keys. The attacks can be countered depending on the strength of the derived key and process. We outline some of the practical limitations of using BCI technology for the cryptographic key generation.

Ethical issues: Abusing the BCI technology to trick a user into inputting a thought for deriving meaningful interpretations. *Protection from user non-compliance*: The EEG biometric template should not be easy to transfer to other parties so as to share the key using the same BKG system. This can be prevented by not storing the EEG in a raw form. *Electrodes*: There is no consensus on the number of electrodes and electrode positions for authentication or key generation processes. *Larger Dataset*: More number of distinguishable features have to be evaluated to generate keys in future from larger datasets (e.g. 1 million people). *Emergency*: Performing a behavioral activity or task in an emergency, as opposed to a normal situation, will result in a change in the brain signals due to emotional stress. The system should still be able to generate a key. *Coercion Attack*: Similar to an emergency situation, performing an activity under duress will also result in a change in the EEG patterns. However, in this case, the system should not generate a key.

3.12. Conclusion

A unique key for each subject was obtained using EEG signals by collecting data from distinguishable mental activities. We studied the feasibility of deriving a cancelable biometrics-based Neurokey using various mental tasks. Uniqueness and consistency amongst the subjects and

their keys can be asserted from the results achieved using different datasets. Cryptographic systems based on biometrics such as fingerprinting have evolved over time with extensive research work and marketing technologies leading to a reduction in their error/failure rates. It is a challenging task to characterize EEG variations for cryptographic purposes but we envision to bring the error rates down with better grade recording devices and feature fusion mechanisms. Hybrid algorithms for feature mapping to binary codewords are under progress. We would also like to explore the possibility of combining the EEG data with fMRI, and study the correlations for producing the Neurokeys. We ascertained the strength of the obtained Neurokeys by using entropy and NIST's statistical tests. Additionally, it seems promising to combine other synchrony measures with EEG features.

3.13. Dataset Acknowledgements

We would like to acknowledge the late Prof. Henri Begleiter at the Neurodynamics Laboratory at the State University of New York Health Centre at Brooklyn, USA, who generated the data and UCI Machine Repository for making it available online. The authors also thank the assistance of Dr. Charles Anderson of Colorado State University, USA, for maintaining a repository of 1989 Keirn and Aunon data and making it available for experimentation.

3.14. Acknowledgements

This work is partially supported by the National Science Foundation under grants CNS -0751205, CNS-0821736 and CNS-1229700.

CHAPTER 4

DETECTING ON-ROAD DRIVER DISTRACTION EVENTS USING A SINGLE CHANNEL DRY SENSOR EEG

4.1. Structured Abstract

Background: Driver distraction is one of the primary factors of accidents, followed by drunk driving and speeding. It has become a significant concern in safety and health measures taken by National Highway Traffic Safety Administration.

Introduction: The integration of information and communication technology has led mobile phones to constitute a significant part of cognitive distraction, in association with visual, acoustic and manual distractions. Our aim is to utilize the capabilities of these mobile phones to identify a distracted drivers behavior by analyzing his/her neurological response from the Electroencephalograms or brain signals in various multitasking scenarios while driving.

Materials and Methods: A 14 electrodes headset was used to record the brain signals while driving in the pilot study with two subjects and a single dry electrode headset with 13 subjects in the main study. Subjects completed typical tasks involving distractions such as texting, calling, using the camera on a mobile phone, reading an article, and operating Google Glass while driving. We used a naturalistic on-the-road driving study as opposed to a virtual-reality driving simulator to perform the distracted driving maneuvers, consisting of over 100 short duration trials (three to five seconds) for a subject.

Results: We detected significant changes in the time-frequency spectrum of the EEG signals during distracted driving compared to the normal driving. We overcame one of the biggest challenges in EEG analysis - reducing the number of electrodes by isolating one electrode (FC5) from 14 electrode locations to identify certain distractions. Our machine learning methods achieved a mean accuracy (averaged over the subjects and tasks) of $91.54 \pm 5.23\%$ to detect a distracted driving event. Identifying the type of distraction for a driver can be certainly difficult as there is an overlap in the brain activations of the neurological mechanisms. However, we achieved a reasonable mean accuracy of $76.99 \pm 8.63\%$ to distinguish between the five distraction cases in our study

(read, text, call, and snapshot) using a single electrode. A distraction metric was also calculated to rank the severity of a distraction task. Lastly, an assistive real-time distraction alert system was developed using an android application based on the communication protocol between the EEG device and a mobile phone.

Conclusion: This study localized the everyday distraction events to one part of the brain. A clear indication of distracted behavior was identified using the EEG signals in a real world scenario in contrast to a simulated driving environment. Our real-time assistance application adapted to a drivers mental state can address the safety concerns resulting from driver distraction.

4.2. Introduction

Electroencephalography (EEG) is a technique for the measurement of electrical activity or the potential difference between different parts of the brain. It occurs as a result of ionic current flows when neurons communicate with each other. The novel idea of using EEG to communicate with a computer emerged in the early 70's with the research initiated by Vidal [138]. Since then, many diverse areas such as robotics, gaming, and neurofeedback applications use this technique [26]. Brain-computer interfaces (BCI) are being adopted increasingly for real-time monitoring of patients, controlling wheelchairs to assist physically challenged people, and neural prosthetics [146]. Hence, the future developments are focused on recording and transmitting EEG signals using a wireless platform and at the same time supporting mobility for such applications [79, 16, 143].

In the recent past, many investigations have been made for driver distraction behavior. Specifically, the U.S. National Highway Traffic Safety Administration (NHTSA) has given significant attention to this issue [41, 117, 67]. It reported nearly 3,154 deaths in 2013 resulting from distracted driving crashes. NHTSA defines driver distraction as *"any activity that takes a drivers attention away from the task of driving"*. Their recent guidelines [100] have listed manual text entry, reading and displaying graphics unrelated to driving as unsafe driver distractions. According to a study on drivers willingness to engage in various sorts of potentially distracting tasks, highest mean ratings were shown in activities like entering text messages from the phone, looking up stored phone numbers, picking up and reading a message on PDA and sending emails [71]. It

influenced us to formulate an experiment to study an individuals brain pattern involved in common distraction activities.

Measuring whether a driver is distracted or not is not an easy task and may involve analysis of many parameters. There must be proper metrics and measurements available to quantify driver distraction accurately. Obtaining data directly from the brain to measure distraction sounds more natural and plausible. According to a review by Dong et al. [28], there are primarily three types of inattention detection methods. They are biological signal processing approaches, subjective report approaches and behavior signal processing approaches. Under biological signal processing approaches, EEG plays a critical role in detecting driver distractions. Further, their study highlights EEG technique as one of the most accurate methods of detecting driver inattention. Their findings inspired the usage of EEG in our research to study about driver distraction.

Most of the existing work for analyzing driver distraction using EEG was performed in simulated environments [60, 123, 70, 81]. Faro et al. [35] in their study of analyzing driver status observed that channel locations F7, F8, FC5 (according to international $10-20$ system, Figure 4.1) play an active role in detecting distraction. They observed the frontal areas as the most significant channels for 18 out of 20 peoples' sample. Using a virtual-reality (VR) based simulator, Lin et al. [80] observed increased powers in the theta, and beta frequency bands in the frontal cortex while studying the dynamics of dual-task driving performance. They also proposed that motor area was not related to the distraction effects as most of the brain resources were occupied in the frontal area to deal with the two tasks. Also, the correlation was low between EEG dynamics in motor area and its corresponding response times.

Detecting driver emotions using EEG can also be very useful in observing driver distraction. Fan et al. [34] explained the importance of emotions towards driver safety. Their research claims to detect human emotion using EEG with an accuracy of 72.25% for the targeted group samples. Studies in the past have also evaluated drivers' mental workload [112]. Lei, Welke and Roetting [75] assessed this workload using EEG data when drivers were performing multiple tasks simultaneously. They also used a virtual driving simulator to present each subject with four different blocks of lane change tasks and observed that EEG is very effective tool for evaluating a

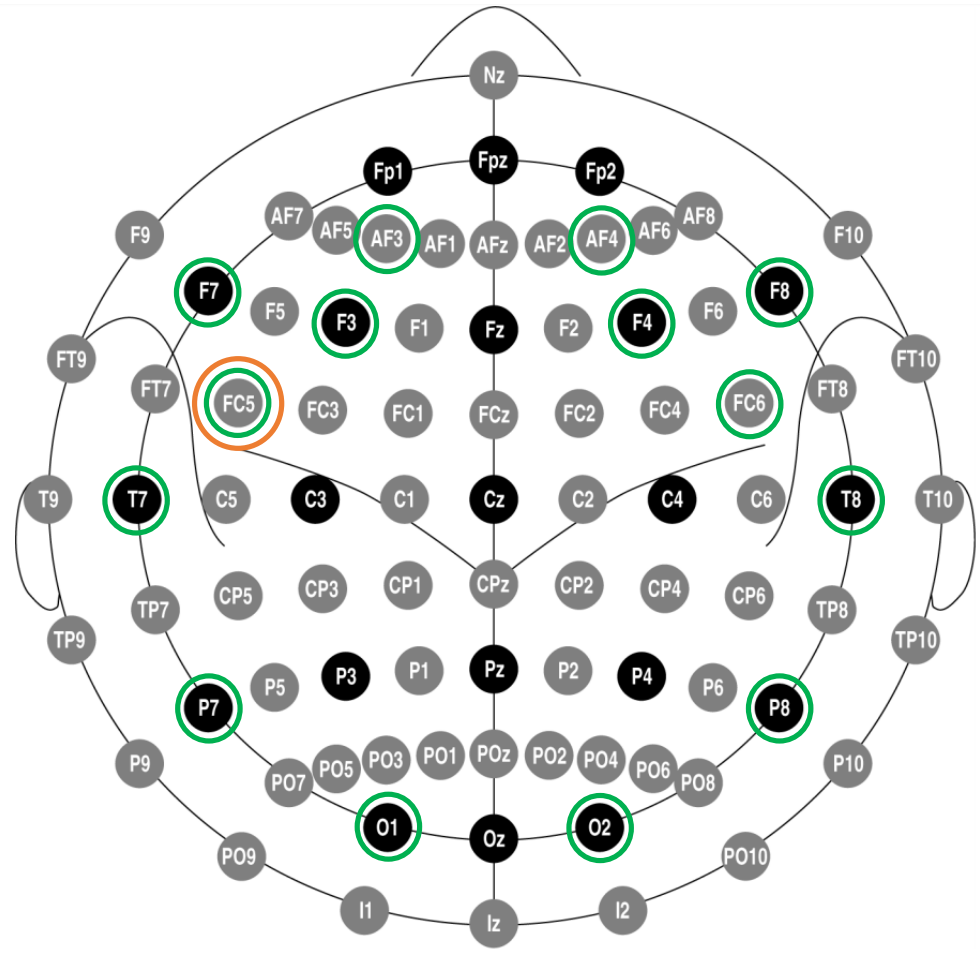

FIGURE 4.1. 10-10 Electrode positioning system. Black circles indicate positions of the original 10-20 system, gray circles indicate additional positions introduced in the 10-10 extension [103]. The letters F, T, C, P and O stand for frontal, temporal, central, parietal, and occipital lobes, respectively. The electrodes used in EPOC headset are marked in green color and Neurosky electrode placement in orange.

drivers mental workload. An EEG-based drowsiness estimation system used the EEG power spectrum methods to estimate indirectly a driver's drowsiness level in a VR-based driving simulator [83]. Another work by Lin et al. showed the use of independent component analysis (ICA) in estimating driver's drowsiness effectively [82].

4.2.1. Contributions

Current literature focuses on the use of simulated driving in distraction studies using EEG. In this work, we collected responses from human subjects during on-the-road driving in a real environment that incorporates complexities arising from multisensory cues as opposed to virtual-

reality driving that involves only distal cues and non-vestibular self-motion cues [113, 51, 120]. The newer generation of EEG recording devices [96, 30] have eased the signal acquisition process and storage. Our aim is to utilize these devices to develop a reliable and robust application that supports mobility as well as simplification of high-dimensional EEG data that generates safe real-time feedbacks for the drivers'. A user acceptable assistive application is highly desirable to prevent fatal accidents resulting from distracted driving.

The key contributions of this paper are:

- Performed extensive on-the-road trials with 15 subjects in a real-life naturalistic driving setup where the brain responses are much more complex and intriguing than a simulated driving environment. Nearly all the prior studies focused on the use of simulated study [80, 142, 141].
- Localized the identification of common distractions to one electrode (FC5) from 14 electrode locations. All the previous work performed classification and prediction with more than one electrode [28]. Using a single dry sensor EEG also increases the usability and acceptability of our system.
- Established a system to understand and distinguish between multiple scenarios of everyday driver distractions such as reading, texting, calling and taking a snapshot.
- Developed a real-time training and calibration of a mobile application to provide safety alerts to the drivers based on their level of cognitive distraction computed using the EEG spectrum.

The methodology of the driver distraction system consists of three main stages; *process* the EEG signals, *analyze* using time, frequency and independent components, and *classify* them into various types of distraction events (Figure 4.2). The rest of the paper discusses scenarios of distraction and the methods that help to recognize such behaviors. The last section is dedicated to the feasibility of detecting these events on a mobile platform.

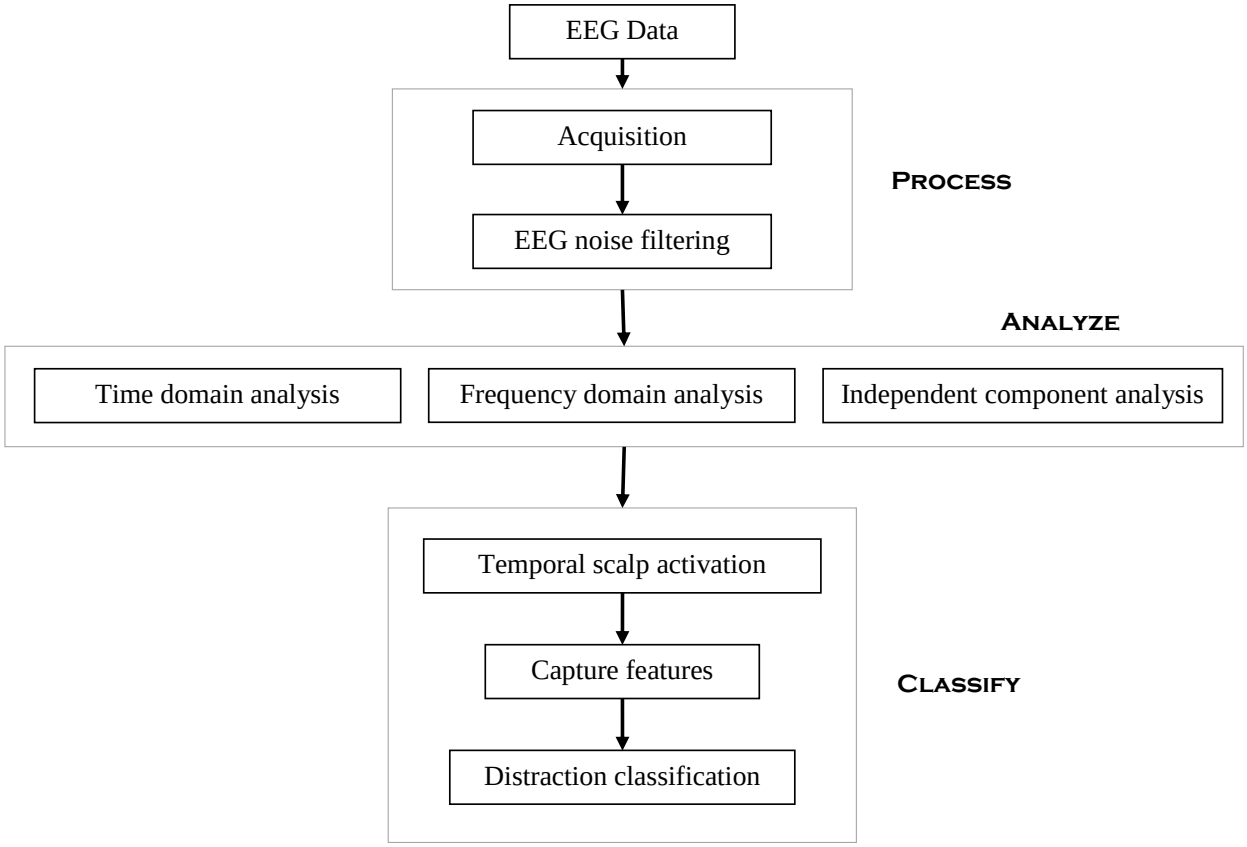

FIGURE 4.2. A schematic depiction of the processing stages of the distraction detection system. The first process stage deals with EEG signal acquisition and filtering. In the analyze stage, three techniques time, frequency and independent components were used to understand the signals behavior in distractions. The classify stage incorporates feature formation, selection, and classification evaluation of various distraction events.

4.3. Materials and Methods

4.3.1. Ethics Statement

Ethical approval for the study was obtained from the Institutional Review Board at University of North Texas (Denton, Texas, USA). All participants provided written informed consent to participate in the study and also consented to the publication of the data and media.

4.3.2. Driving Tasks

The aim of this experiment was to quantify driver distractions using EEG while a subject performed certain activities along with driving a car in a real world scenario. The scope of this study was constrained to the common distractions while driving [117, 65, 3] as follows:

(1) *Base (undistracted)*: Normal driving behavior of a subject without engaging in any tasks while driving

(2) *Read*: Subject was presented with an unseen article on a printed paper to read while driving

(3) *Text*: Involved composing and sending a message while driving by using any of the standard messaging services on the mobile phone

(4) *Call*: Subject browsed his/her contact list and made a call to the desired person

(5) *Snapshot*: Subject operated the phones camera that involved taking pictures either using the front or back camera

In addition, one of the subjects volunteered for using Google Glass to perform the above activities of read, text, call or snapshot while driving. Google glass was becoming a popular device for navigation and other activities at the time we were collecting data for our study. We wanted to observe the changes in the brain signals while using this device in driving. We also performed a pretending to text activity to observe the differences from an actual distraction task. In this activity, the driver looked at his phone screen intermittently while driving. The testing conditions were purposely kept simple in order to implement a controlled driving environment by isolating only the designated distraction. Adding complicated driving courses and behaviors such as hard turns, lane changes can cause more complex brain activity that could mask or mislead the driver distraction signals.

4.3.3. Driving Location

The road section adjacent to a parking lot on the University campus was chosen for the study (Figure 4.3). We conducted the experiment during the time the parking lot was rarely used to ensure a safe environment for the study. The path driven was a straight and curved stretch of nearly one mile. There was a minor risk of accident associated with performing the tasks while driving. Therefore, principal investigator and the student investigator constantly kept a check for any undesirable events such as subjects moving out of the lane while driving, monitoring incoming traffic on the opposite lane, and rare cases of any pedestrians being present to make sure of the safety on the road. There was no case of any injury or accident at the end of data collection process

FIGURE 4.3. A view of the road section inside the university campus used to conduct the distracted driving experiment.

from any subject.

4.3.4. EEG Acquisition Devices

The distracted driving study was conducted using two different EEG recording devices; Emotiv's EPOC neuroheadset [30] and Neurosky's Mindband [96]. EPOC is a portable device to record EEG data from 14 saline electrodes placed according to the international $10-20$ system (Figure 4.1). Its sampling rate is 128 Hz. It has a built-in gyroscope that generates optimal positional information for cursor and camera controls allowing a total range of motion. The Neurosky headband contains a single sensor dry electrode with an ear clip reference to record signals from the scalp. Its sampling rate is 512 Hz and records signals up to 100Hz. It has a rechargeable battery, and a stretchable fabric makes it very convenient to wear and adjustable to different head sizes. A significant benefit over Emotiv is that it has a single dry electrode and needs no preparation.

Since, the data collection was carried out in a dynamic environment with multiple subjects, we used conductive gel in some cases to ensure good contact with the Neurosky electrode. Quality of the signals was monitored using the signal strength information from the electrode (good strength equivalent to 200 is solid contact with the skin/scalp).

4.3.5. Data Collection

The data was recorded for 15 right handed subjects, nine males, and five females with ages between 24 to 28 years, and one male with age 55 years. In the pilot study with two subjects, EEG data was recorded from both the 14 electrodes and single electrode headsets. In the main study with 13 subjects, EEG data was collected using the single electrode device (explained in forthcoming sections). A session consisted of performing one trial of each distraction activity (read, text, call, and snapshot). The recording time for each task was nearly 60 seconds over the pre-defined road route. We avoided contaminating the EEG readings of participants with any known factors such as tiredness or boredom. At the end of every session, the participants either chose to come back or continue with the data collection. The variation in sessions was dependent upon the willingness of participants to volunteer for more than one session. Hence, the number of sessions varied from two to four for the subjects. The details of the complete dataset are shown in Table 4.1.

The experiment was carried out by two people; one performed the driving task, and the other person recorded the data as well as gave the audio prompts for the desired activity. The driver was asked to relax for few seconds before a prompt to start driving. Similarly, audio cue was given to perform a certain distraction activity (text or read) and finally, the driver was asked to stop the vehicle safely. The subject was not aware of the order in which he/she will perform the distraction tasks. We wanted to carry the distraction activity as a controlled event to visualize the maximum effect of distraction in the EEG activity. Also, we did not want to bias the EEG signals with any known criteria prior to performing the distraction activity and intended to keep the experimental conditions similar for all participants.

A laptop was used to establish a wireless connection to the EEG headsets and record the data for further processing. A video of the driver was also recorded simultaneously throughout the experiment for reference and verification of the distraction tasks. Both the EEG and video

TABLE 4.1. Statistics of the dataset. Each row corresponds to the details of the trials for a subject performing the various distraction tasks. Duration of each trial varies from three to five seconds.

Subject	Interface	Baseline	Text	Read	Snapshot	Call	Total
		Number of trials					
1	BCI	20	20	20	20	20	100
2	BCI	20	20	20	20	20	100
3	BCI	25	25	25	25	25	125
4	BCI	25	25	25	25	25	125
5	BCI	15	15	15	15	15	75
6	BCI	25	25	25	25	25	125
7	BCI	30	30	30	30	30	150
8	BCI	30	30	30	30	30	150
9	BCI	30	30	30	30	30	150
10	BCI	25	25	25	25	25	125
11	BCI	15	15	15	15	15	75
12	BCI	25	25	25	25	25	125
13	BCI	35	35	35	35	35	175
14	BCI	30	30	30	30	30	150
15	BMI	60	69	69	69	69	336

BCI - brain-computer interface, BMI - brain-mobile interface

recording were synchronized at all times. The same EEG data was also collected synchronously on the smartphone using the mobile API (application interface) described in the section on brain mobile application interface. During the whole experiment, the second person in the vehicle also kept a check on any undesirable events. In such a situation, the experiment was aborted and started again.

4.4. Driver Distraction Identification

The challenge in this experiment was whether we could localize the identification of distracted activity to only a few scalp locations. *The data collected from 14 electrodes added many parameters and constraints for carrying out effective real-time analysis on the recorded brain signals. Also, the subjects preferred to wear an EEG cap with less number of electrodes.* So, the initial phase of the experiment involved reducing the electrode positions for distraction identification using a 14 electrode headset. We performed three analysis - *time domain, frequency domain and independent component analysis* to discover the electrodes capable of detecting distraction with reasonable accuracy.

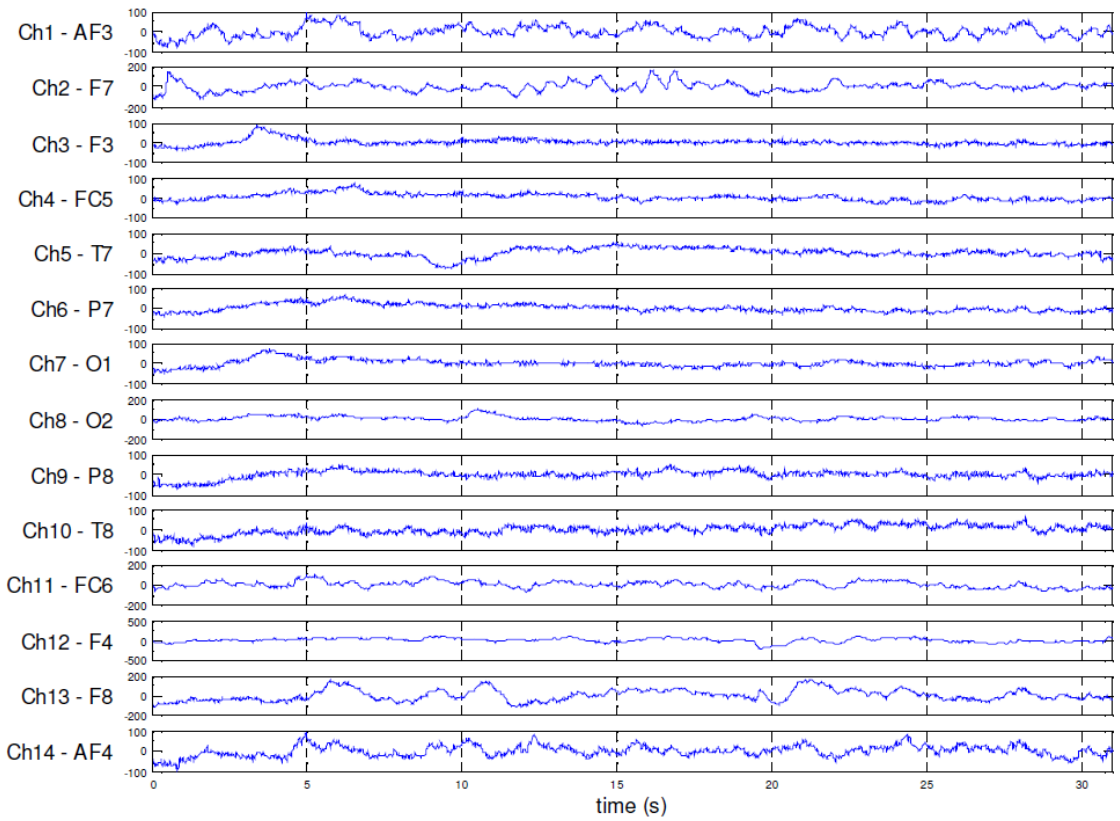

FIGURE 4.4. EEG signals from a base profile (undistracted driving) trial of a subject using the 14 electrodes headset.

4.4.1. Time Domain Analysis

A base trial (undistracted activity) was recorded before each distracted driving task trial using 14 electrodes. This collection generated a large number of data readings. Therefore, for illustration purpose, we plot the brain activity of only one trial of two activity types for a subject. Figures 4.4 and 4.5 show the brain activity during normal driving and sending a text message while driving. O1, O2, FC5 and FC6 electrodes showed a rhythmic pattern of occurrence of high and low frequency in the EEG signals of text activity compared to the baseline signals (statistical tests detailed in Results and Discussion section).

Shweizer et al. fMRI study suggested that brain activation shifted dramatically from the posterior, visual, and spatial areas to the prefrontal cortex during distracted driving [124]. We also observed that channel-4 (FC5) clearly showed sudden bursts of high and low frequency in the brain signals compared to other electrodes for various types of distraction events.

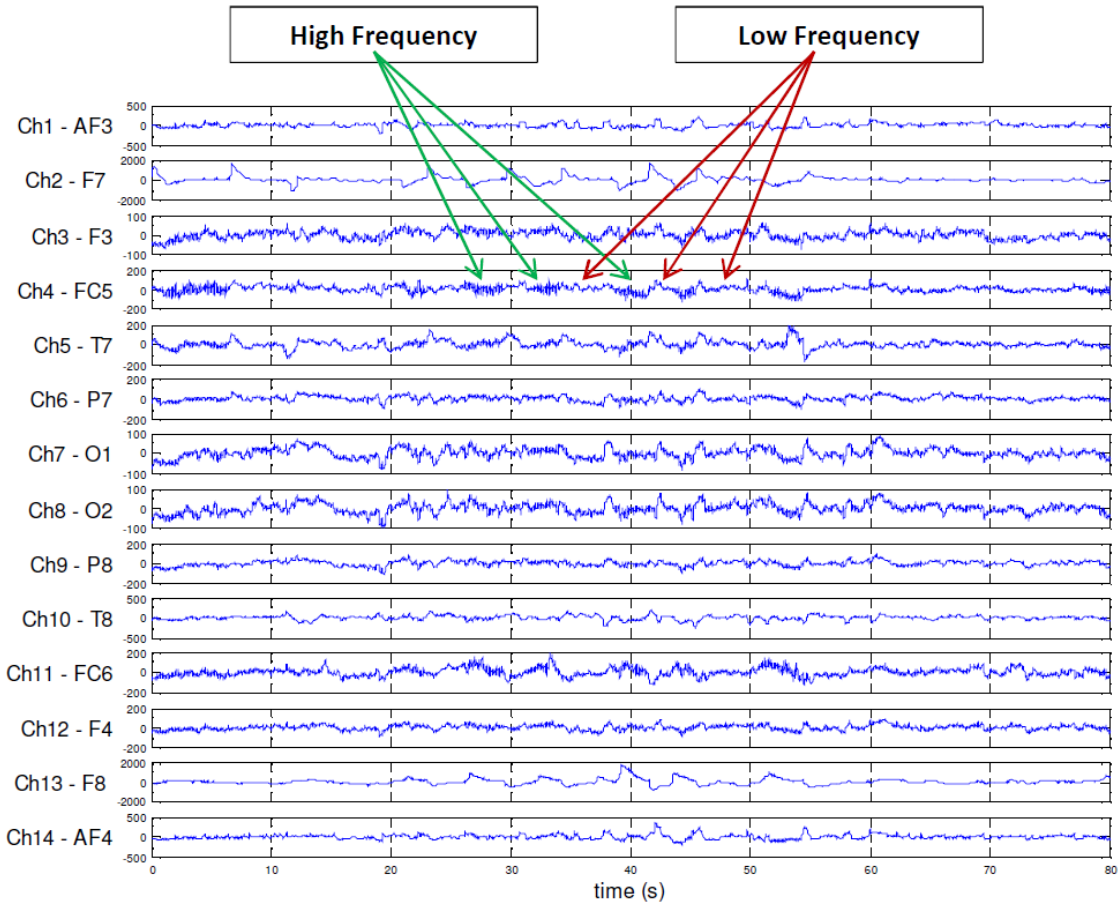

FIGURE 4.5. EEG signals from a texting while driving trial of a subject using the 14 electrodes headset. Signals corresponding to the O1, O2, FC5 and FC6 electrode regions exhibit alternating high-low frequency patterns in the raw EEG compared to the baseline signals (Figure 4.4).

We further investigated to verify if the EEG behavior identified in the FC5 channel correlated to driver's distracted activity. As the recorded video of the driver was synchronized with the EEG data recording, it was easy to find a correlation between our observations and the behavior exhibited by the EEG signals. Figure 4.6 shows the moments of distraction extracted from the video frames of the distracted activity. The time of the extracted event shown under each frame explains the corresponding EEG pattern. The text while driving activity showed the appearance of rhythmic occurrence of EEG bursts corresponding to the action of typing a text while looking at the screen of the phone.

We also analyzed the activities of distraction associated with operating Google Glass (read, text, call and snapshot). Reading activity caused the maximum bursts with more power in high

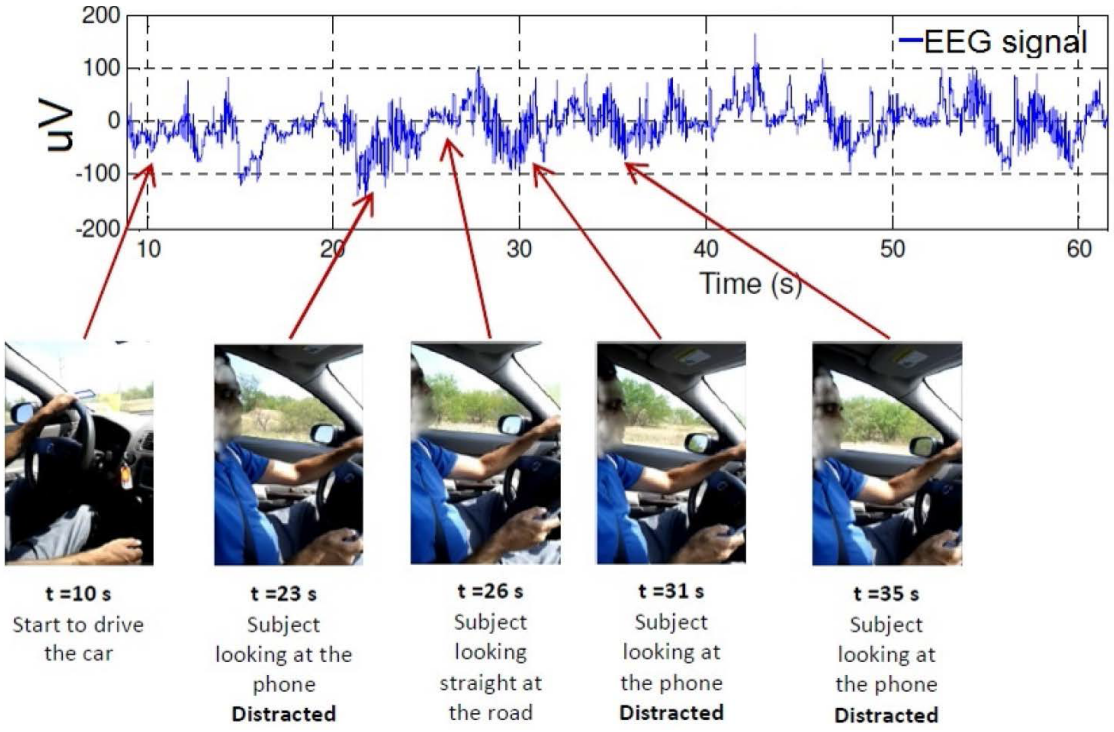

FIGURE 4.6. An example of the time frames extracted from the video recording of a texting while driving activity. These recordings were used to verify the observed changes in the EEG signals corresponding to the distraction events captured in the video frames.

frequencies. It could be because it was difficult to focus on the small glass projection. The text was next, and the call activity showed the least activity. These findings were in conjunction with our previous two scenarios of reading an article in hand and texting while driving. Also, the same FC5 channel as shown in Figure 4.7 proved to be associated with this type of distraction activity as well.

4.4.2. Time-Frequency Analysis

Similar to the previous experiment with the 14 electrodes headset, EEG signal acquisition, and video recording were synchronized while collecting the data. The recording was started a few seconds before the distraction activity to verify the base profile. We observed a similar pattern of high and low alternating frequency bursts in the time-frequency data obtained from the single electrode band for other tasks such as reading while driving (Figures 4.8 and 4.9). Likewise, the time-frequency spectrum of other distraction tasks obtained from the single electrode also

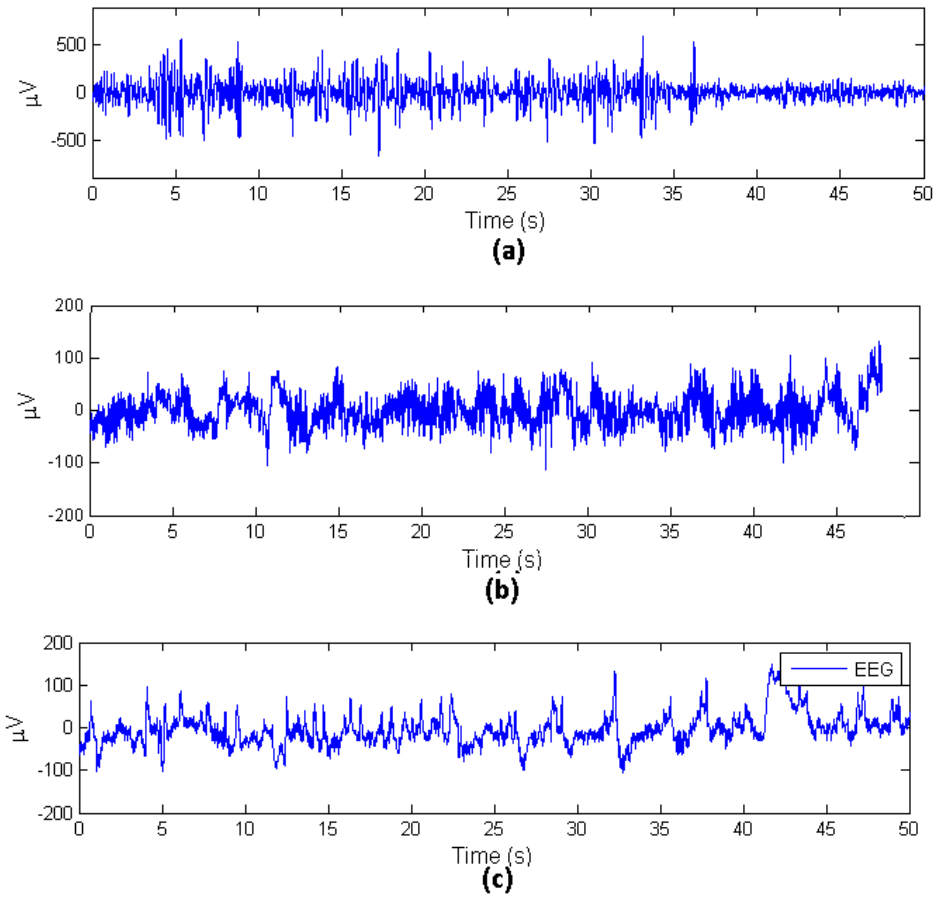

FIGURE 4.7. EEG signals from the distraction trials of a subject using Google Glass while driving. There were differences in the pattern of the raw EEG signals of the read (a), text (b), and call (c) activities. These changes were quantified using the spectrum features during the classification phase (Table 3).

showed similar changes with different signatures in average power during the distraction time span (Figure 4.10). The change was spread across the higher frequency bands except the low frequencies between $1-4$ Hz. EEG signals have inherent characteristics that lower frequency components have higher magnitude compared to higher frequency components. No difference observed in the intensity for frequencies above 10 Hz in baseline is because the magnitude of lower frequencies have masked the subtle changes in the higher frequency components. We observed this behavior in power spectrums of all the subjects. However, again for illustration purposes, the spectrum plots show activities from only a single subject. *Thus, the power spectrum analysis further strengthened our hypothesis of identifying distraction from FC5 location (statistical tests detailed in Results and*

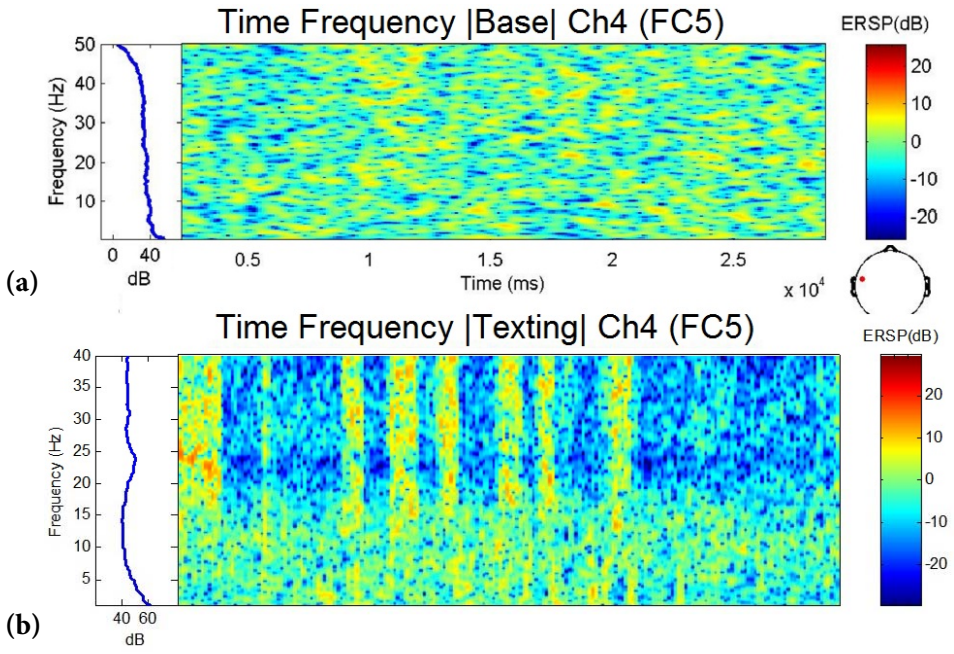

FIGURE 4.8. Time-frequency plot of the FC5 scalp location comparing the baseline (a) and texting activity (b) of a subject while driving. The left part of each figure shows power (dB) in the various EEG frequencies averaged over time, and the right part shows the detail time-frequency power spectrum. There was an overall increase in the total power of the texting activity. Also, the observed rhythmic appearance of high-low frequency in time domain EEG signals corresponded to a pattern mainly in the frequency range of 20 Hz to 40 Hz.

Discussion section).

4.4.3. Independent Component Analysis

The 2D scalp map for each component of the independent component analysis (ICA) of all 14 channels is shown in Figure 4.11. Again, ICA was carried out for all the activities, but we discuss the components of one distraction type (texting) to facilitate our discussion. The components were calculated for the entire duration of a trial [24]. ICA is a popular method to separate linearly mixed sources. However, even when the sources are not truly independent, it converges to a maximally independent space of sources separation, which was desired by our study. Component 13 accounts for a significant EEG variance observed in the distraction activity of texting. Component 4 contributes to the eye movement artifacts in the frontal region.

The ICA algorithm has no apriori knowledge about the electrode positions for the EEG signals and gives us maximally independent sources of cortical synchrony [89, 6]. Figure 4.12

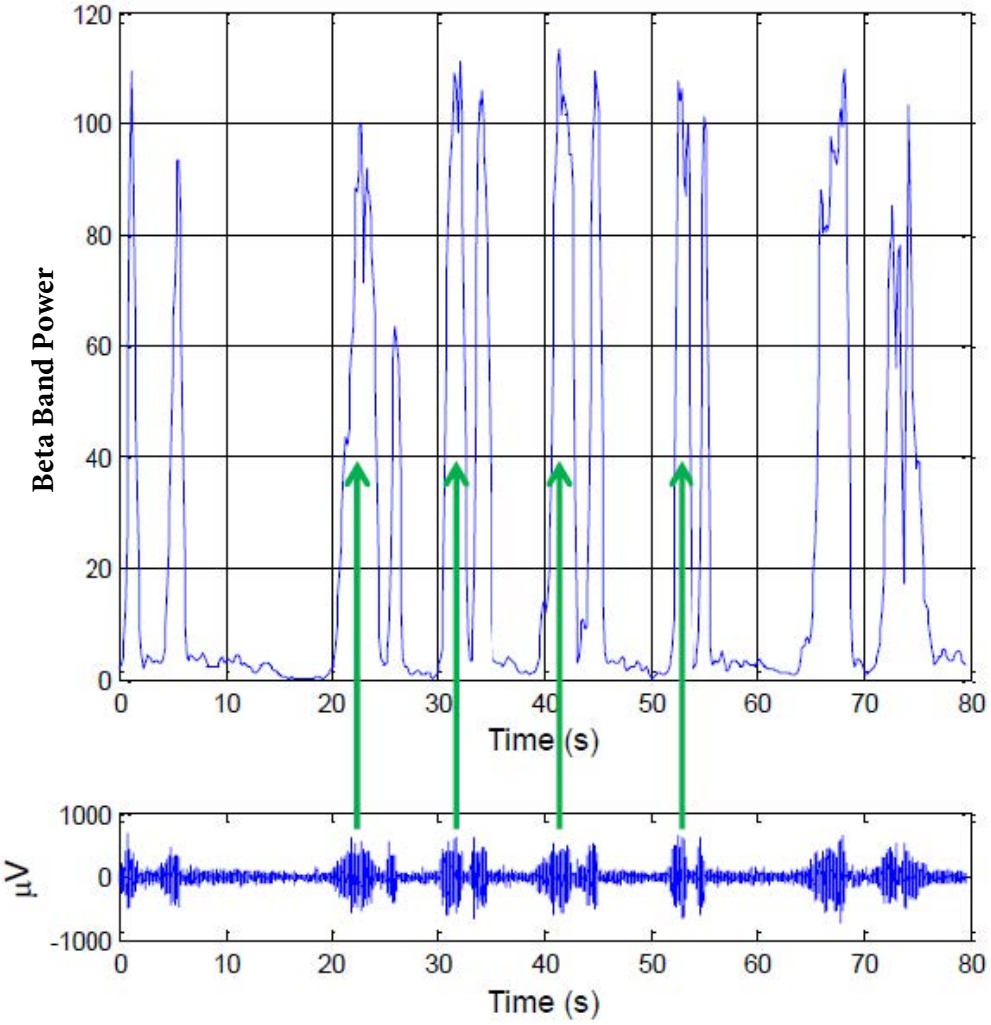

FIGURE 4.9. Correlation between the beta frequency band (12 Hz - 30 Hz) and the raw EEG signals from a reading while driving task of a subject using the single electrode headband. The concentrations of high-low bursts in the raw EEG clearly corresponded to the increase in the power of the beta frequency band at the FC5 location.

shows the topographical distribution of power at the center frequencies of the EEG bands (theta-θ, alpha-α, beta-β, gamma-γ) and each colored trace represents power spectrum of the texting activity in a channel. We can see the scalp distribution of power at 25 Hz (beta-β) and 34 Hz (gamma-γ) of a texting task were concentrated in regions around FC5 and FC6 electrodes. Similarly, the scalp map distribution (Figure 4.11) of the components shows that IC 13 accounts for a significant variance in the activity spectrum. Also, it was evident that IC 13 has the highest contribution to the activity at FC5 electrode at 25 Hz as shown in Figure 4.15. We compared the activity

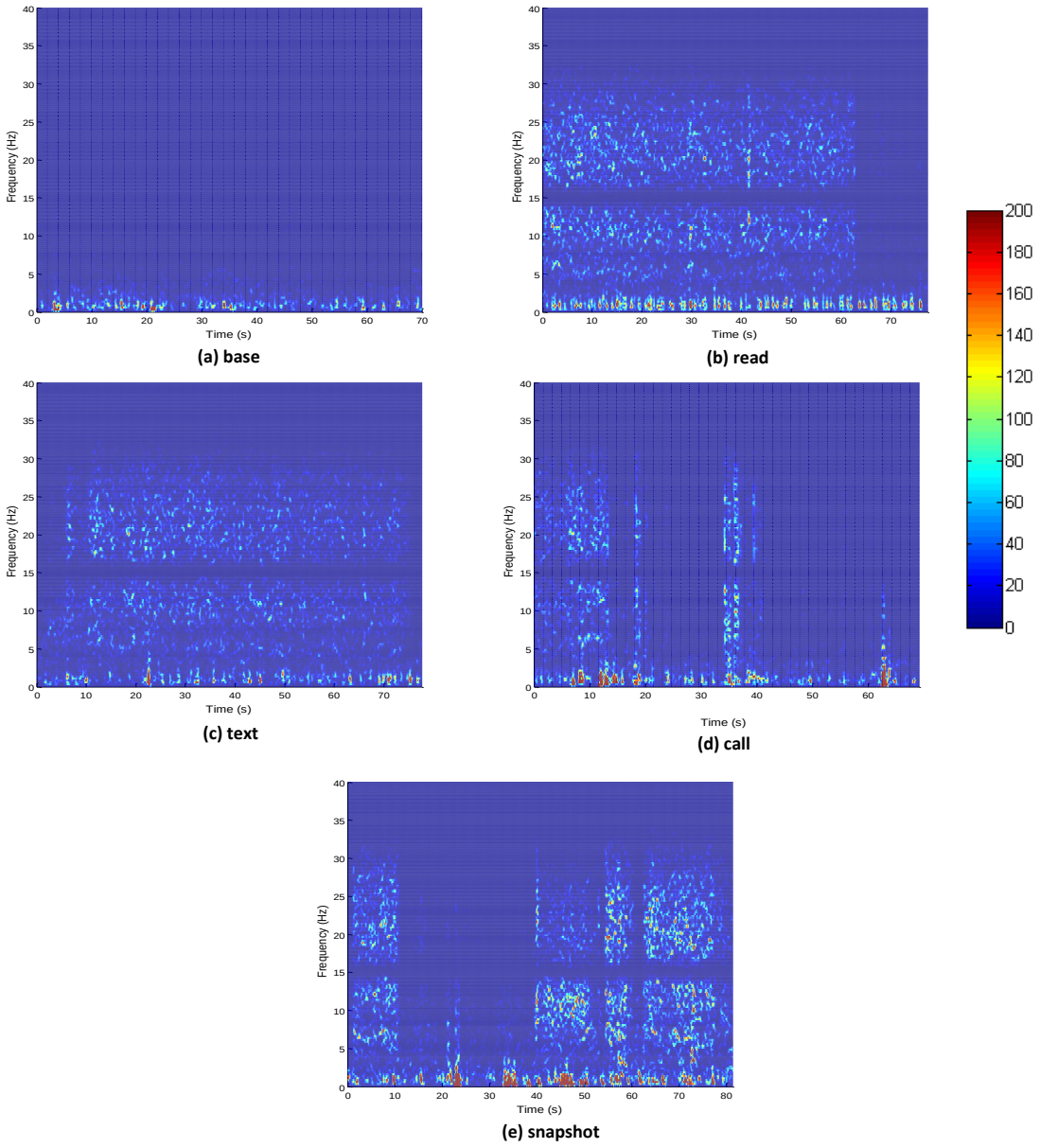

FIGURE 4.10. Time-frequency representation of the distraction activities (read, text, call, snapshot) from one driving session of a subject recorded using the single electrode headband at FC5 location. All the distracted driving maneuvers exhibited an increase in the total EEG power spectrum compared to baseline (undistracted driving).

spectra of all components at this electrode and contribution of IC 13 to other scalp locations to validate this (Appendix B). The activity spectrum plots in Figures 4.13 and 4.14 showed a perfect synchronization between the neural activations recorded at FC5 electrode and the cortex source identified by Component 13. Hence, it was reasonable to conclude that the activity observed in

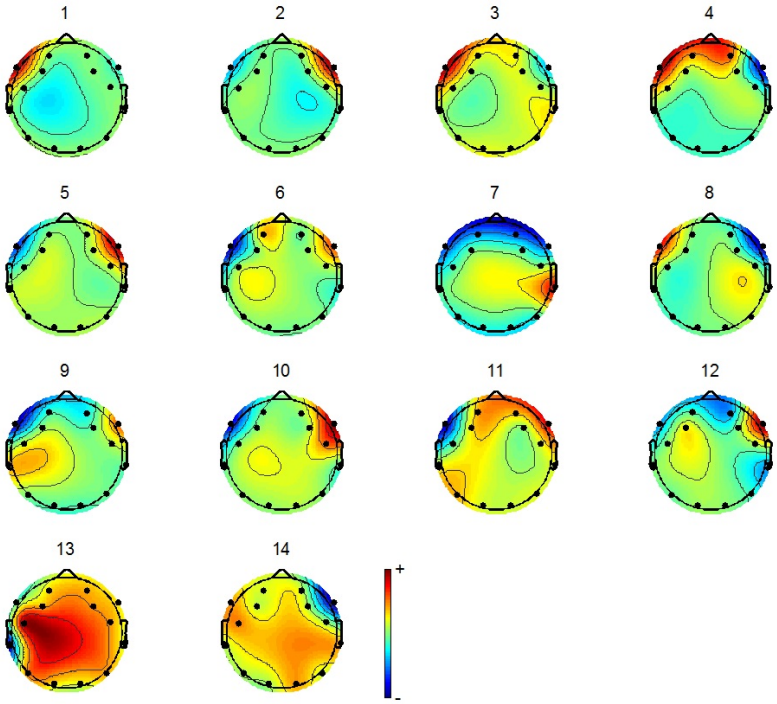

FIGURE 4.11. 2D scalp map projection for all the independent components. These components were obtained from the independent component analysis (ICA) of the 14 channels EEG data for a texting trial of a subject. ICA helped to unmix the multi-channel EEG data into a sum of linearly independent, spatially fixed cortical sources.

FC5 electrode could be used as a cortical source to identify distractions without any significant loss of distraction related information (ignoring the smaller contributions of other cortical sources to the power distributions in higher frequency bands such as beta and gamma). This favors the use of the single electrode (FC5) compared to that of bulky 14-electrode system.

4.5. Driver Distraction Quantification

People develop different kinds of driving habits over time. The level of concentration, skill and reaction times vary among subjects. EEG signals of each person while driving are different (significant or minute), even if they are performing the same activities. Our goal was to study the effects of the various types of distraction on these signals. Therefore, we looked into the problem of distraction classification for each subject separately through the existing machine learning models. Later, we shall discuss how this information can be used to calibrate an application to detect the distraction levels and create an index to measure such distractions.

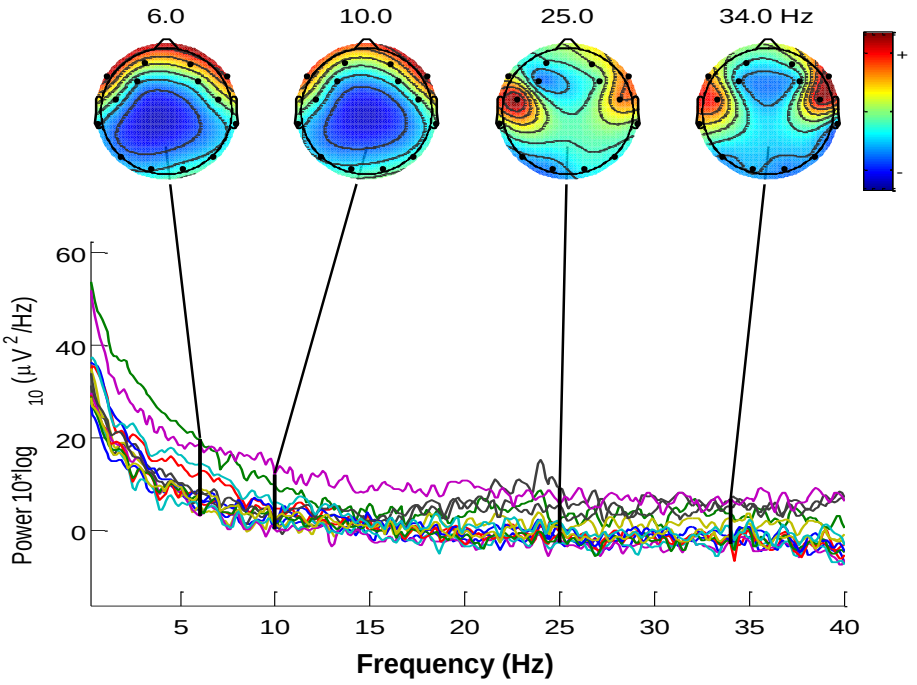

FIGURE 4.12. The electrode spectra and associated topographical distribution of power at the specified center frequencies of the EEG bands (theta-θ, alpha-α, beta-β, gamma-γ).

4.5.1. Quantification

We studied the distraction classification problem as a two-class problem and a five-class problem. In the two-class problem, the distraction class was the positive class a grouping of all the distraction tasks (read, text, call and snapshot). The other category, the base class was the negative class which represented a normal driving pattern of a subject. For the five-class problem, each of the tasks performed while driving were considered a separate category base, text, read, call, and snapshot and we performed multi-class machine learning assessment. Since each task recording was nearly 60 seconds, we split the baseline and distraction tasks to form multiple trials of three to five seconds. This smart sub-sampling of the tasks was done to increase the instances and have a balanced dataset for classification. Also, it was difficult to precisely perform a distraction activity for three to five seconds. Hence, the same distraction activity was carried out for a longer time and repeated in multiple sessions to reliably capture distraction signatures. Secondly, the variations in brain dynamics were better captured in smaller intervals than using the whole reading as a single

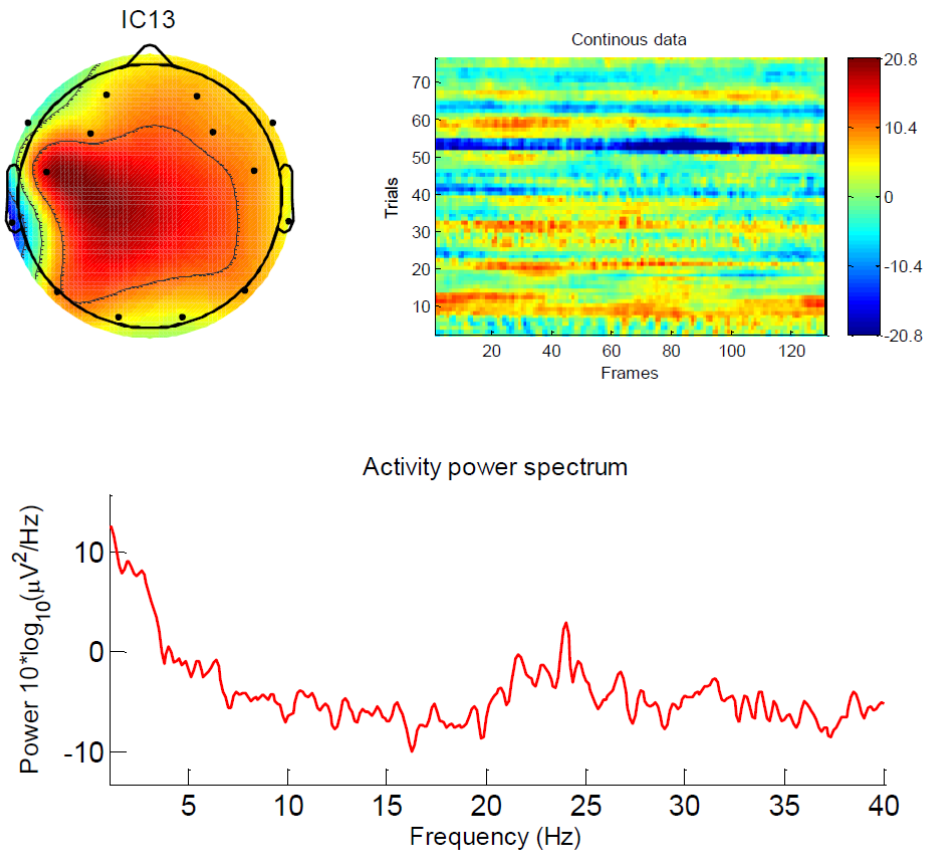

FIGURE 4.13. Activity power spectrum and the scalp map projection of component 13 for a texting trial of a subject (same trial as in Figure 4.11). This dipole-like scalp map distribution of component 13 has a beta band peak near 25 Hz and accounts for a significant EEG variance observed in the distraction activity of the texting trial.

event.

Additionally, we compare the performance of distraction classification between 14 channels and one channel (FC5) for the pilot study subjects. Table 4.1 shows the details of the complete dataset with the number of trials for each task. Subject 2 performed the distraction maneuvers using the Google glass and 14 electrodes headset. Subject 15's data was recorded on the mobile phone to test the real-time application for distraction detection. Therefore, we label the data obtained from either the brain-computer interface (BCI) or the brain-mobile interface (BMI).

4.5.2. Feature Extraction

The feature extraction process was the same for the data obtained from both the 14 electrodes and single electrode headsets. We used two approaches for feature extraction.

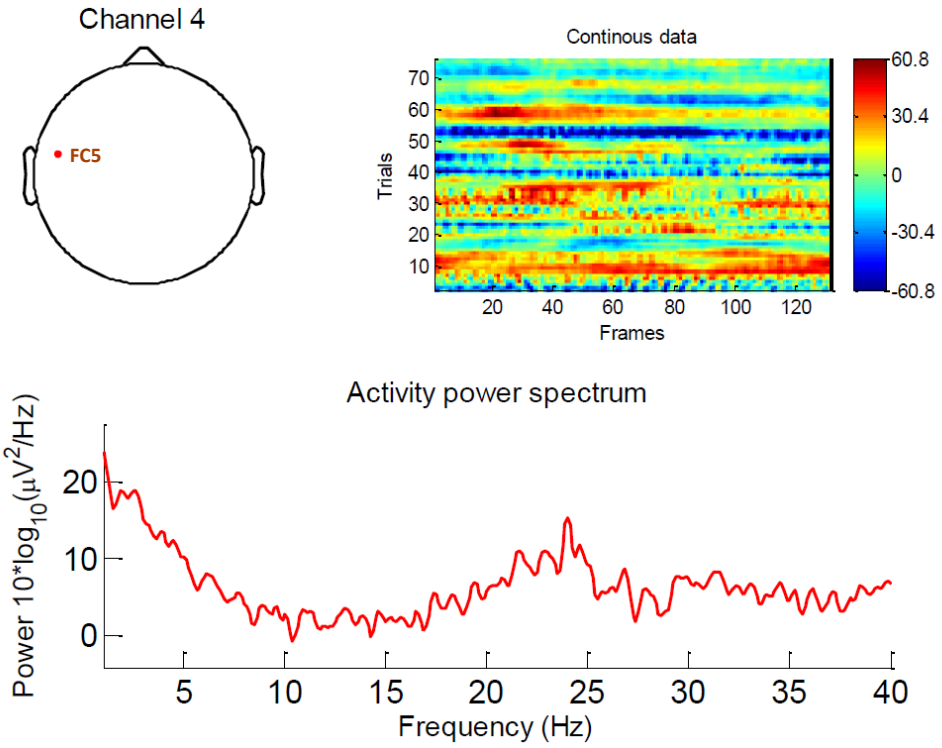

FIGURE 4.14. Activity power spectrum of FC5 channel for the same texting trial of a subject as in Figure 4.13. The power spectrum showed a perfect synchronization between the neural activations recorded at FC5 electrode and the cortex source identified by component 13 with a similar beta band peak near 25 Hz.

- *Fast Fourier Transform (FFT):* First, the raw time domain data was converted to frequency-time spectrums. Then, the window size was increased to the whole EEG reading duration of a trial, so that it will eliminate the time axis of the plots and only produce the frequency spectrum. Thus, the time window for the FFT was the total EEG recording duration of a trial. The attributes consisted of 5 bands, namely Delta (1-4 Hz), Theta (4-8 Hz), Alpha (8-12 Hz), Beta (12-30 Hz) and Gamma (31-40 Hz). The power values in each window were averaged to produce the feature value. Hence, for 14 channels there were $14 \times 5 = 70$ values in the final feature vector for each EEG reading. Similarly, for the single electrode we had five values in the feature vector of a trial (Figure 16).
- *Discrete Wavelet Transform (DWT):* We used the Daubechies family (db8) as the mother wavelet for the transform. Its irregular shape and compact nature help in analyzing signals with discontinuities and sharp changes such as EEG signals. Instead of using all the

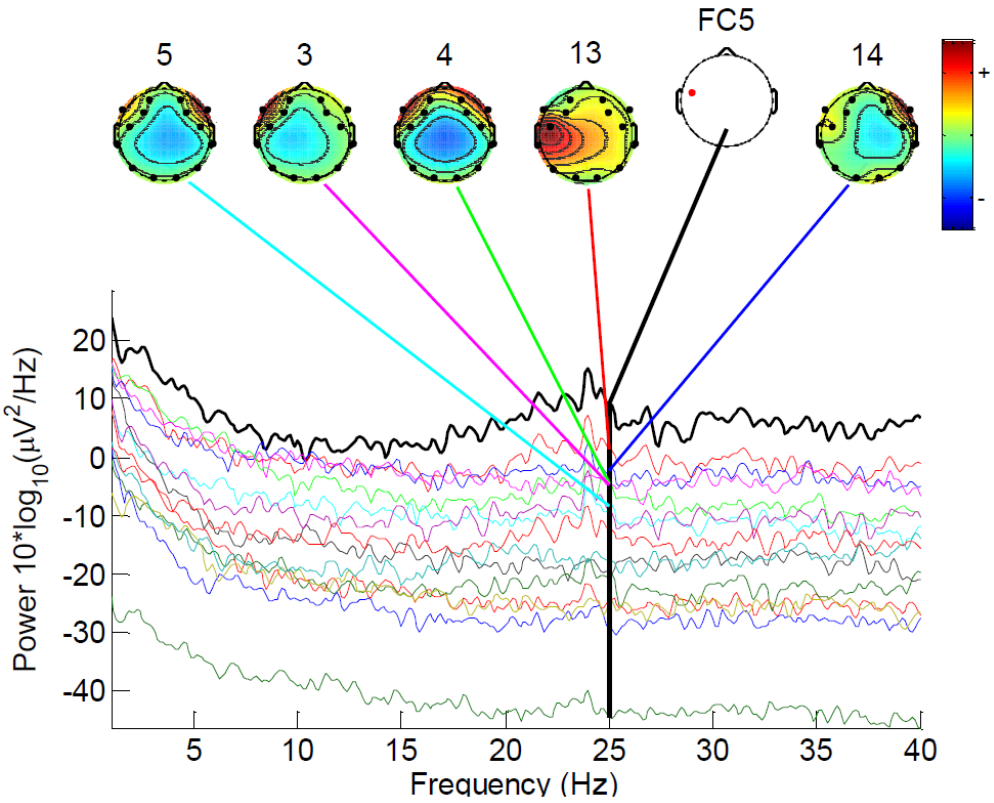

FIGURE 4.15. Contributions of the five largest independent components as a percentage of the total power at FC5 electrode at frequency 25 Hz for the texting trial (same trial as Figure 12) of a subject. Component 13 accounted for the maximum variance compared to other independent components with more than 87% of the power at the FC5 electrode.

coefficients at each decomposition level, we extracted the information from the wavelet coefficients only at the levels corresponding to the five frequency bands mentioned in FFT feature extraction (Figure 4.16). The mean of the absolute values of the coefficients and their average power in these levels were used as features. Thus, the DWT feature vector was composed of 10 features for an electrode.

Once the feature vectors were extracted from an each EEG reading, they were organized into an ARFF (Attribute-Relation File Format) file format for Weka [48] tool to process various machine learning models.

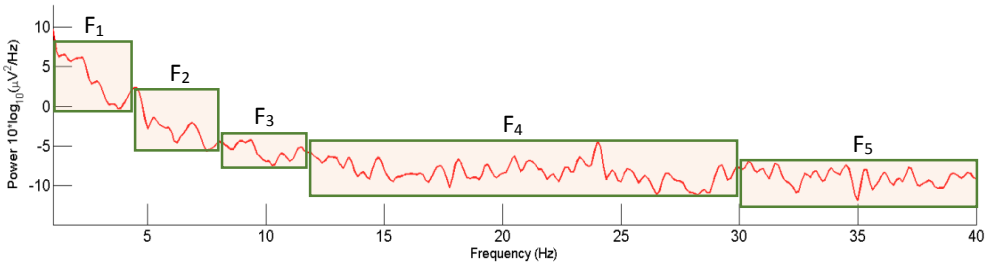

(a) Fast Fourier Transform (FFT) features

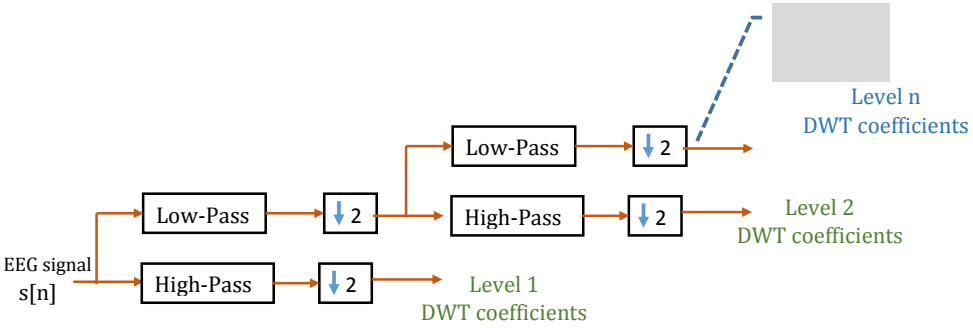

(b) Discerete Wavelet Transfrom (DWT) features

FIGURE 4.16. The process of extracting features from the frequency spectrum of EEG to form feature vectors used in distraction classification. Fast Fourier Transform (FFT) and Discrete Wavelet Transform (DWT) were the two methods used to obtain the relevant features. Using FFT (a), power values in each frequency band of the transformed signal were averaged for the feature vector. Using DWT (b), mean of the absolute values of the coefficients and average power of the coefficients in each level wavelet band were averaged to produce the feature vector.

4.6. Results and Discussion

4.6.1. Classification

The distraction classification was performed using supervised learning models. We include the brain-computer interface (BCI) and brain-mobile interface (BMI) to compare the classification performance using both the interfaces. Bayesian Network and Multilayer Perceptron were the two classifiers that gave good performance in our experiments of classifying distraction and it's types. K-fold cross validation was conducted for each classifier. The training set was randomly divided into K disjoint sets of equal size, K-1 folds used for training and the remaining one for testing with each time a different set held out as the test set. The overall performance was analyzed by using various indexes such as accuracy, precision, recall, F-score and AUC (area under curve). F-score

TABLE 4.2. Classification performance of the two class distraction problem for each subject measured with Bayesian Networks and Multilayer Perceptron using k-fold cross validation. The true class consisted of the distraction events, and the other class was the base driving (undistracted) activity.

Subject	Electrodes	Interface	Classifier	Precision	Recall	Accuracy %	F-Measure	AUC
1	14	BCI	Bayesian Network	0.962	0.958	95.83	0.958	0.986
1	one	BCI	Bayesian Network	0.917	0.917	91.66	0.917	0.847
2	14	BCI	Multilayer Perceptron	0.96	0.957	95.65	0.956	1
3	one	BCI	Bayesian Network	0.955	0.95	95	0.95	0.97
4	one	BCI	Multilayer Perceptron	0.951	0.947	94.73	0.946	1
5	one	BCI	Multilayer Perceptron	1	1	100	1	1
6	one	BCI	Multilayer Perceptron	0.907	0.889	88.88	0.886	0.775
7	one	BCI	Multilayer Perceptron	0.929	0.92	92	0.918	0.923
8	one	BCI	Bayesian Network	1	1	100	1	1
9	one	BCI	Multilayer Perceptron	0.946	0.938	93.75	0.938	0.908
10	one	BCI	Bayesian Network	0.904	0.882	88.23	0.88	0.757
11	one	BCI	Multilayer Perceptron	0.944	0.938	93.75	0.937	0.898
12	one	BCI	Bayesian Network	0.9	0.875	87.5	0.873	0.906
13	one	BCI	Bayesian Network	0.889	0.84	84	0.843	0.774
14	one	BCI	Multilayer Perceptron	0.864	0.813	81.25	0.806	0.695
15	one	BMI	Multilayer Perceptron	0.87	0.868	86.84	0.869	0.923

BCI - brain-computer interface, BMI - brain-mobile interface, AUC - Area under curve

is a measure that combines precision and recall, and is computed as the harmonic mean of them. The equations below describe the relationship between all the measures.

$$Accuracy = \frac{T_p + T_n}{T_p + T_n + F_p + F_n}$$

$$Precision = \frac{Tp}{Tp + Fp}$$

$$Recall = \frac{Tp}{Tp + Fn}$$

$$F - measure = \frac{2 \cdot Precision \cdot Recall}{Precision + Recall}$$

where *T_p = True positive, T_n = True negative, F_p = False positive and F_n = False negative*

Tables 4.2 and 4.3 show the distraction performance of the classifiers for the two-class (base, distract) and five-class (base, read, text, call, camera) problem respectively for each subject.

Similarly, we analyzed the complete dataset consisting of all the subjects together to study

TABLE 4.3. Classification performance of the five class distraction problem for each subject measured with Bayesian Networks and Multilayer Perceptron using k-fold cross validation. Each of the tasks performed while driving were considered a separate class - base (undistracted), text, read, call, and snapshot.

Subject	Electrodes	Interface	Classifier	Precision	Recall	Accuracy %	F-Measure	AUC
1	14	BCI	Bayesian Network	0.961	0.947	94.73	0.946	1
1	one	BCI	Bayesian Network	0.876	0.871	87.09	0.871	0.993
2	14	BCI	Multilayer Perceptron	0.941	0.929	92.85	0.929	0.981
3	one	BCI	Multilayer Perceptron	0.857	0.848	84.8	0.847	0.956
4	one	BCI	Multilayer Perceptron	0.856	0.856	85.6	0.856	0.966
5	one	BCI	Bayesian Network	0.804	0.8	80	0.803	0.953
6	one	BCI	Multilayer Perceptron	0.728	0.728	72.8	0.727	0.921
7	one	BCI	Multilayer Perceptron	0.816	0.813	81.33	0.814	0.95
8	one	BCI	Multilayer Perceptron	0.724	0.7	70	0.698	0.881
9	one	BCI	Multilayer Perceptron	0.835	0.768	76.8	0.777	0.92
10	one	BCI	Bayesian Network	0.823	0.792	79.2	0.794	0.935
11	one	BCI	Multilayer Perceptron	0.726	0.724	72.4	0.719	0.882
12	one	BCI	Multilayer Perceptron	0.71	0.672	67.2	0.676	0.873
13	one	BCI	Multilayer Perceptron	0.607	0.6	60	0.599	0.837
14	one	BCI	Multilayer Perceptron	0.665	0.651	66	0.667	0.868
15	one	BMI	Multilayer Perceptron	0.79	0.789	78.86	0.789	0.918

BCI - brain-computer interface, BMI - brain-mobile interface, AUC - Area under curve

the two-class and the five-class problem (Table 4.4). The performance measures were weak compared to the subjective classification of distraction because of the difference in the EEG response among the subjects while performing similar tasks. Five-class classification measures were worse than the two-class problem. The normalized confusion matrices of the five-class problem were compared among different subjects (Figure 4.17 and Appendix A). It clearly reflects the variation in the classification of the same distraction activities for the subjects. Hence, a real-time distraction detection application requires calibration for each driver, as discussed in the section below.

4.6.2. Distraction Index

We can observe the differences in the active regions of the frequency bands for various distraction activities. However, it's difficult to quantify these distractions from raw EEG signals, time-frequency plots or even machine learning models, especially for real-time alerts. Therefore, we developed an index of distraction using the signal power in various frequency bands of EEG as

TABLE 4.4. Overall classification performance of the two class and the five class distraction problem using the trials from all subjects. Baseline (undistracted) driving, and collectively the distracted driving activities constituted the two class problem. The various tasks performed while driving - base (undistracted), text, read, call, and snapshot separately formed the five class problem.

Classifier	Classes	Precision	Recall	Accuracy (%)	F-measure	AUC
Bayesian Network	Two class	0.776	0.774	77.37	0.774	0.81
	Five class	0.502	0.509	50.93	0.498	0.816
Multilayer Perceptron	Two class	0.81	0.81	80.99	0.809	0.803
	Five class	0.511	0.511	51.06	0.51	0.792

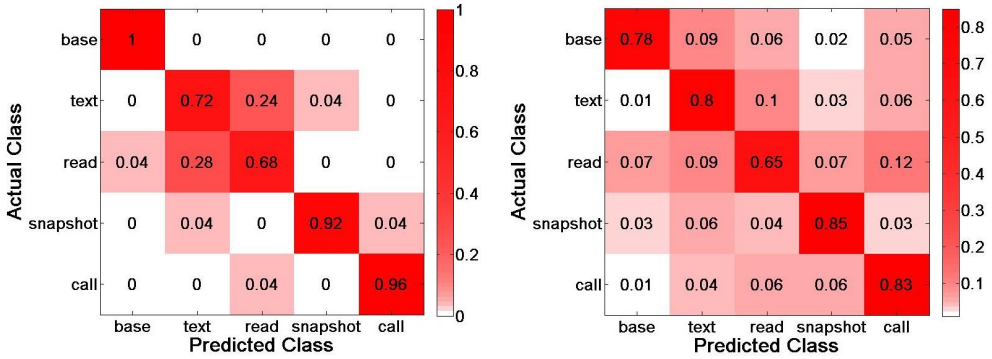

(a) Subject 4 (b) Subject 15

FIGURE 4.17. Normalized confusion matrices of two subjects to depict the performance of the system to distinguish between various types of distraction (read, text, call, and snapshot). The normalized counts on the diagonal are the true positives for each class and the counts not on the diagonal are the errors for each class. The classifier performance for a subject was independent of the other subjects.

follows;

$$DistractionIndex(DI) = \theta/\alpha + \alpha/\beta + \beta/\gamma$$

where θ is the average EEG power between 4-8 Hz, α - between 8-12 Hz, β - between 12-30 Hz, and γ - between 31-40 Hz.

The reasons to include these EEG frequency bands was to capture their varying contribution in distraction. The ratios were important because the common noise in all the bands such as muscle artifacts will be mitigated. EEG signals have inherent characteristics that lower frequency components have higher magnitude compared to higher frequency components. Hence, each term (e.g. θ/α) in the index was specifically a ratio of the adjacent band so that no band masks the contribution of another frequency band. The addition of the three ratios increases the dynamic

TABLE 4.5. Users perception of the level of distraction for the various driving tasks compared to the order obtained by our distraction index metric (Figure 18).

Subject	User's perception of distraction tasks in descending order	User's perception of least distraction task
1	Snapshot, Text, Read, Call	None
2	Read, Text, Snapshot, Call	None
3	Snapshot, Text, Read, Call	Call
4	Text, Snapshot, Read, Call	None
5	Text and Read, Snapshot, Call	Call
6	Text, Read, Snapshot, Call	None
7	Read, Text, Snapshot, Call	Call
8	Read, Text, Snapshot, Call	None
9	Snapshot, Text, Read, Call	Call
10	Text, Snapshot, Read, Call	Call
11	Snapshot, Read, Text, Call	Call
12	Snapshot, Read, Text, Call	Call
13	Snapshot, Text, Read, Call	None
14	Read, Snapshot, Text, Call	None
15	Snapshot, Read, Text, Call	None

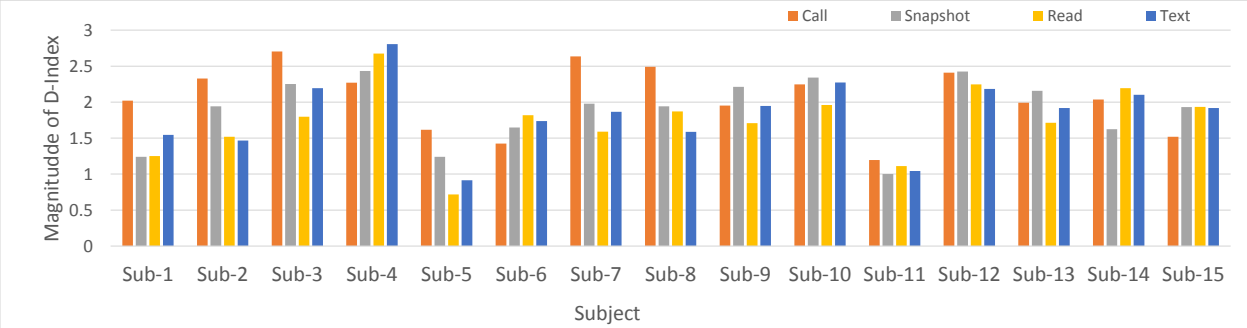

FIGURE 4.18. Distraction Index (D-Index) of various types of distractions (read, text, call, and snapshot) for each subject. Features from the time-frequency spectrum were used to rank these distractions. The rank was obtained from the value of distraction index given by a summation of power ratios obtained in different frequency spectrums of the EEG for an activity ($\theta/\alpha + \alpha/\beta + \beta/\gamma$).

range of the index and helps in evaluating the extent of distraction. We also ranked the tasks in order of the severity of distraction and compared it to the actual order of distractions rated by the subjects (Table 4.5 and Figure 4.18). An average over all the trials was taken to represent the mean Distraction Index for each task of a subject. The differences in the levels of distraction were certainly unique to the activity and subject.

TABLE 4.6. Average EEG power ($\mu V^2/Hz$) in the activity spectrum of 15 subjects during normal/base driving and various distracted driving scenarios.

Subject	Baseline	Distraction
1	4.322328629	8.106168937
2	2.664582	3.4866521
3	3.111189679	7.875135417
4	2.086580297	9.029101508
5	2.336924079	5.267485052
6	1.585887914	4.56627038
7	1.836878292	2.757522033
8	1.083730232	2.590520998
9	4.449198532	5.391230252
10	2.604087967	6.304723748
11	1.803099442	3.435682585
12	2.150271466	8.187098718
13	3.682609891	4.267558023
14	3.857001751	4.310074392
15	3.346612251	6.025901425

4.6.3. Statistical Analysis

Nonparametric test - Wilcoxon matched pairs signed rank test [92] was used to compare between the base and distraction activities as we had two paired groups with sample size 15.

H_0 (null hypothesis): There was no difference in the average EEG power of the subjects in normal (base) driving compared to distracted driving scenario. The critical value for this two-sided test with n=15 (sample size) and α=0.05 (level of significance) is 25 and the decision rule is to reject H_0 if $W \leq 25$ (test statistic) [1]. Table 4.6 shows the average EEG power in the activity spectrum of 15 subjects during normal/base driving and various distracted driving scenarios. We obtained p = 6.1035e-05 and signed rank (W) = 0. Since $W \leq 25$, we can reject the null hypothesis that there was no difference between the average power spectrums of the two groups.

Nonparametric Friedman's test [92] was used to examine whether performing distraction tasks while driving caused any difference in the average EEG power measured at various electrodes (14) for a subject, using a two-way layout as shown in Table 4.7.

H_0 (null hypothesis): There was no difference in the average EEG power measured at the 14 electrodes for the various distraction distractions performed by a subject with α=0.05 (level of significance). We obtained that there was a statistically significant difference in the average EEG

power of various electrodes during distraction while driving, $\chi^2(2) = 34.54$, p = 0.001.

To examine where the differences actually occurred, we ran separate post hoc test - Wilcoxon signed-rank tests on the three combinations based on our previous observations. We used one-tailed test with n=16 (sample size) and α = (0.05/3 = 0.0166) (Bonferroni corrected level of significance). The summary of the test is as follows:

- *FC5 to FC6* - Test revealed an increase in the average EEG power at FC5 compared to FC6 (p = 0.0015, zval: 2.9733)
- *FC5 to O1* - Test revealed an increase in the average EEG power at FC5 compared to O1 (p = 0.0039, zval: 2.6630)
- *FC5 to O2* - Test revealed an increase in the average EEG power at FC5 compared to O2 (p = 0.0070, zval: 2.4562)

4.6.4. Discussion

Previous studies have revealed the effects of distracted driving regarding the attentional resources of one brain region being compromised over another. The observations indicated a substantial shift in brain activations from posterior (back of head area) to anterior (forehead area) regions, particularly in prefrontal area that is critical to driving [144] [29] [68]. In our study through EEG signals, we also observed similar demands on the mental processing of different tasks while driving.

Qualitative analysis of the subjects' EEG signals using time domain, frequency domain and independent component analysis led to FC5 scalp location as the most appropriate identifiable location for determining a distraction event (Figure 4.6, 4.9 and 4.15). The machine learning results were in agreement with our observations from the distraction analysis. The mean classification results using one electrode for both the two-class (91.54 $\pm$ 5.23)% and five-class problems (76.99 $\pm$ 8.63)% were reasonable across all the subjects (Tables 4.2 and 4.3). The F-measures and ROC areas were reasonably high as well (greater than 0.7). We see that the classification accuracy dropped from 95.83% to 91.66% using only the single electrode for the two-class problem in the pilot study for subject 1. However, the processing overhead and overall training time was signifi-

TABLE 4.7. Average EEG power ($\mu V^2/Hz$) measured at various electrodes (14) for a subject performing different distraction tasks while driving.

Activity	Trial	AF3	F7	F3	FC5	T7	P7	O1
Call	1	2.4214752	2.4981809	2.3926721	2.4672167	2.4537251	2.5601602	2.8574317
	2	2.4347413	2.4729524	2.4361315	2.3754349	2.4241006	2.6834061	2.7273037
	3	2.4279513	2.4650245	2.4330645	2.4140978	2.4705017	2.522824	2.676507
	4	2.5287697	2.5791395	2.5299034	2.517122	2.4597104	2.8035517	3.1059065
Read	1	2.6744332	4.0664635	2.6502247	4.4818392	3.8846357	2.7514007	2.7116179
	2	2.9250038	2.9563489	2.8790686	3.3520169	3.1556339	2.7855651	2.7135143
	3	2.635082	3.5064738	2.5460846	5.0874629	3.5924051	2.6608219	2.599179
	4	2.6065793	3.4197419	2.6382325	3.9598022	2.9867475	2.5310094	2.4755123
Snapshot	1	3.2478967	3.5448542	3.9311559	4.0561976	3.4324446	3.5578644	3.6534033
	2	2.8223073	4.2352448	2.8834374	4.7531309	2.7212167	2.6228042	3.3407328
	3	2.6893418	2.9432366	2.7538092	3.6618721	2.5144477	2.415884	2.4211514
	4	2.6671553	3.0878718	2.7727659	3.7537279	2.5740485	2.4142389	2.3955367
Text	1	2.9869101	4.2868524	3.1079965	5.8076501	3.3425231	2.6736579	2.6249413
	2	2.5955961	2.7717819	2.4941945	2.9578588	2.5736146	2.3959432	2.413789
	3	2.4637313	3.039103	2.547775	3.0722754	2.5503836	2.4926076	2.3438687
	4	2.4745536	2.4191566	2.4521291	2.3884513	2.4261627	2.430717	2.3713632
Activity	Trial	O2	P8	T8	FC6	F4	F8	AF4
Call	1	2.8621693	2.5580797	2.3760216	2.4576824	2.4028533	2.4821734	2.4983783
	2	2.7133338	2.5219572	2.4690683	2.4598217	2.4115481	2.4615436	2.4418302
	3	2.6805191	2.5085919	2.4453657	2.3933685	2.4249372	2.4244306	2.4233027
	4	3.0501297	2.8355846	2.6063755	2.5199046	2.4523113	2.494493	2.5130088
Read	1	2.7799065	2.7040005	2.6929064	3.6230438	2.6564288	5.0124846	2.9661417
	2	2.8175149	2.426374	2.5852654	2.8593514	2.6942704	3.2400942	2.9929171
	3	2.614526	2.5878289	2.6682968	3.1144288	2.6079624	3.3645532	2.7210817
	4	2.5711627	2.4911165	2.5489254	3.1336505	2.518424	4.1870437	2.6842604
Snapshot	1	3.839448	3.120744	3.3499269	3.3758676	3.3225701	3.4972935	3.2727661
	2	3.1243985	2.7641568	2.6531153	2.9631443	2.6733487	3.0371733	2.7402406
	3	2.4218996	2.4387803	2.4160261	2.6179724	2.6229534	2.7957058	3.064657
	4	2.4215443	2.4266396	2.4192357	2.5572968	2.5817022	2.8330786	2.8972125
Text	1	2.6944857	2.6453888	2.9356737	4.284204	3.0896397	5.5555711	3.5289237
	2	2.4593246	2.386148	2.4703412	2.6398413	2.4761744	3.1388083	2.6252344
	3	2.4223473	2.4383831	2.5079806	2.8174579	2.4746096	3.0528491	2.7614758
	4	2.411974	2.4470479	2.3850336	2.4338882	2.4373732	2.373611	2.5013528

cantly reduced from 14 electrodes down to one electrode with a small compromise in classification results. On the other hand, distinguishing between different kinds of distractions using a single electrode was relatively difficult as reflected by the accuracies of the five-class problem for all the subjects (Table 4.3). There was a significant drop in classifier performance for subject one, from 94.73% (14 electrodes) to 87.09% (one electrode). The normalised confusion matrix of classi-

fication highlights these variations in detecting different types of distractions (Figure 4.17). For instance, the subtle differences in brain activations during a read and text activity while driving for subject 4 were hard to capture by the feature extraction mechanisms employing a single electrode. Nearly 25% of the time classifier misclassified text as a reading activity and vice-versa.

The individual differences in classification results have interesting implications. It suggests that the brain activations of each subject are different (significant or minute) even when they are carrying out the same distraction activity. The machine learning outcomes of training the classifiers with data from all the subjects help us to understand this (Table 4.4). We clearly observed that there was no improvement in mean classification results of the two-class problem. The performance of the classifiers was worse even with the increase in the training and testing instances for the five-class problem (read, text, call and snapshot). It clearly signifies that a general classifier cannot be obtained for the entire population to provide metrics for distracted driving by just increasing the amount of training data. Hence, the need for an application that provides individual calibration was tested using the data from subject 15, acquired by the brain-mobile interface (BMI). We achieved 86.84% and 78.86% accuracy for the two-class and the five-class problems respectively. Wang et al. [140] showed the potential to predict the start of a map viewing distraction event during navigation while driving. Their study produced interesting results with nearly 81% accuracy of prediction, however, conducted only in a simulated environment with 36 active EEG electrodes and a single distraction task. A combination of our mobile phone based detection application coupled with their prediction algorithm could form a robust framework for predicting driver intentions a-priori to the distraction events.

The feature vectors also play a significant role in the overall classification of the distraction events. We observed that the DWT features alone gave good classification accuracies for the two-class problem. So, the size of feature vector was reduced by deselecting the FFT features. However, we needed more features for the five-class problem to improve the classification. Hence, the combined FFT-DWT feature vector was used for the classification of various distraction tasks, although, using both DWT and FFT feature vectors will add overhead in the application for real-time alerts. In addition to the features selection, probabilistic classifiers such as Bayesian Network

and Multilayer Perceptron were chosen as the machine learning methods because of their extensive use in brain research based on EEG. The overall performance of these classifiers varied among the subjects. Comparing all the measures - recall, precision, accuracy, F-measure and ROC area, we observed that Multilayer Perceptron achieved better classification results for many subjects in our dataset, even though Bayesian Networks offered a computationally efficient approach. Therefore, classifier selection also showed a dependence on the individual differences in the synchronous brain activations of the drivers'.

Our findings suggest that quantifying drivers' distraction events and generating real-time alerts is possible through a single electrode placed at FC5 location. The system offers a comfortable, wearable EEG option without compromising mobility, and usability. A limitation of this study is the assumption that the tasks while driving (read, text, call and snapshot) were the only source of distraction in a given frame of time. Our replication of the on-road driving incorporates many other complexities that are not addressed by simulated driving such as anxiety and attention that are absent in a virtual environment as there are no real consequences of distraction tasks. Another limitation is that we did not test the cognitive abilities of the subjects before the data collection. The subjects confirmed that they had no known neurological disorders before participating in the study. Also, our current study did not involve younger ($<$24 yrs) and older drivers ($>$55 yrs) or gender based comparisons of driving behaviors - that may be interesting areas for further study.

The following section describes the prototype of the driver alert system that can communicate with the EEG headset, retrieve data, and perform the necessary signal processing to generate safe feedbacks to the distracted driver in real-time.

4.7. Brain Mobile Application Interface

We intended to use mobile computing resources to extract useful cognitive information from the brain signals to determine the real-time distraction level of a driver. Therefore, we developed a reliable interface between the brain sensor and the mobile phone. It provides ease of mobility for recording and processing the data in any driving environment. An Android API was used to display the raw EEG data and power in various frequency bands simultaneously while the data was being collected. We performed onboard processing in the phone to analyze, and compare

these power levels in various EEG frequency bands. The expected primary results were displayed using the existing API; otherwise the rest of the data was stored in the phone memory or sent to a cloud [11]. The cloud analysis of this mobile data can be advantageous to not only to the current driver but also the other vehicles/drivers for vehicle to vehicle (V2V) communication network in future.

4.7.1. Design

The brainwaves were captured via a single EEG sensor [96]. The formula for converting raw EEG values to voltage is given by equation below [98];

$$ScalpVoltage = \frac{Rawvalue \times \frac{(inputvoltage)}{4096}}{2000} \tag{12}$$

where the input voltage is 1.8v, 2000x is the gain, and 4096 is the value range. Bluetooth protocol was used to establish the communication to the headband (Figure 4.19). An Android API was used to retrieve the EEG data on the smartphone [97]. The messages exchanged between the integrated chip in the headband, and API were parsed to obtain the necessary data on the phone. All the data was obtained at a frequency of 1 Hz except the raw data that was sampled at 512 Hz. Figure 4.20 shows our Android API, which retrieves the raw EEG data and the power plots of different frequency bands.

Our brain-mobile interface API implements a real-time capturing of EEG signals on the phone without any delay. The system consists of two modes: (1) Recording mode and (2) Replay mode. In the recording mode, the application shows the contact strength of the headband at the top to indicate a user the signal quality - a complete status bar for full strength. User records the EEG data via a toggle button on the screen. All the calculated EEG parameters are made available to the user on the go. In the replay mode, the saved files in the phone memory can be retrieved for display and further analysis off the phone for driver behavior metrics (Figure 4.21).

4.7.2. Mobile EEG Data Processing

Distraction occurs in a high-low frequency pattern as observed in the power spectrums of the data from the subjects. Hence, a peak detection algorithm is useful at the start of a distraction

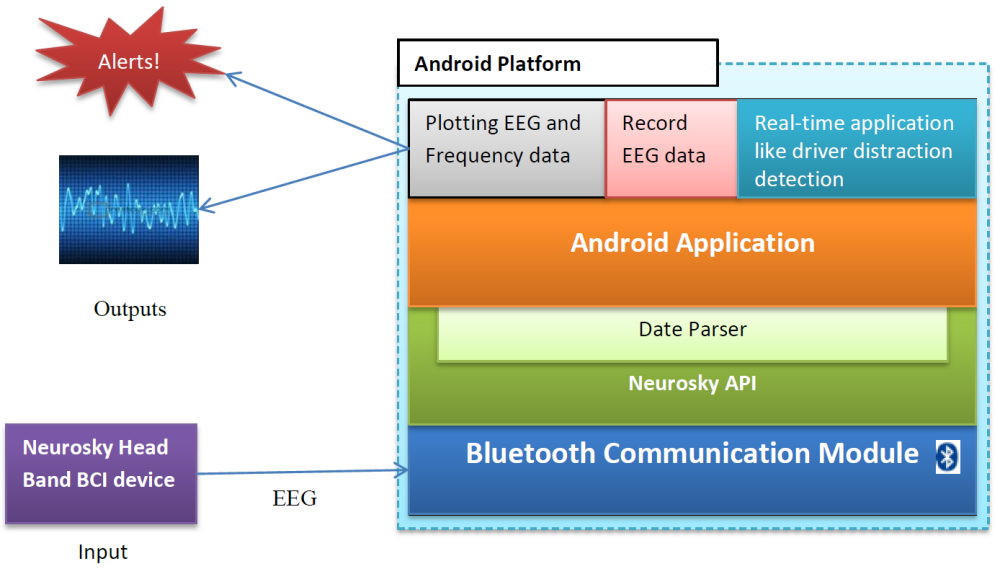

FIGURE 4.19. The architecture of the Brain Mobile system used to obtain and process EEG data on the smartphone using an Android application interface.

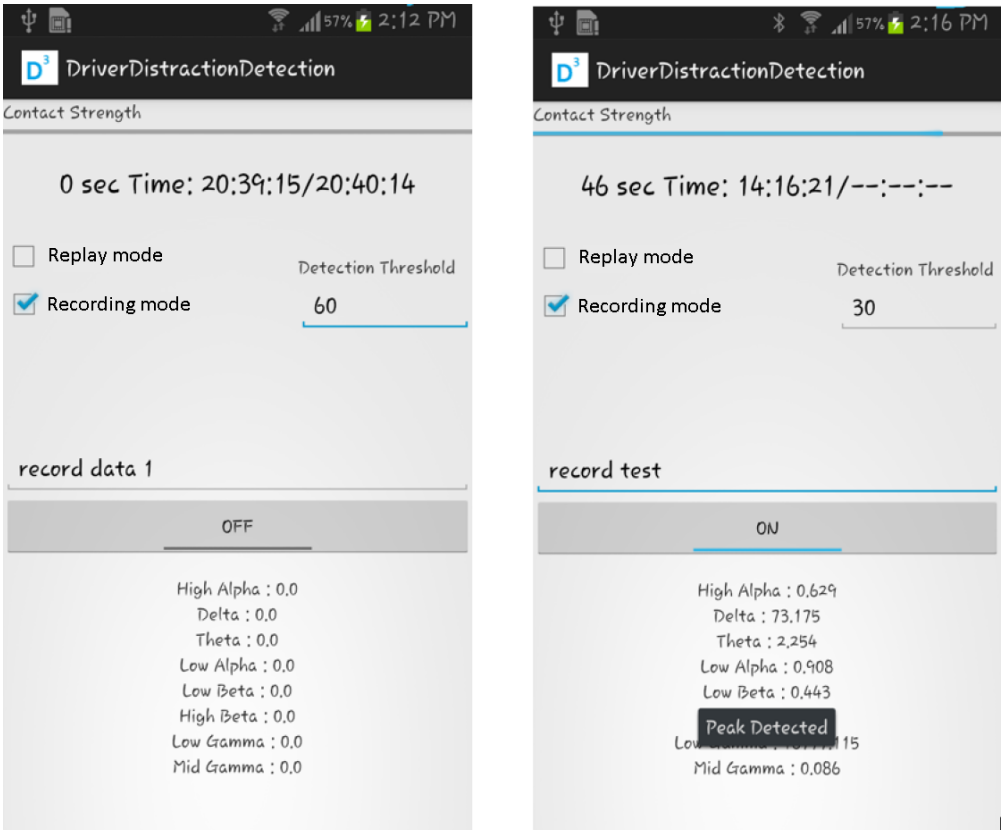

FIGURE 4.20. An example screen from the Android application interface. The application displays connection strength with the headband (top), the raw EEG signals, and power values of each frequency band (bottom). A voice prompt alerts the user when the peak detection algorithm detects a distraction event.

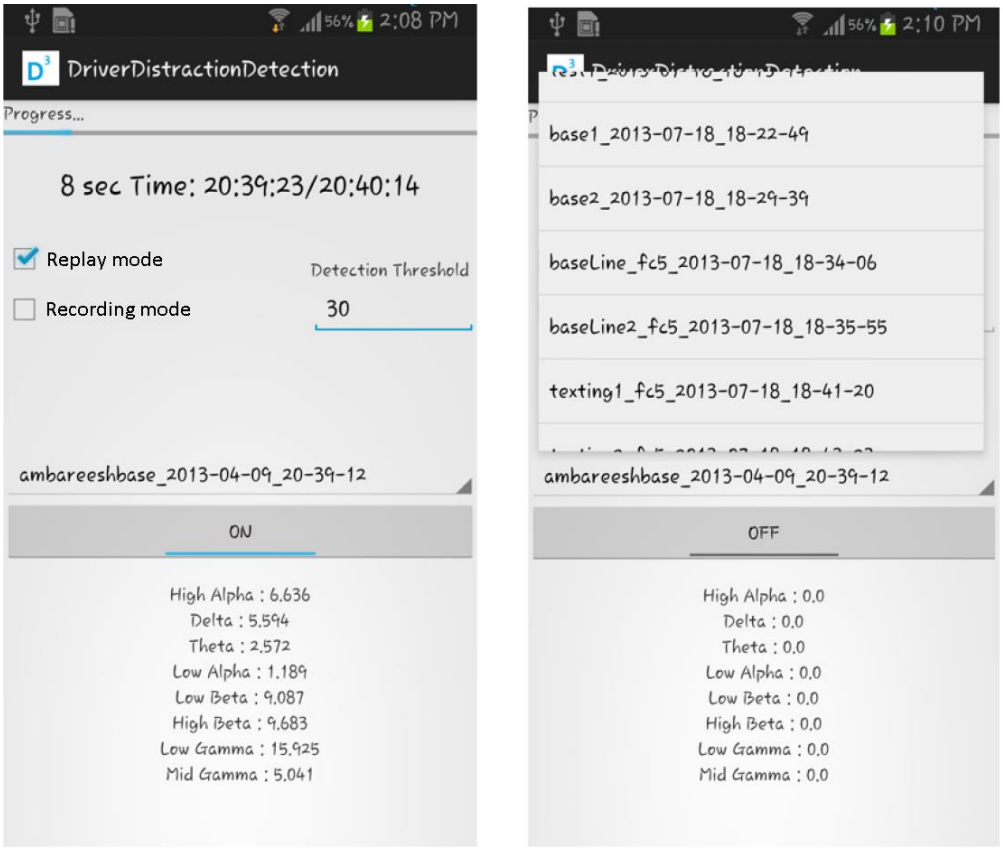

FIGURE 4.21. An example screen from the Android application interface in the replay mode. The replay mode is used to calibrate and test the peak detection algorithm for each subject separately to minimize false alerts.

event. Our detection algorithm was tailored to various customized thresholds for a subject and tested during the replay mode of the API (Figure 4.22). The alerts were in the form voice prompts to the user if the power in frequency bands or a combination of frequency bands passed the customized threshold level. The instantaneous value of the Distraction Index was used to differentiate the extent of distraction.

4.8. Conclusion

In sum, we have shown that using a single dry sensor in the frontal region of the scalp (FC5) is sufficient to detect driver distraction using an individuals' EEG signals in a mobile environment. We tested our mobile application interface for detecting distraction events using peaks in the higher frequency bands of EEG data. Our real-time detection and feedback can help to bring about the cultural change needed in distraction driving intuitively and create safer driving scenarios. The

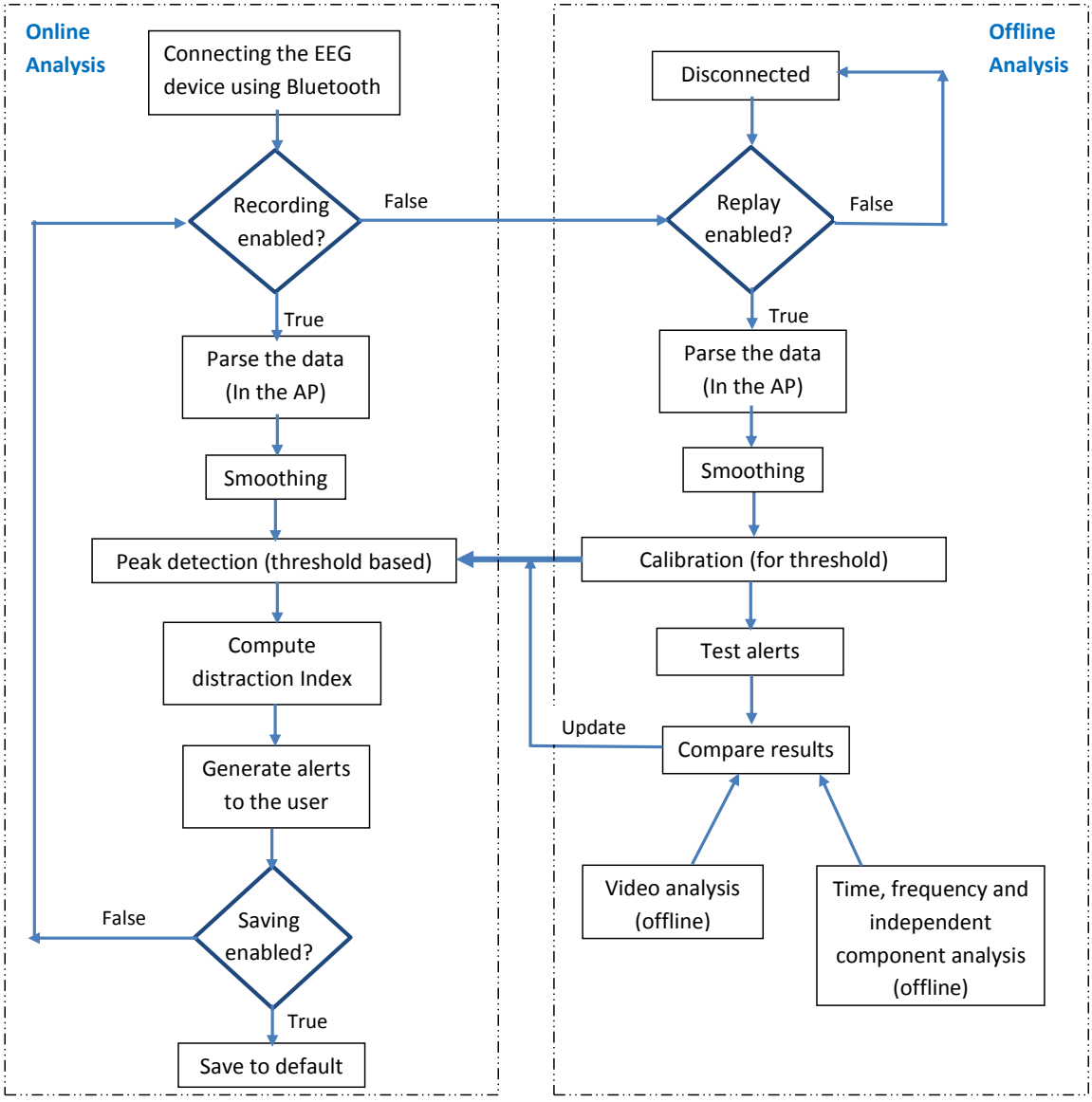

FIGURE 4.22. Flowchart representing functionality of the system.

scientific understanding of distracted driving is necessary to guide policies and support laws to answer critical questions for investment in next car technologies.

We are working on identifying other driver behaviors such as taking turns, lane changes, sudden acceleration, braking time and reaction time using the brain signals. This multi-paradigm integration into a single mobile application will lead to predicting drivers' behavior based on their current state. We would also like to study the activations in occipital lobes corresponding to distraction tasks, that may be helpful in understanding relations between cognitive and visual distractions.

It would be a substantial improvement in ensuring the health and safety of the drivers and other drivers who are becoming a part of the vehicle-to-vehicle communication network. The classification performance can be further improved using statistical feature selection algorithms. Classifier fusion methods [32] can also be used to extract EEG feature vectors that can further improve the detection capability of a distraction activity.

4.9. Acknowledgements

This work is partially supported by the National Science Foundation under grants CNS -0751205, and CNS-1229700.

CHAPTER 5

QUANTIFYING CEREBRAL AUTOREGULATION ASSESSMENT USING ELECTROENCEPHALOGRAMS

5.1. Structured Abstract

Objective: To obtain an index of dynamic cerebral autoregulation by correlating cerebral blood flow (CBF) and blood pressure (BP) variation with electroencephalograms (EEG).

Design: Prospective cohort study.

Setting: University Research Lab.

Participants: A random sample of seven university students was asked to participate in the study, and five agreed (ages 22-28 years). Interventions: Participants received five minutes of training on how to evoke changes in blood pressure by means of valsalva, sit-stand, handgrip maneuvers, and releasing arm cuffs that were inflated above systolic pressure.

Outcome Measure(s): Instantaneous BP changes were measured with a smartphone application using a customized stethoscope. Estimated CBF response from EEG signals was computed using Hilbert transform and canonical hemodynamic response function. Quantitative EEG parameters such as relative power spectrum and composite band indices were used to quantify the relationship between EEG and BP, and estimated CBF and BP.

Results: Pearson correlations showed that the rise and fall of estimated CBF from EEG was significantly associated with changes in instantaneous BP ($r = 0.81$, $p<0.03$). The fall back of estimated CBF to the baseline value took about six to fifteen seconds, depending upon the subjects and method of evoking changes in BP. Among all the indices, variability in composite alpha index

---

Parts of this chapter have been previously published in Garima Bajwa, Ram Dantu, and Arvind Nana "Quantifying Dynamic Cerebral Autoregulation using Electroencephalograms." *Archives of Physical Medicine and Rehabilitation*, 96 no. 10 (2015), e69., reproduced with permission from Elsevier (http://dx.doi.org/10.1016/j.apmr.2015.08.231) [12], and Garima Bajwa and Ram Dantu, "Cerebral Autoregulation Assessment using Electroencephalograms." *Proceedings of the 8th International Conference on Body Area Networks*, 327-330 (2013), reproduced with permission from ACM (http://dx.doi.org/10.4108/icst.bodynets.2013.253703) [8].

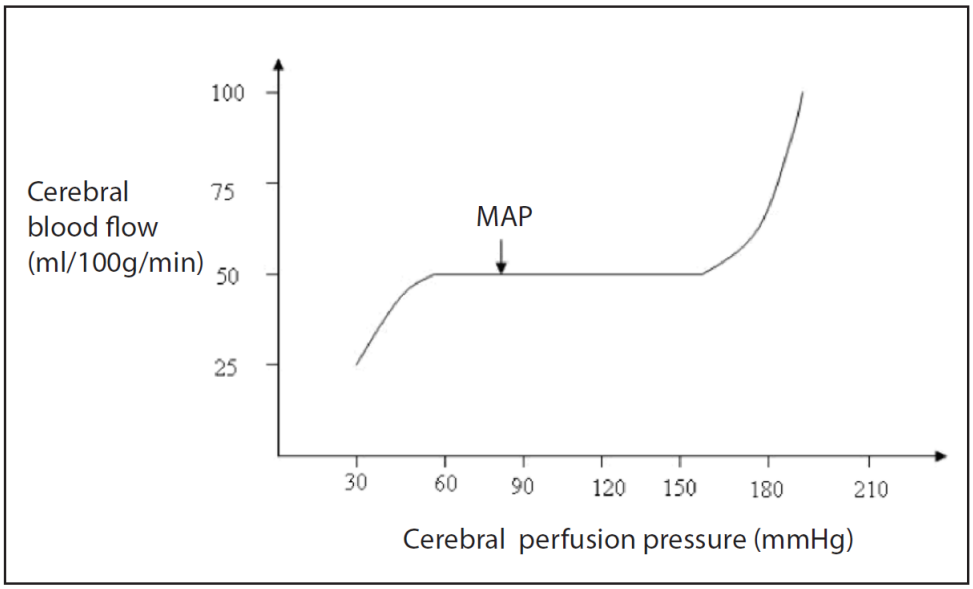

FIGURE 5.1. Relationship between Cerebral Blood Flow and Cerebral Perfusion Pressure [125]

showed the most significant change, about two to eight times increase for changes in evoked BP. These observations were dominant in temporal and occipital brain regions.

Conclusion: Our results suggest that both relative power spectrum and composite band indices obtained from EEG are associated with changes in BP; and behavior of estimated CBF is correlated with BP. Therefore, EEG metrics can be used as a firsthand screening tool to check impaired cerebral autoregulation, especially critical for people at higher risk of developing stroke.

5.2. Introduction

Cerebral blood flow (CBF) is the measure of blood supply to the brain in a given time and typically varies between 50 to 54 ml/100g/min (100g of brain tissue). Brain needs continuous adequate supply of blood for its proper functioning. Cerebral autoregulation (CA) refers to the intrinsic ability of the brain to maintain constant cerebral blood flow despite changes in perfusion pressure due to active modulation of cerebrovascular resistance/conductance as shown in Figure 5.1 [125]. It is as fundamental as any other vital sign (heartbeat, respiratory rate, temperature, blood pressure and oxygen saturation). A major limitation in measuring the regulation of cerebral blood flow is the lack of a gold standard for its assessment.

It becomes increasingly important to monitor CA in a number of common disorders such

TABLE 5.1. Requirements for a methodology to be used for cerebral blood flow monitoring

Properties needed for a CBF monitoring technique	*EEG (Fulfils)*
Quantitative Results	Features needed
High Spatial resolution	No
Continuous Measurements (if clinically required)	Yes
No influence on the normal brain function	Yes
No or minimal risk to the patient	Yes
Cost Effectiveness	Yes
Application in clinical setting	May be

as hyper/hypotension, stroke, trauma, concussion or other serious mental illness requiring intensive care. Monitoring of cerebral blood flow is extremely useful for population at higher risk of developing stroke. It comes handy as an alternate way of planning effective strategies to minimize consequences of cerebral ischemia. The symptoms of a brain injury detected by hospital examination often occur at late stages of brain health deterioration [25]. Some clinical ways of CBF measurement include using xenon-133, thermal diffusion technique, laser doppler flowmetry (LDF), jugular venous oximetry, trancranial doppler sonography and near infrared spectroscopy (NIRS)[148]. MRI techniques for calculating CBF in acute settings is not feasible for practical applications. All the above mentioned techniques lack the possibility of detecting flow abnormalities that can occur between short spans over different times before causing a significant/irreversible brain damage. The focus of the present study was to explore the possibility of a quantitative measure of cerebral autoregulation by non-invasive means using individuals' EEG signals. We outline the essential properties needed for a methodology to be used for measuring cerebral blood flow in Table 5.1 and correspondingly highlight the features that EEG fulfils [149].

5.2.1. Hypothesis

The focus of our present study is to establish a quantitative measure of cerebral autoregulation by non-invasive means using individuals' EEG signals. The primary reason is that brain can tolerate only very short periods of lack of blood supply (3 - 8 min) as the neurons possess very limited capacity of anaerobic metabolism [74]. Hence, adequate blood supply is required at all the

times.

In order to quantify the relationship between the cerebral blood flow and mean arterial pressure (MAP), the changes in EEG with respect to mean arterial pressure have to be understood. Also, the canonical hemodynamic response functions can be used to estimate the CBF from EEG [63]. So, having established the two individually, we can deduce the changes in EEG corresponding to the ones arising in CBF because of changes in MAP. Thus, also reflecting the variation in CBF because of changes in MAP. In the following subsections, we discuss different scenarios relating CBF and MAP to changes observed in EEG signals, proving our hypothesis for real-time monitoring of CA. Our method of estimating the CBF covers only regional response with no influence on normal brain functioning.

5.3. Physiology of Autoregulation

Ample literature confirms the existence of neurovascular coupling between EEG signals and CBF [15][85]. EEG-CBF correlation can be considered as a result of the change in local neuronal activity, which affects local blood flow regulation. This is because regional metabolic demand increases, requiring more oxygen and energy. As a result, the byproducts of metabolism (CO2, NO, lactate etc.) act as vasodilators causing relaxation of smooth blood vessels and increases blood flow. As CBF serves to deliver metabolic substrates and also washes away waste products of metabolism, focal increases in CBF closely follow neural activity and hence, measures local changes in EEG signal. Figure 5.2 shows the mechanism of neurovascular coupling [38].

Using statistical parametric mapping's (SPM) canonical HRF function that serves as a good link function for the neurovascular coupling [129], we demonstrate observed changes in CBF with EEG recorded activities. The estimated CBF was obtained from EEG signals via a linear convolution of canonical HRF with the neural activity (as measured from the instantaneous EEG signal activity). The methodology for estimating CBF from EEG is given in Figure 5.3.

CBF is dependent on a number of factors but can be broadly related to cerebral perfusion pressure (CPP) and cerebrovascular resistance (CVR) [149] by the equation given below:

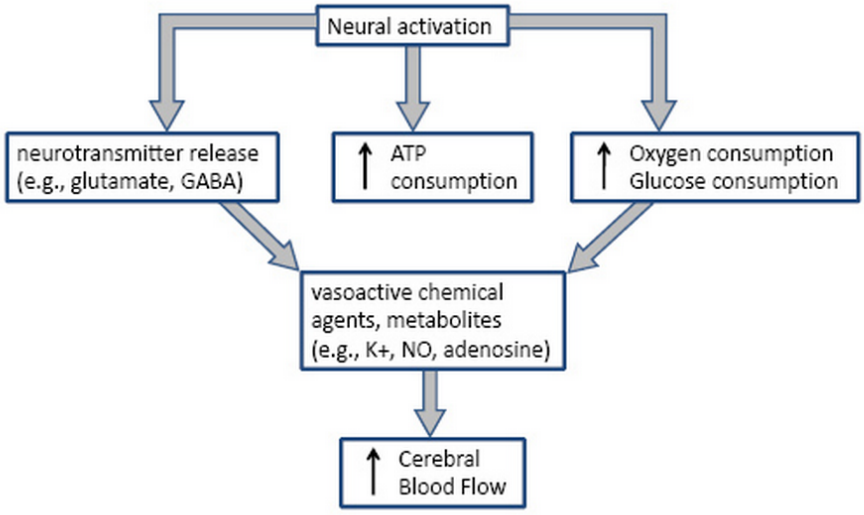

FIGURE 5.2. Flowchart showing vascular response as a result of neuronal activity [38]

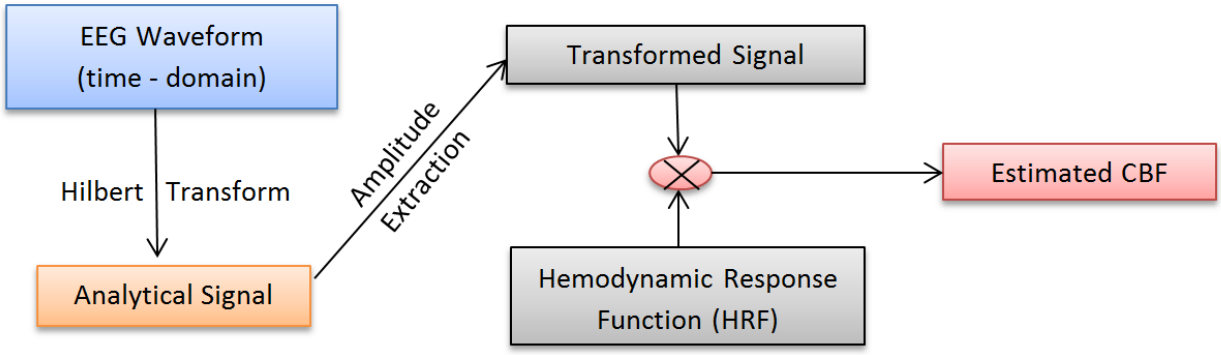

FIGURE 5.3. Flowchart of methodology for estimating CBF from the EEG signal data.

$$CBF = \frac{(CPP)}{(CVR)} \tag{13}$$

(14) $$CPP = MAP - ICP$$

(15) $$MAP = DP + \frac{(SP - DP)}{3}$$

where MAP = Mean Arterial Pressure, ICP = Intracranial pressure, DP = Diastolic Pressure, SP = Systolic Pressure.

5.4. Methodology

Ethics Statement: Ethical approval for the study was obtained from the Institutional Review Board at University of North Texas (Denton, Texas, USA). All participants provided written informed consent to participate in the study and also consented to the publication of the data and media.

Cerebral autoregulation refers to maintaining a constant flow of blood over a range of mean arterial pressures (60-160 mmHg) assuming in normal adults ICP is less than 10mmHg (constant) [40]. In order to quantify cerebral autoregulation, variation in MAP was evoked by using different activities for producing fluctuations in blood pressure as discussed in following sections. A random sample of seven university students was asked to participate in the study, and five agreed (ages 22-28 years). Participants received five minutes of training on how to evoke changes in blood pressure by means of valsalva, sit-stand, handgrip maneuvers, and releasing arm cuffs that were inflated above systolic pressure.

5.4.1. Procedure 1: Arm Cuff Inflation

Large quantitative variation in EEG signals corresponding to changes in MAP can be induced pharmacologically but may expose subjects to risk of stroke. Previously, mean arterial pressures have been elevated with the application of leg compression cuffs with no changes in heart rate, cardiac output, thoracic impedance and central venous pressure [109][145]. Similar approach was adopted in this experiment using a sphygmomanometer and the EEG headband. Figure 5.4 shows the experimental setup to study the changes in EEG signals corresponding to changes in mean arterial pressure. It is harder to measure MAP compared to the blood pressure. Hence, the change in MAP can be reflected by evoking changes in instantaneous blood pressure as they are

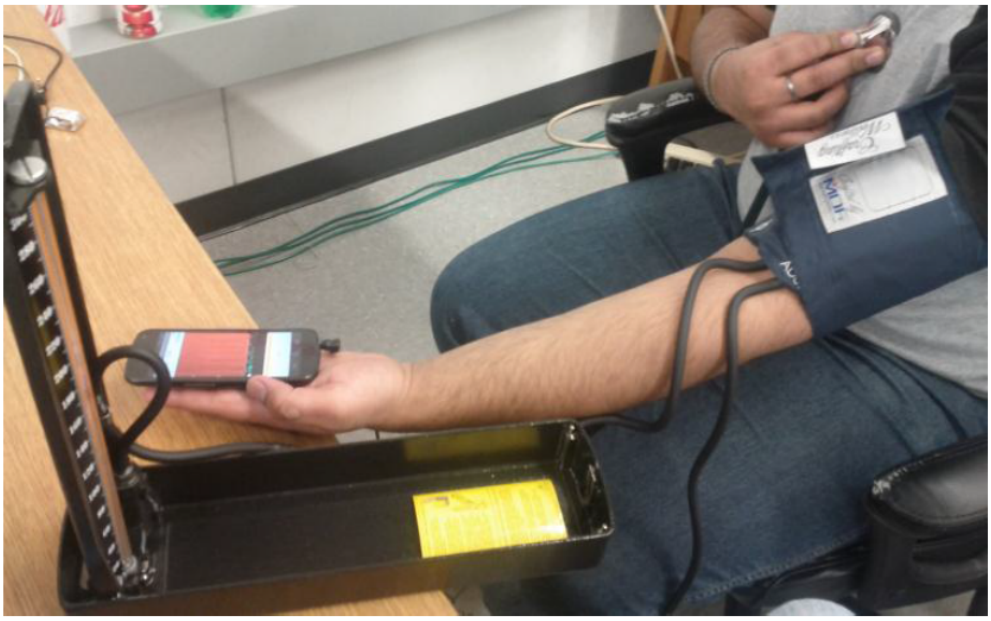

FIGURE 5.4. Experimental setup to acquire simultaneous recording of blood pressure and EEG signals during arm cuff inflation.

related according to equation 15. The EEG signals were recorded on the laptop via a Bluetooth interface using the single dry electrode headband from Neurosky Incorporation [96].

The subjects were seated in a chair with closed eyes and data was recorded from the FP1 location according to the 10-20 international system of electrode placement [58]. The cuff was inflated in the arm to restrict blood flow (140 mmHg) and held constant for the time the EEG signals were recorded from the subject (10 secs). The blood pressure was also recorded simultaneously along with the EEG data by using the blood pressure android application on a smart phone using a combination of inbuilt camera, external stethoscope and microphone [17]. Data was recorded with five trials each for the baseline and arm cuff inflation activity.

5.4.2. Procedure 2: Posture Transitions

In this experiment, variation in blood pressure is studied by posture transition between supine, sit, and stand positions [137]. Figure 5.5 shows the experimental setup to study the changes in EEG signals corresponding to changes in mean arterial pressure. In the supine position (left of Figure 5.5), blood flows relatively easy to the brain and feet because gravity is evenly affecting the body. The heart does not have to fight against gravity to push blood to the brain. However, when

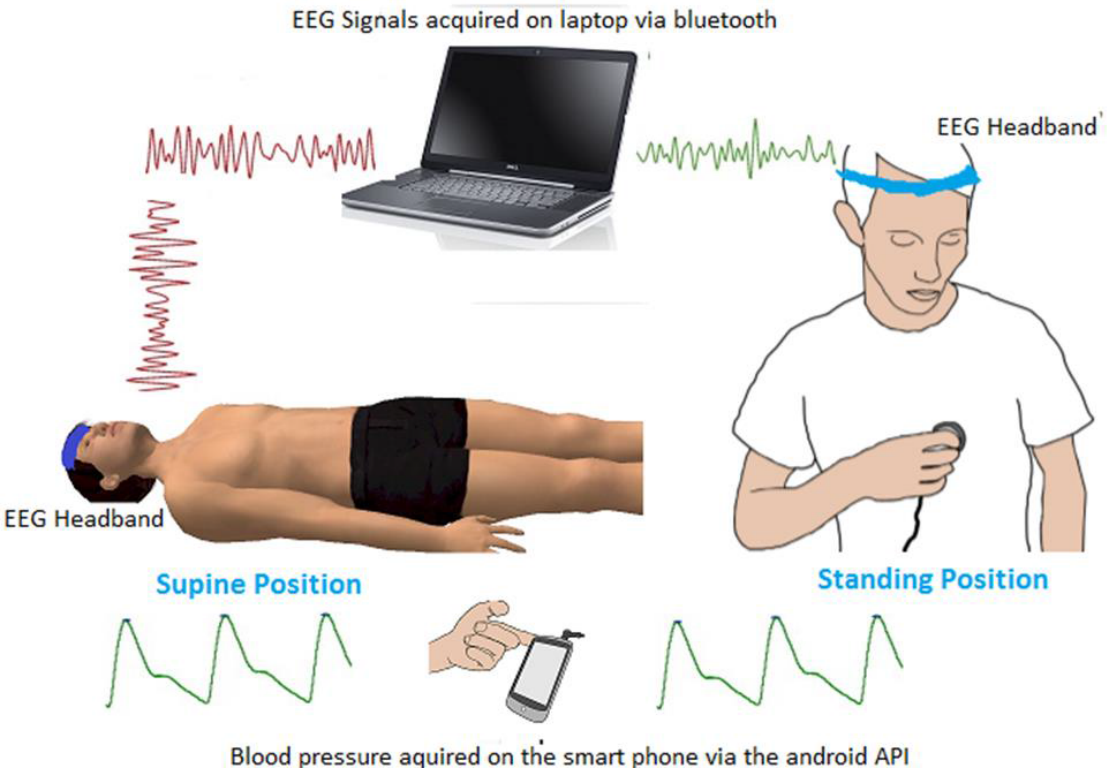

FIGURE 5.5. Set up of the system to acquire simultaneous recording of blood pressure and EEG signals during sit stand maneuvers.

we move from supine position to a standing position, there is an initial drop in the blood pressure followed by rise in the blood pressure [130].

5.4.3. Procedure 3: Sustained Handgrip Test

The subjects were seated comfortably in a chair and asked to exert maximal hand grip strength on the pneumatic dynamometer with their dominant hand. After recording the maximum voluntary contraction (MVC), they were asked to exert 30-40% of MVC for one to two minutes with the dominant hand [33]. The blood pressure and heart rate were measured in the other free hand at rest just before the release of hand grip pressure using the smartphone as mentioned previously. It has been established that heart rate and blood pressure approximately increase linearly with handgrip contractions above 15% MVC [84, 54].

5.4.4. Procedure 4: Valsalva maneuver

In this activity, data was first recorded while the person is breathing normally for nearly 30 seconds. This was the baseline reading of the subject for normal cerebral blood flow estimation. Then, the subject was asked to inhale the air and hold the breath. An audio prompt was used to indicate the start of holding breath and forceful exhaling to bring momentary blood pressure variation. Again, the data is recorded for 30 seconds. A decrease in the pressure during the strain period followed by an overshoot with the release of the strain is considered a normal response to valsalva [76].

5.5. Observations

This section provides a discussion of the observations in terms of the derived EEG parameters and estimated CBF variations.

5.5.1. EEG Parameters

Studying EEG signals in time domain or only its power spectrum, changes in the underlying brain activity were difficult to observe as illustrated by Figures 5.6 and 5.7. EEG parameters were derived from the decomposed frequency bands of the power spectrum of EEG signal. They were used to quantify the changes in EEG activity compared to the baseline activity. The relative frequency power change was defined as Delta (1-4)(δ), Theta (4-8)(θ), Alpha (8-12)(α), Beta (12-30)(β), Gamma (30-50)(γ) Hz frequency power divided by the Total power (1-50 Hz), calculated over every 0.25 seconds time windows. The analysis was carried out for all the activities and subjects, but we discuss a trial of each activity of a subject to facilitate our discussion. The changes were observed in all subjects as shown in the statistical analysis section.

Figure 5.8 shows the power variation in these bands during the stand (blue) and supine position (red). We observe a higher order relative power in stand position compared to supine position. Similar trend is observed in the relative power variation of arm cuff inflation activity compared to baseline activity as shown in Figure 5.9. Using these quantified EEG (Q-EEG) parameters, changes related to blood pressure and EEG were studied quantitatively in next section.

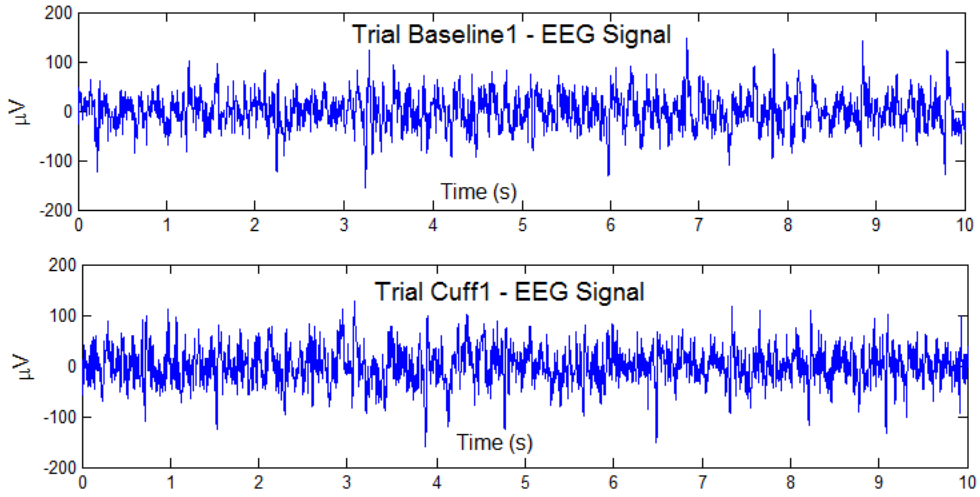

FIGURE 5.6. EEG signal recording during baseline and arm cuff inflation activities

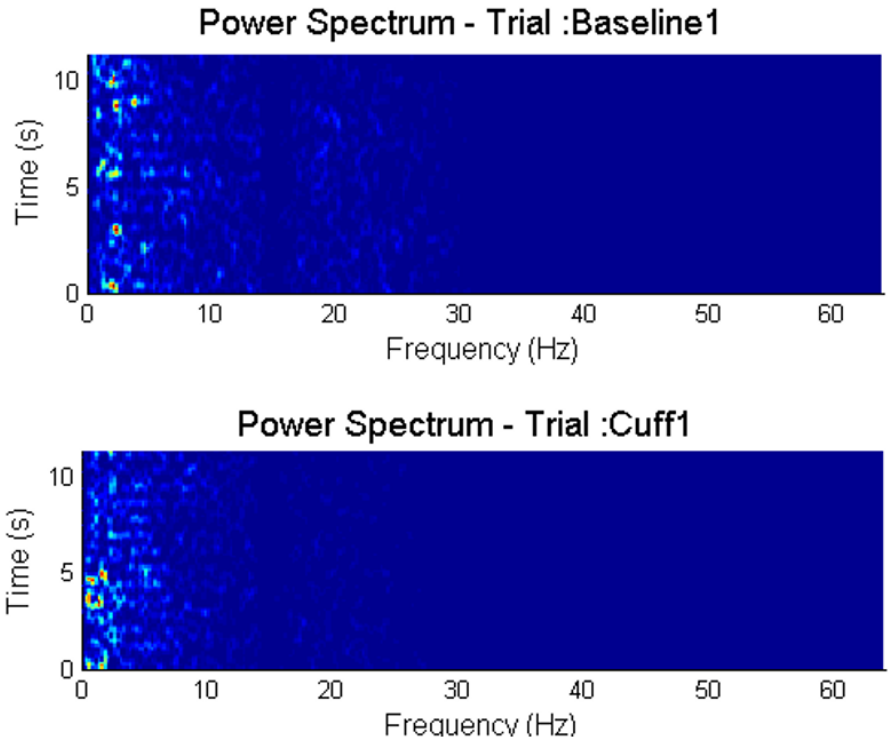

FIGURE 5.7. EEG power spectrum of baseline and arm cuff inflation activities

5.5.2. CBF Variations

CBF is estimated using the flowchart given by Figure 5.3. A comparison in the variation of estimated CBF from the above activities is discussed here. It takes around 2 seconds for the estimated CBF to reach to a peak value and then settle to a baseline value for supine position EEG

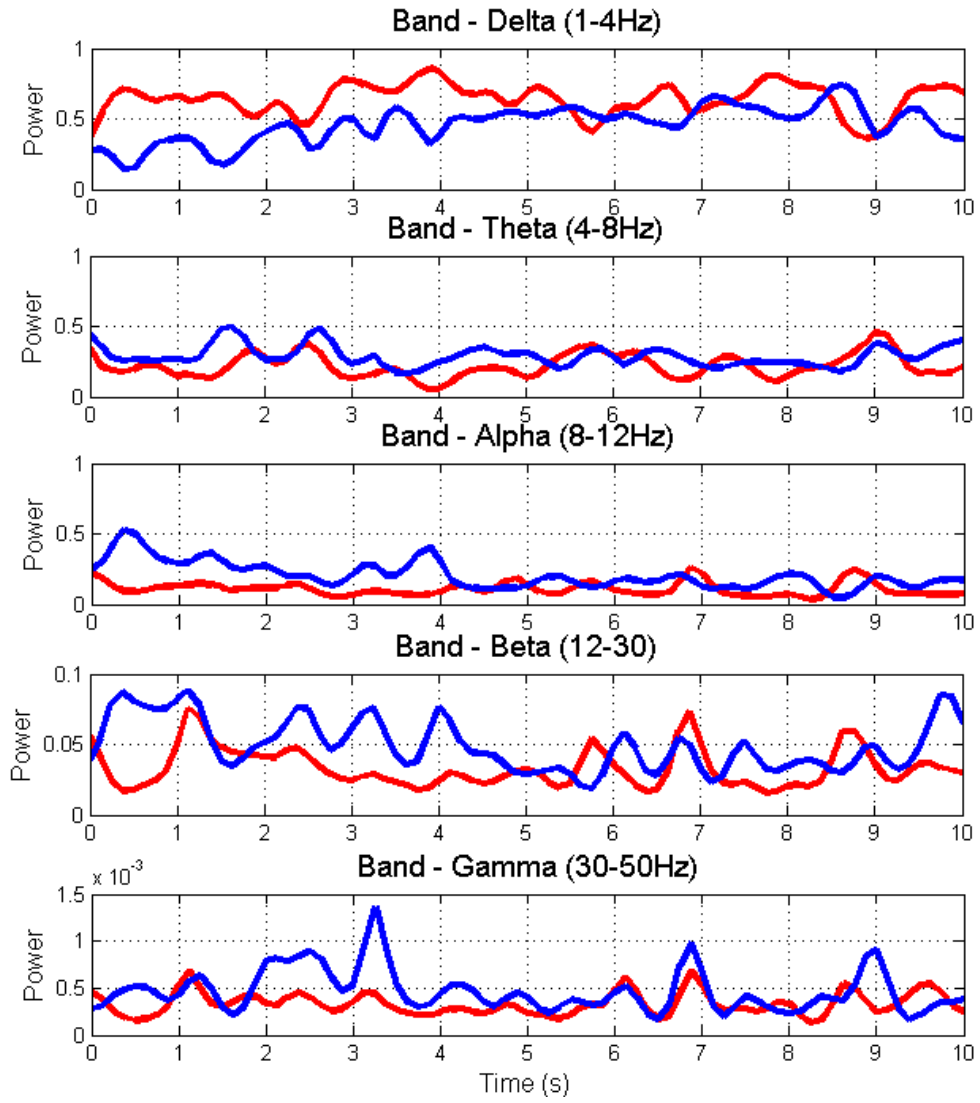

FIGURE 5.8. Relative power variation in frequency bands during the Supine (red) and Stand Position (blue)

recording as shown in Figure 5.10. It is interesting to see that the there is a rise in the peak of estimated CBF for stand position compared to supine whereas no visible changes are observed in EEG waveforms in time domain to detect any such phenomenon. Also, it takes 8 seconds for the estimated CBF to fall back to the baseline value for the stand position.

The above observation also co-incides with rest and arm cuff inflation activity. Inflating arm cuffs causes temporary increase in mean arterial pressure reflected in the increased estimated CBF values as shown in Figure 5.11. The fall back of estimated CBF to baseline in arm cuffs takes

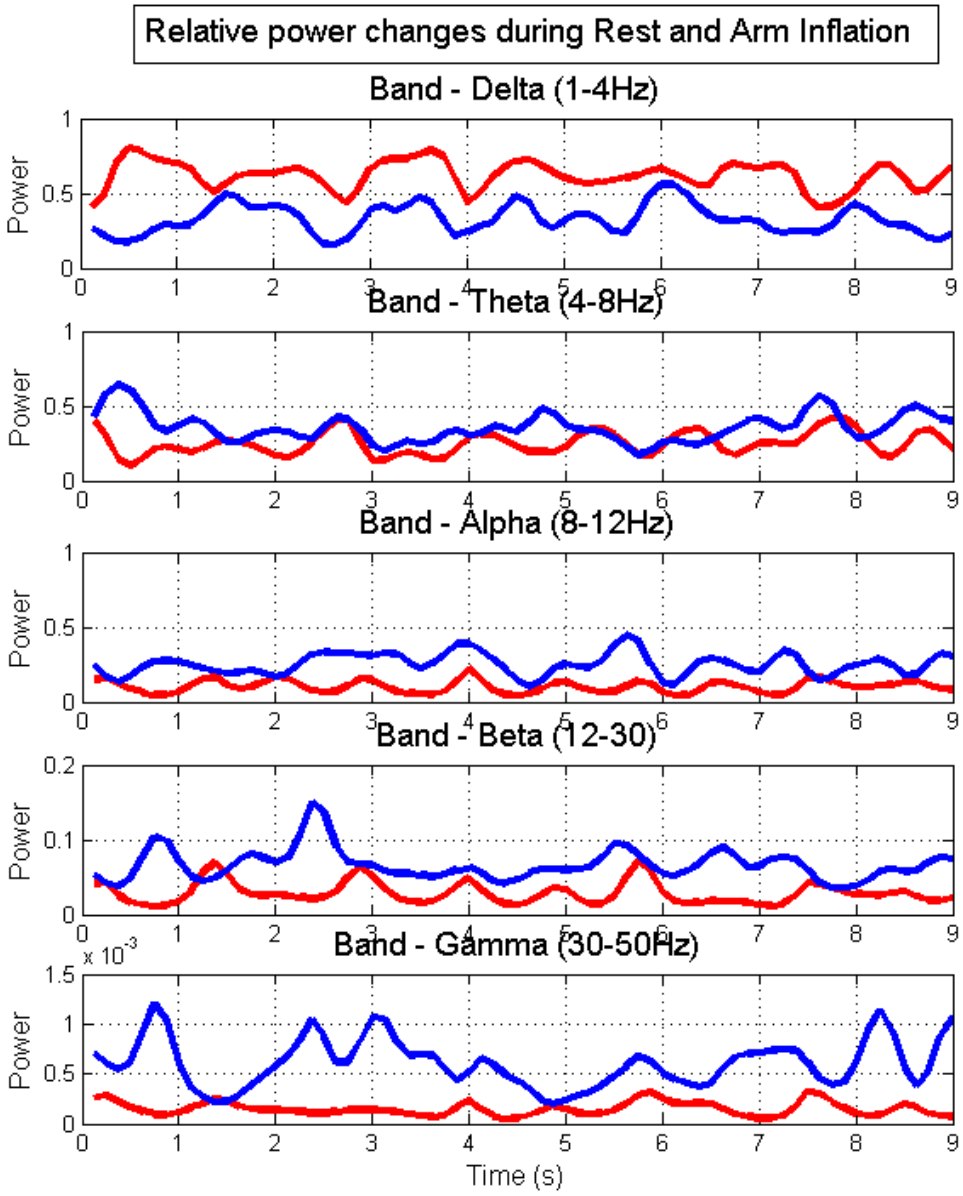

FIGURE 5.9. Relative power variation in frequency bands during Baseline (red) and Arm Cuff Inflation (blue)

about 6 seconds which again strengthens our observation of detecting increase in estimated CBF with increase in blood pressure. The changes in CBF while performing valsalva is shown in Figure 5.12. An example of mean changes in blood pressure for handgrip activity is shown in Table 5.2 that was used to evaluate the correlations between estimated CBF from EEG and blood pressure. The percentage change in systolic and diastolic pressure for each subject varies. For most of the subjects the change nearly 15 mmHg indicating a normal response. The systolic pressure change

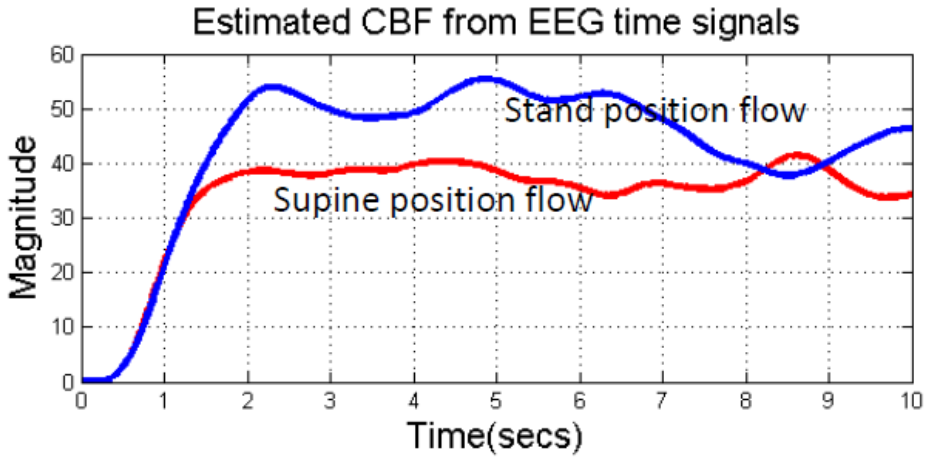

FIGURE 5.10. Comparison of estimated CBF for Supine (red) and Stand Position (blue)

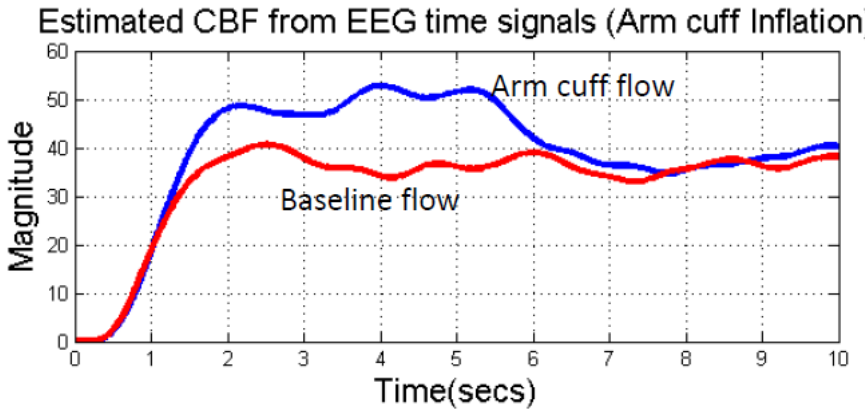

FIGURE 5.11. Comparison of estimated CBF for Baseline (red) and Arm Cuff Inflation (blue)

in each subject closely follows the diastolic. This indicates that autoregulation mechanisms can be reflected by analyzing the behavior of EEG signals in different quantitative ways.

5.6. Statistical Analysis

Frequency domain EEG can be quantified in several ways such as band separation, power, amplitude, mean, standard deviation etc. to observe trends different from the baseline. In this study, composite band index is used to characterise the changes that occur due to variation evoked in blood pressure [37]. Power in the frequency bands is calculated every 1 second and averaged over the entire duration of each EEG recording (10 secs). The standard deviation and mean power

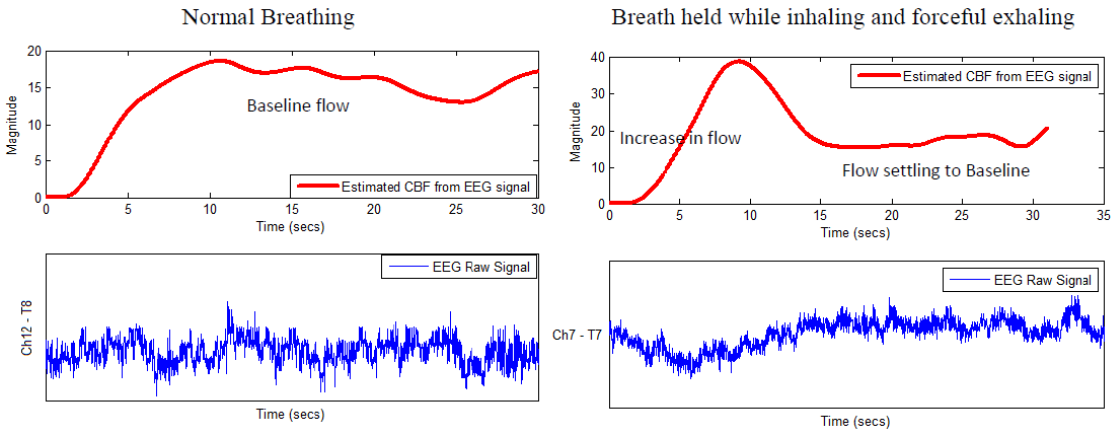

FIGURE 5.12. Comparison of estimated CBF for normal breathing and valsalva maneuver

TABLE 5.2. Systolic and Diastolic variation in blood pressure in a sustained handgrip activity

	Baseline		Sustained Handgrip	
Subject	Systolic	Diastolic	Systolic	Diastolic
1	103	64	114	75
2	97	56	110	72
3	102	63	108	69
4	111	74	119	83
5	108	69	120	88

are multiplied to obtain the composite band index as given in equations below:

$$Mu = \frac{1}{N} \cdot \sum_{i=1}^{N} P_i \tag{16}$$

$$Sig = \sqrt{\frac{1}{N} \sum_{i=1}^{N} (P_i - Mu)^2}. \tag{17}$$

$$CompositeBandIndex = Mu_k \cdot Sig_k \tag{18}$$

where 'k' represents the five frequency bands namely δ, θ, α, β and γ

The composite band indices of supine position and stand position are summarized in Tables

TABLE 5.3. Composite Band Index for Supine Position

Subject	δ	θ	α	β	γ
1	47.71	12.08	2.34	0.39	8.79 E-05
2	52.91	12.14	3.61	0.22	2.96 E-05
3	42.42	11.55	1.58	0.10	1.99 E-05
4	46.84	3.36	0.36	0.032	0.31 E-05
5	56.84	9.40	0.61	0.03	1.91 E-05

TABLE 5.4. Composite Band Index for Stand Position

Subject	δ	θ	α	β	γ
1	90.75	29.17	4.45	0.15	2.05 E-05
2	75.85	7.561	3.45	0.07	1.35 E-05
3	69.42	38.88	23.00	0.66	1.78 E-05
4	79.39	66.90	26.18	1.14	2.90 E-05
5	62.45	9.30	4.00	0.32	7.97 E-05

5.3 and 5.4 respectively.

Among all the indices, variability in composite alpha index shows the most significant change for rise in mean arterial pressure in the experiments. Magnitude of variability observed in composite beta and gamma indices was low compared to alpha index. Delta and theta indices do not follow any definite pattern in their variability. The variability in the alpha index can be easily visualized by the box plot shown in Figure 5.13. We observed that the baseline, and supine position activity exhibit similar behavior indicating low variability and stand position behaves analogous to arm cuff inflation indicating high variability.

Pearson correlations showed that the rise and fall of estimated CBF from EEG was significantly associated with changes in instantaneous BP ($r = 0.81$, $p<0.03$). Among all the indices, variability in composite alpha index showed the most significant change, about two to eight times increase for changes in evoked BP. These observations were dominant in temporal and occipital brain regions.

5.7. Conclusion

This paper presented the scope of EEG as a monitoring tool for the mechanism of Cerebral Autoregulation. Our results suggest that both relative power spectrum and composite band indices obtained from EEG are associated with changes in BP; and behavior of estimated CBF is correlated

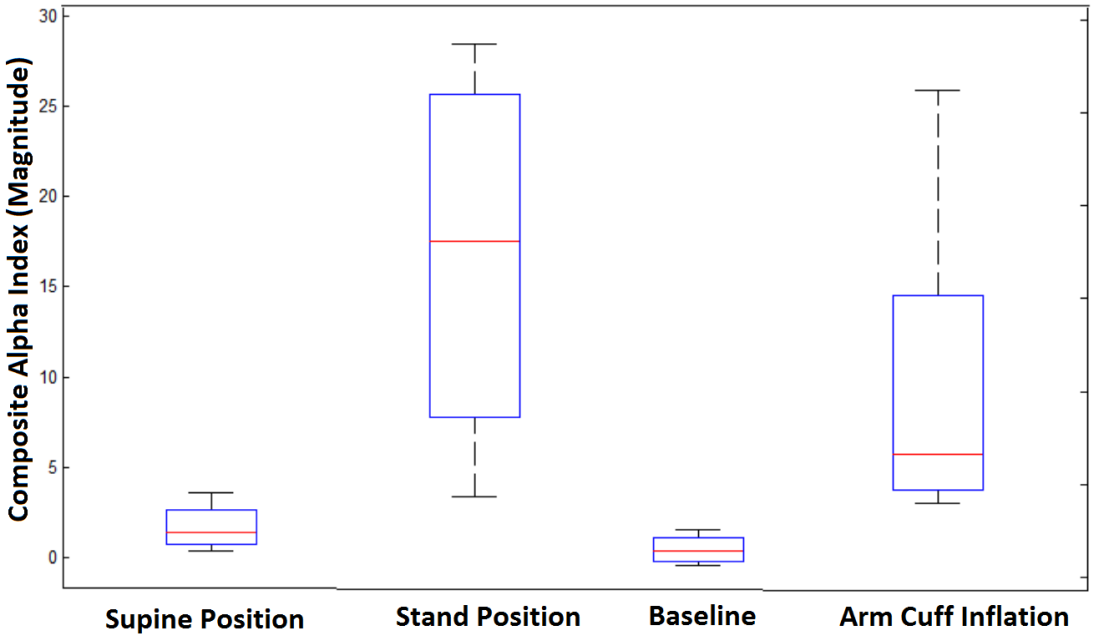

FIGURE 5.13. Mean variability in composite alpha band index for various activities in the study.

with BP. The observation was strengthened by analyzing the change in behavior (rise and fall) of estimated cerebral blood flow as well. Therefore, EEG metrics can be used as a firsthand screening tool to check impaired cerebral autoregulation, especially critical for people at higher risk of developing stroke.

We are currently working on porting our quantitative EEG measures over to an Android mobile platform which is capable of recording and transmitting EEG signals in real-time. Although, we are able to show the possibility of quantifying Cerebral Autoregulation via EEG, appropriate cut-offs have to be determined to state if the change in parameters are significant to be alarmed. Last, it is important to analyze the sensitivity of this approach to avoid confusion with artifacts.

5.8. Acknowledgements

This work is partially supported by the National Science Foundation under grants CNS-0751205, CNS-0821736 and CNS-1229700.

CHAPTER 6

COGNITIVE TASK RECOGNITION

6.1. Introduction

Cognitive task classification has gained attention over the past decade because of its implied usage in BCI (brain-computer interface) technology. The ability to distinguish between any two states of the user can be used as an input to the computer to design applications based on the varied response from the user [73]. There are various existing brain sensing technologies like functional magnetic resonance imaging (fMRI), electrocorticography (ECoG) etc. but Electroencephalography (EEG) proves to be a relatively simpler, less costly, silent, non-invasive sensing technology for BCI research. It is used to detect the changes in brain activity that helps in diagnosing brain related abnormalities like epilepsy, head injury, sleep disorders, memory impairment etc. Nowadays, EEG signals are widely being used for brain-computer interface (BCI) including detecting neurodegenerative diseases, PC based gaming, and operator controlled robots. Cognitive task recognition can be specifically useful to disabled people - who can control and interact with the world by thinking about a particular event.

6.2. Background

The process of cognitive task recognition can be done in two ways; operant conditioning or pattern recognition [126]. In operant conditioning method, the user has to get accustomed to train their brainwaves in order to achieve the desired output results via a feedback loop. In pattern recognition method, advanced signal processing and machine learning techniques are used to differentiate between the different brainwaves associated with different mental tasks.

Fitzgibbon et al. studied eight different cognitive tasks and found statistical differences in the spectral power of EEG signals while subjects performed these tasks [36]. But only statistical differences do not qualify to prove the classification between such tasks. Keirn and Aunon recorded EEG signals for subjects performing five mental tasks to indicate hemispheric differences in the mapping of brain functions [62]. They obtained accuracy about 75 90% while comparing pair of these tasks using within the subject models. Numerous researchers have re-used the data set

obtained by Keirn and Aunon to study the issue of task classification from EEG signals. Palaniappan was able to obtain an accuracy of about 97.5% using Keirn data for separable pairs of tasks which was different of each subject. This made the model less general to be used in different BCI applications [106].

Liang et al. have evaluated the performance of the tasks based on Keirn dataset using three classifiers, namely Back propagation Neural Network (BPNN), Support Vector Machines (SVM) and Extreme Learning Machine (ELM) [77]. They obtained that ELM needed nearly 1 to 2 orders of magnitude less training time in contrast to other two methods with about the same classification accuracy for all three. However, better testing accuracy may achieved by smoothing the raw outputs for all three classifiers. Lastly, the optimal classifier parameters for ELM are obtained relatively in lower time span than the other two classifiers.

Anderson used two and three layered neural networks with 10 fold cross validation to classify the EEG data into the respective five mental tasks classes [4]. They were able to increase the efficiency from 54% to 96% by proposing an approach to average the output of the neural network over consecutive half-second windows. Thus this higher classification accuracy was obtained by a run done with averaging over 20 consecutive windows.

6.3. Data Collection

6.3.1. Ethics Statement

Ethical approval for the study was obtained from the Institutional Review Board at University of North Texas (Denton, Texas, USA). All participants provided written informed consent to participate in the study and also consented to the publication of the data and media.

6.3.2. Tasks

In our study, we collected the EEG data from three participants while they performed four cognitive activities using the commercially available single electrode Neurosky band [96]. The duration of a trial was 10 secs and the subjects completed two trials of each of the following task.

- Baseline: In this task, the subject was asked to close his eyes and relax as much as possible without thinking anything in particular.

- Focus: The subject focuses on two different objects; rubik cube and baseball in different trials.
- Read: A 100 word paragraph was presented to the subject on the computer screen with instructions to find a particular word.
- Math: The subject was given two multiplication problems in the two trials.

6.4. Feature Extraction

We have used several methods to extract features from the single channel EEG signal. Different methods produced different size of feature vector (number of input is different). Following is the description of different feature extraction methods.

- Average power of frequency bands with one second time window: In this method, we converted the EEG data into frequency domain usinf FT Transform. Then the standard EEG frequency bands, Delta (0.5-4Hz), Theta (4-8Hz), Alpha (8-13Hz), Beta (13-30Hz), and Gamma (36-44Hz) were calculated for each channel. The data was split into one sec non-overlapping windows. Since the data set has 10 seconds of data for each channel this will produce 50 (10*5) features. The class type was determined as usual.
- Logarithmic power of frequency bands with the whole signal: This method was similar to the previous method. But, we used the whole 10 seconds of data from the channel to obtain the frequency power spectrum. The logarithmic power of each band was then used as the feature.
- Logarithmic power of frequency bands with one second window: Here, the logarithmic power of each frequency band per second of the data was used as feature. Thus, increasing the total of number of features for classification.

Figure 6.1 gives a general idea of the feature extraction methodology.

WEKA is a tool that can be used to analyze the dataset by applying it to various classification models [48]. WEKA accepts ARFF file format. Since our data set was in MATLAB cell array format, we wrote a set of different Matlab scripts to produce appropriate ARFF file for each of the feature extraction methods. Then for each of these ARFF file (that correspond to each feature

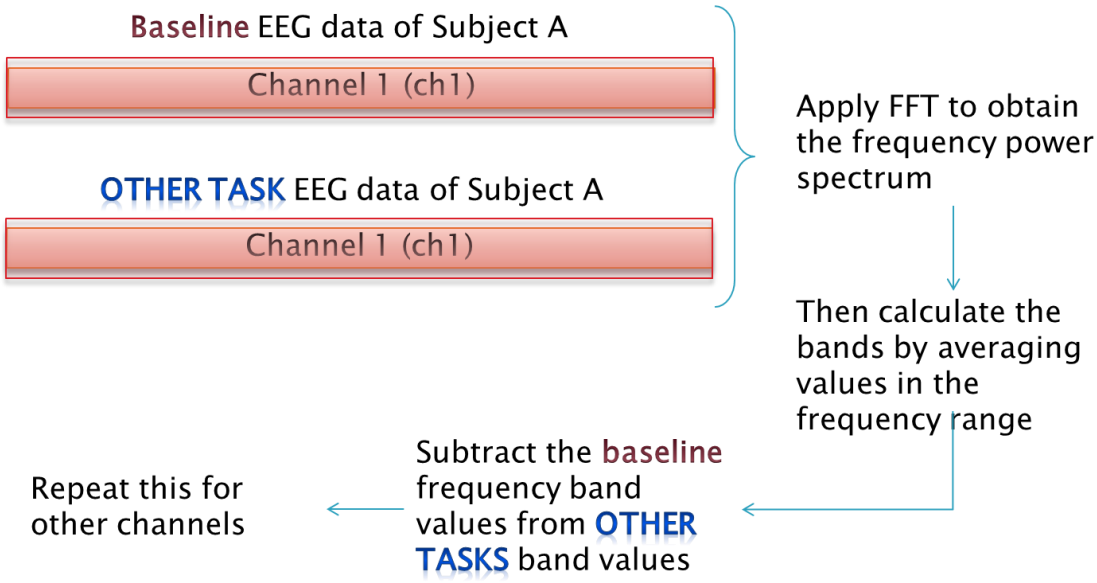

FIGURE 6.1. An overview of the feature extraction methodology

extraction methods), we tested multiple classifiers and obtained the results. The model was always validated using train-set and test-set in a predictive validation strategy where train set is used to build the model (train the model) and then the test-set was used to test the model. Confusion matrix and measures that were derived from the confusion matrix was used to evaluate the performance of the model. The dataset was split into train-set and test-set based on 10-fold cross validation technique.

6.5. Results and Discussion

The prefrontal lobe is associated with behavior, short-term/working memory tasks, and reasoning [22]. So, using only FP1 region for recording EEG signals to classify the tasks is sufficient. But, the reading task in which subject was asked to identify a particular word was a language processing with pattern recognition task. However, we observed power changes in frequency bands even when this activity is carried out (Figures 6.2, 6.3). We observed that there was a significant power level change in the power spectrum of the tasks compared to the baseline. However, it was not very prominent in case of multiplication task which makes the use power bands as a non-optimal option for classifying this task (Figure 6.4). One reason could be that this task was carried out using closed eyes, so more power was concentrated in the lower bands. A very similar

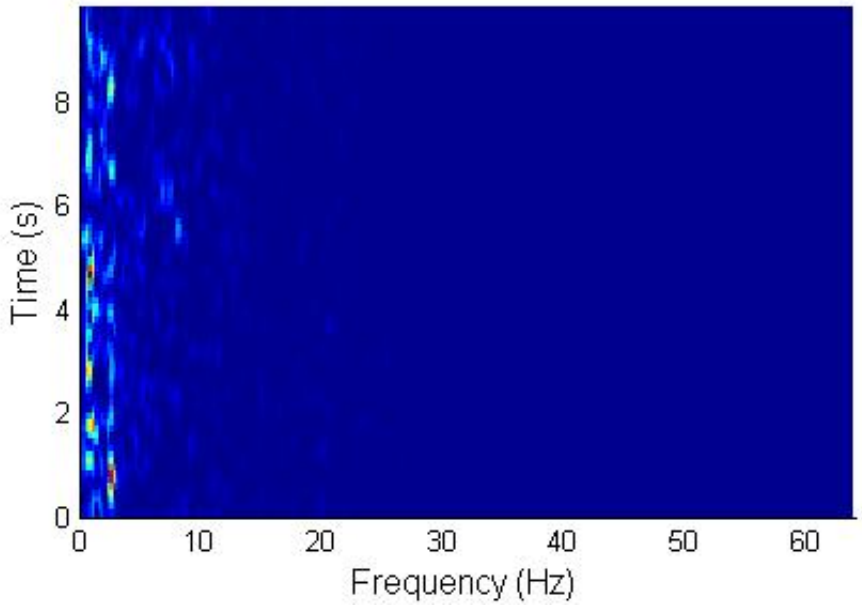

FIGURE 6.2. Power spectrum of the base task of a subject

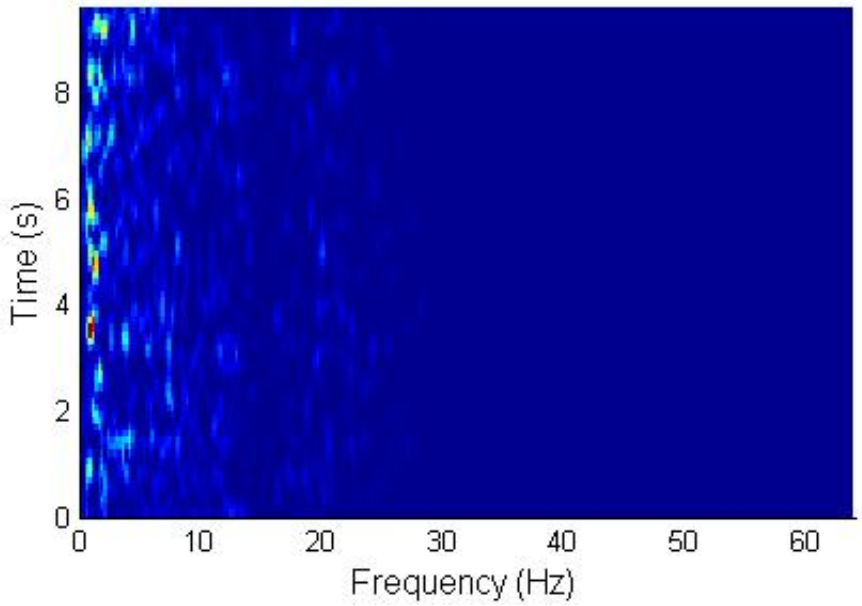

FIGURE 6.3. Power spectrum of the reading task of a subject

pattern in change of power levels of read task and focus task was observed, which causes difficulty in classifying the two tasks generally among all subjects (Figure 6.5.

To determine the ability to predict a task for a particular subject, the classifier was trained using the other subject's data except the one to be predicted. This was repeated for all three

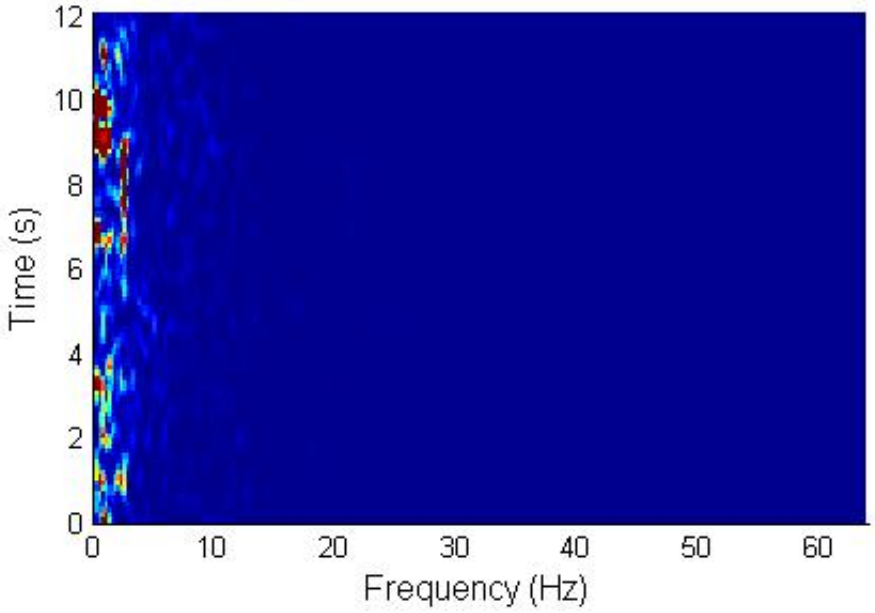

FIGURE 6.4. Power spectrum of the multiplication task of a subject

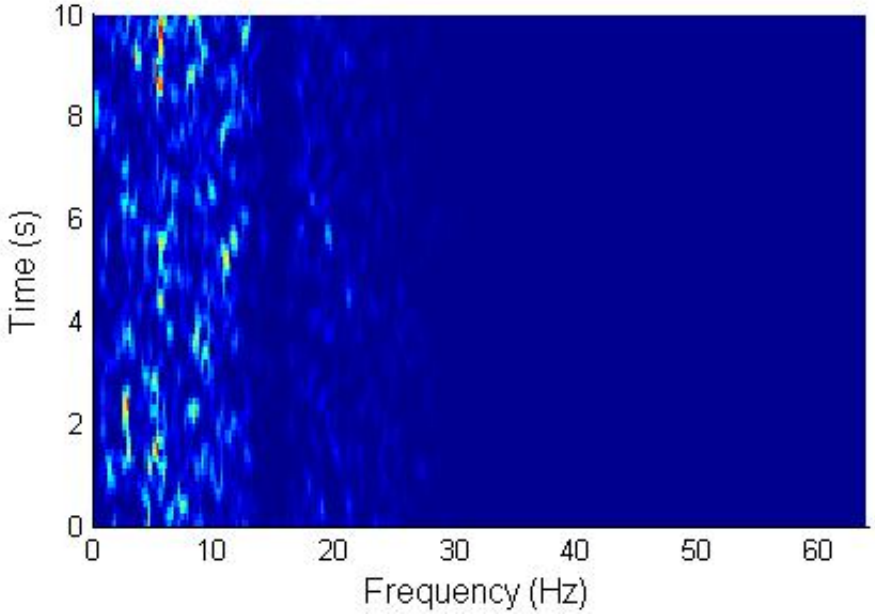

FIGURE 6.5. Power spectrum of the focus task of a subject

subjects. Different classifiers result in different accuracy for classification even within the subjects. A maximum accuracy of classification achieved for the activities was 83.33%. Table 6.1 shows the classification results from the three feature extraction methods.

TABLE 6.1. Accuracies and F-measures for the different feature extraction methods used for the cognitive task recognition

Features	Classifier	Accuracy	F-measure
Average Power features (with windowing)	Multilayer Perceptron, Regression	83.33%	0.742
Logarithmic features	Multilayer Perceptron, Logistic	75%	0.702
Logarithmic features (with windowing)	Bayesian Network, Random Forest	66.66%	0.67

6.6. Conclusion

The rapid emergence of wearable technology has led to a boom in number of quantized self-applications. The integration of body sensor networks and mobile phones with increasing processing capability has motivated me to develop a simple and easy to use infrastructure to make wearable EEG systems as a ubiquitous tool, helping to monitor the activity of brain in unconventional environments. The methods used we used in this study cannot determine a complete ontology of mental states, however spectral differences in frequency bands were observed in these limited tasks performed. The potential applications arising from the ability to differentiate between various cognitive tasks are endless, ranging from disease monitoring, to assisted living to recognition applications.

CHAPTER 7

MOBILE PLATFORM TO FACILITATE EEG KNOWLEDGE DISCOVERY APPLICATIONS

7.1. Introduction

The use of electroencephalography (EEG) to analyze brain activity has existed since 1924 after its invention by a German Scientist Hans Berger [47]. EEG measures the potential difference across the scalp as a result of ionic current flows, when the neurons in the brain communicate with each other. Previously, it was not a fully developed diagnostic tool but has now become viable in diagnosing and treating neurological disorders especially epilepsy, seizures, brain tumors, sleep disorders, coma and brain death.

One of the initial attempts to provide real-time remote EEG monitoring [19] was developed as an internet based EEG information system using the wireless local area network (WLAN) and a WLAN compliant EEG sensor node named pEEG. In another work, [39] proposes architecture based on Cloud Computing and MapReduce for Ubiquitous Learning systems. However, in his scheme only generated EEG data sets and virtual users were used. [31] also offer the use of cloud runtime to allow training of neural networks for EEG classification of different mental tasks from multiple users to use their intended actions for keyboard input or control motion of wheel chair. Their results were based on only pseudo generated EEG streams and a static data set.

The main motivation of our brain-mobile-cloud interface for EEG monitoring is to bridge the enormous gap between diagnosis and treatment of mental disorders. Also, a constraint EEG recording environment cannot accurately determine the onset or presence of many of the complex neural disabilities. As more and more people have access to smart phones, adding mobility in EEG data collection provides unrestrained, remote monitoring of people for more accurate, up-to-date patient data readily available to the doctors. This helps to deliver patient centric care and prioritize the resources of hospitals towards acute patients. It will prevent unnecessary visits to healthcare

Parts of this chapter have been previously published in Garima Bajwa, Ram Dantu, Mohamed Fazeen, and Rajiv M. Jospeph, "Self-tracking via brain-mobile-cloud interface." *AAAI Spring Symposium Series*, 2013, reproduced with permission from AAAI [10].

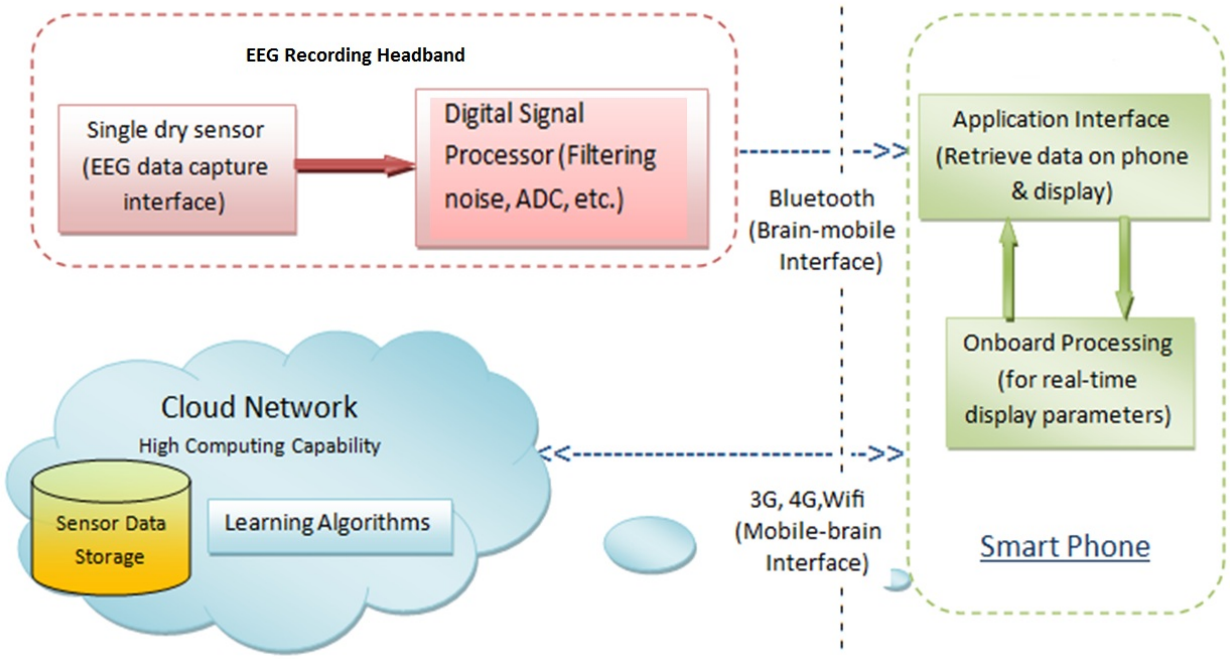

FIGURE 7.1. System design for the brain-mobile-cloud interface

centres thereby cutting overall costs involved in mental healthcare. In the following sections we discuss the proposed infrastructure of the BMCI design, application interface, relevance of our work in applications of self-tracking behavior and finally, some challenges and future work.

7.2. Application Interface Prototype

The system design as shown in Figure 7.1 is a detailed overview of the proposed architecture for brain-mobile-cloud interface. The EEG brain signals are captured using a headband called Mindband [96]. The Bluetooth interface i.e. brain-mobile interface obtains data on the smart phone and the android API displays the collected data from the EEG sensor on the mobile phone. The phone has a 1 GHz processor with 512 MB internal storage. Light weight on board processing can be performed in the smart phone itself for preliminary data analysis. The expected urgent results are displayed using the existing API; otherwise the data is sent to the cloud network via the mobile-cloud interface.

7.2.1. Brain-Mobile Interface

In our system we use the headband as the brain-mobile interface to obtain the EEG data of the user. The headband contains a single sensor dry electrode with an ear clip reference to

record signals from the scalp. It is comfortable and convenient to wear. Additionally, it does some preprocessing of EEG data and provides bluetooth connection for transfer of data to peripheral devices.

7.2.2. Mobile-Cloud Interface

To realize the mobile-cloud interface, we have used the NSL server (Network Security Lab at UNT) to test the upload of raw EEG data file onto the server from the mobile phone. For this process, we used the available Intents from the AndFTP application to perform the upload, download and browsing process. AndFTP is a FTP, SFTP, SCP, FTPS client for android devices [88]. To use these Intents in our current brain-mobile API, the AndFTP application needs to be already installed in the mobile system [5]. The file transfer is performed over a secured SSH connection using Wi-Fi and the authentication process is carried out by verifying a username and password.

7.2.3. Discussion

The observed results in our experimental measurements capture the features that have been reported in the model framework of neurovascular coupling in literature and are in accordance with the underlying assumptions. It highlights the potential use of portable EEG monitoring devices to be used for real time self-tracking of an individuals cerebral blood flow in absence of fMRI, NIRS techniques (assuming the state of the art techniques existing in EEG capturing devices will expand to offer more miniaturized, reliable and cost effective devices). Numerical validation of the measures has to be carried out to provide a better estimate of such measures for clinical relevance and personal health monitoring. Though EEG signals qualitatively characterize the CBF behavior, all the ideas motivating the model may not be correct as neurovascular coupling still remains a subject of debate with researchers and no consensus has been established on exactly which aspect of neural activity drives the hemodynamic response.

Further, we have shown that EEG signals from one channel may be sufficient to detect the intense thinking that can be used to quantize drivers distraction index. Frequency bands can be used for peak detection algorithms to quantify any variations. Such algorithms involve less intensive

TABLE 7.1. Performance Metrics for Data Transfer between the two Interfaces

	Brain-Mobile-Interface	Mobile-Cloud-Interface	
Metrics	EEG Data Transfer to mobile phone	Upload Process	Download Process
Transfer Size	Streaming (raw data at 512 Hz)	2,644 KB	2,644 KB
Transfer Rate	250 kbits/sec (RF data rate)	344.08 KB/s	293.22KB/s

computation in low resource devices like mobile phones as compared to detecting bursts in time domain. Thus, a mobile implementation of these applications would be a major improvement in ensuring the health and safety of an individual.

7.3. Performance Metrics

We used some metrics to evaluate the data transfer speeds of our interfaces, namely; Bluetooth data transfer from headband to mobile phone and upload, download processes for mobile-server-interface. The results of our trials are shown in Table I. We used the same file to perform the upload and download for the mobile-cloud interface to compare the metrics. The impact of transfer rates between the different interfaces is more significant for real-time alerts compared to the diagnosis and processing of data at the health providers side.

The EEG recording of 1 minute from single electrode amounts up to nearly 1.12 Mb of data. As the number of electrodes and the duration of EEG recording increases, the data storage requirement will be enormous. The mobile-cloud interface will be a feasible solution to handle such large data collections.Presently, upload of the EEG data file to server and collection of the raw EEG data from the headband is not supported simultaneous in our application. However, transfer speed of 344 KB/sec during upload is sufficient to allow the data recording and relaying being done simultaneously.

7.4. Conclusion

The BMCI design described in this paper put forwards the idea to carry a wearable headband that is easily connected to the smartphone, which acts as a medium to transfer data to the cloud network for analyses. It provides the ability to use EEG signals with BMCI application

as a means to equip individuals with a self-tracking tool for monitoring their brain signals for symptoms of developing any brain injury. This self-knowledge about ones brain health leads to timely acknowledgment of abnormalities, improved patient centric treatments leading to an overall change in behavioral response of both patients and doctors.

Further use of this application can be extended in driver distraction detection which will lead to safe driving scenarios with timely distracted alerts. More work is in progress to study the relationship of our observations in the EEG data of diseased patients. Also, we need to investigate what kind of risk models can be developed for brain abnormalities/distracted driving based on long-term assessment of EEG self-tracked data in cloud. Lastly, the security and privacy of the EEG data has to be taken care at all times.

7.5. Acknowledgments

This work is partially supported by the National Science Foundation under grants CNS-0751205 and CNS-0821736.

CHAPTER 8

CONCLUSION AND FUTURE WORK

I hypothesize that the wearable EEG would be soon be like a miniaturized chip-sticker that can be readily attached to the scalp, which will allow ease of access for all modern brain-computer-interface applications. Developments in the field of flexible electronics are expected to lead to the advent of even smaller, lighter, and more comfortable wearable devices. Benefits of having EEG in our pocket are manifold - health, memory, mind and learning, and emotions. The work of this dissertation shows how the system of brain-body-environment interaction (BBEI) emerging from multi-disciplinary fields (computer science and neuroscience) will improve real-time understanding of human perception and cognitive skills for innovative applications. Understanding human behavior and actions has always been a topic of interest to psychologists and neurologists. The future work can be inclined towards predicting the brain events before their occurrences and enhancing the accuracy of this estimation by mathematical models.

APPENDIX A

NORMALIZED CONFUSION MATRICES OF SUBJECTS FOR DIFFERENT TYPES OF DISTRACTION

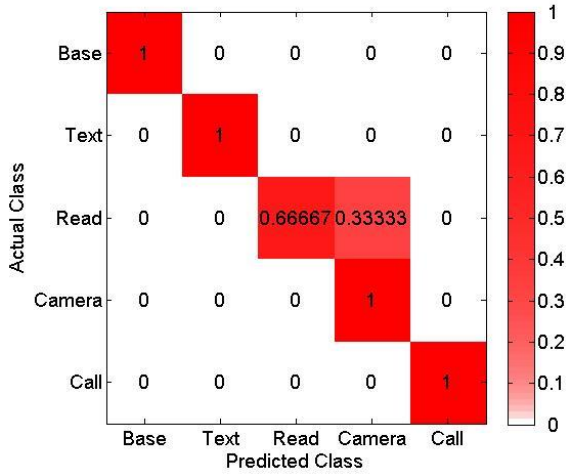

Subject 1 (14 electrodes)

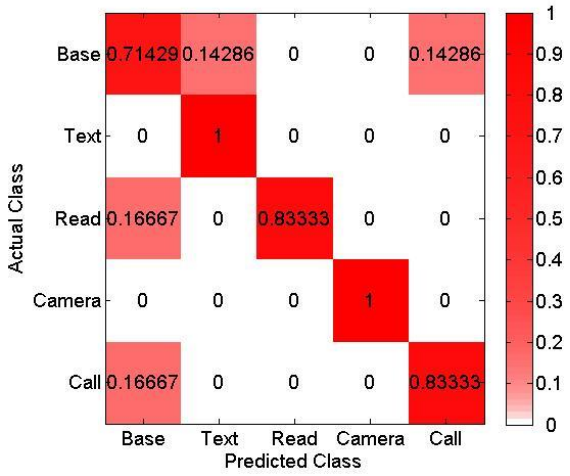

Subject 1 (single electrode)

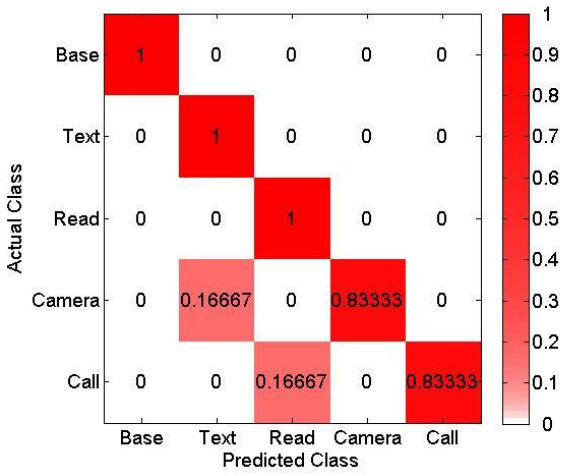

Subject 2

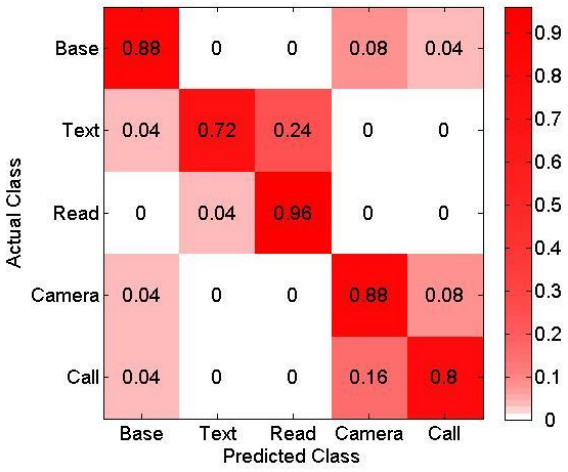

Subject 3

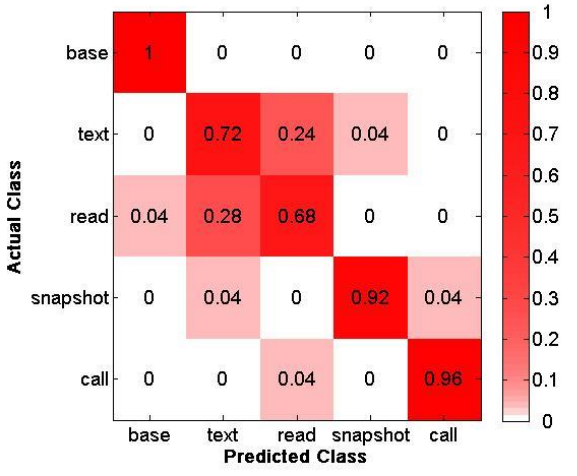

Subject 4

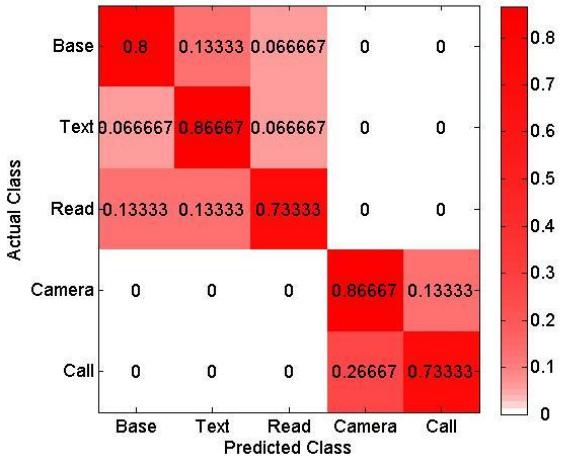

Subject 5

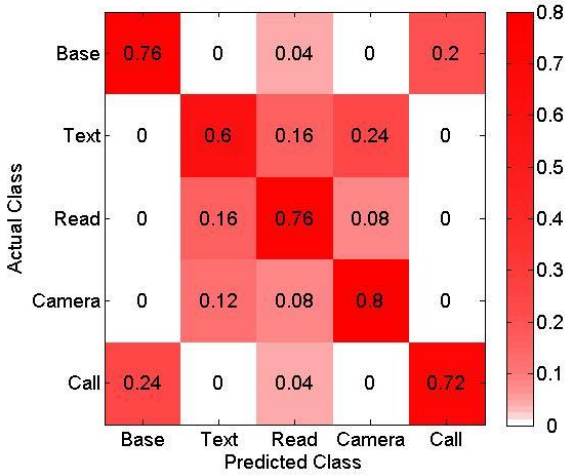

Subject 6

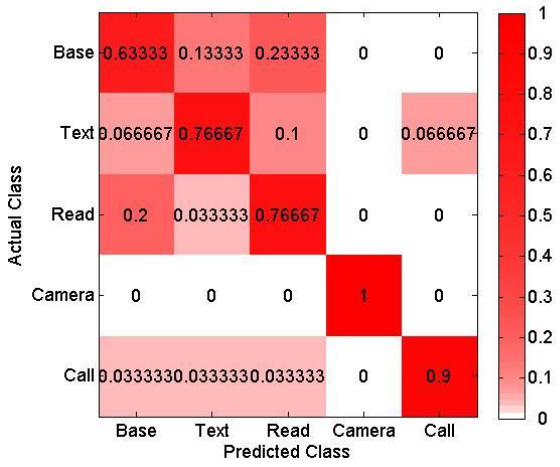

Subject 7

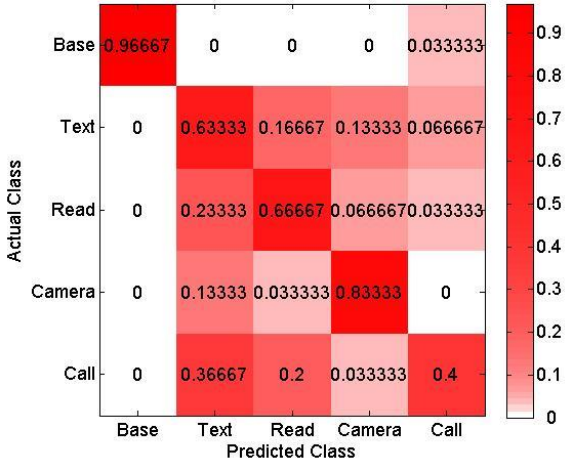

Subject 8

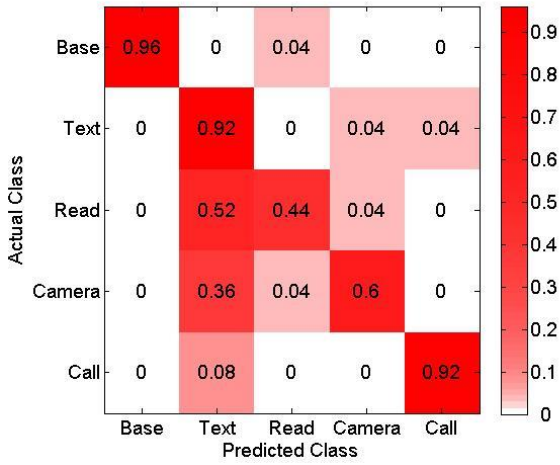

Subject 9

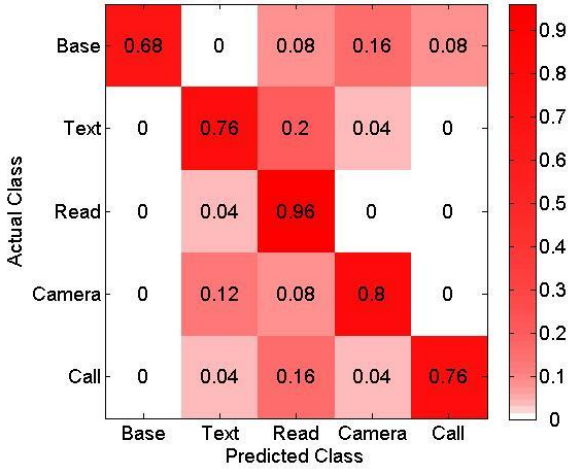

Subject 10

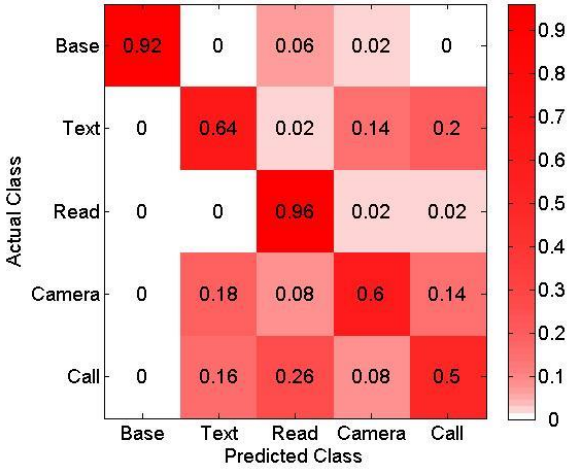

Subject 11

Subject 12

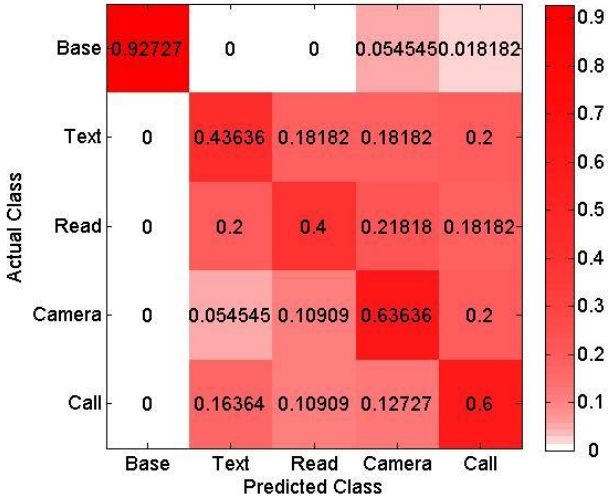

Subject 13

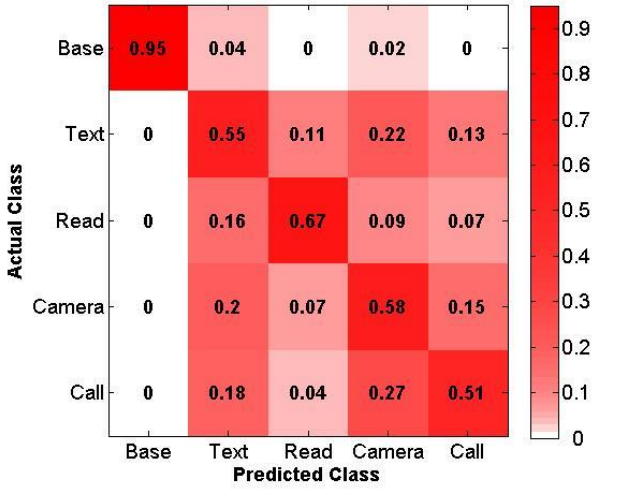

Subject 14

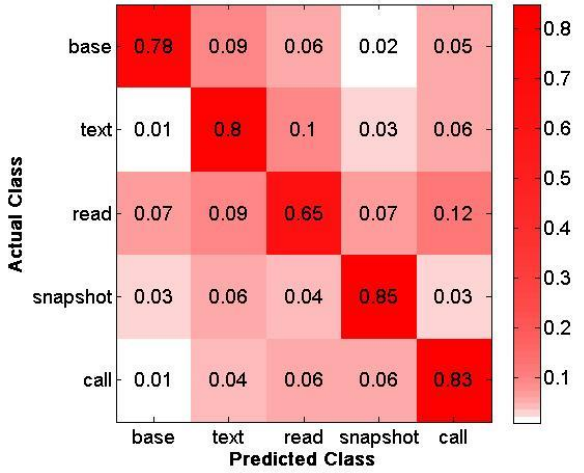

Subject 15

APPENDIX B

ACTIVITY SPECTRA OF ALL COMPONENTS AT FC5 ELECTRODE AND CONTRIBUTION OF IC 13 TO OTHER CHANNELS

Comparison of the activity spectra of all components at FC5 electrode

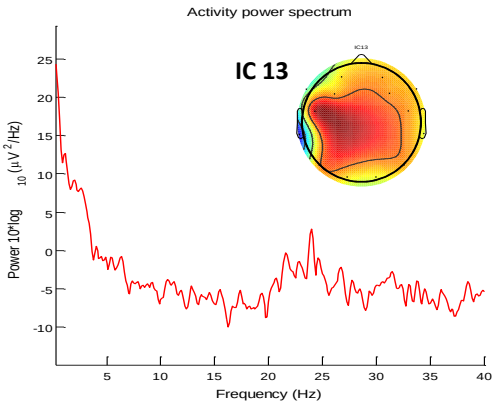

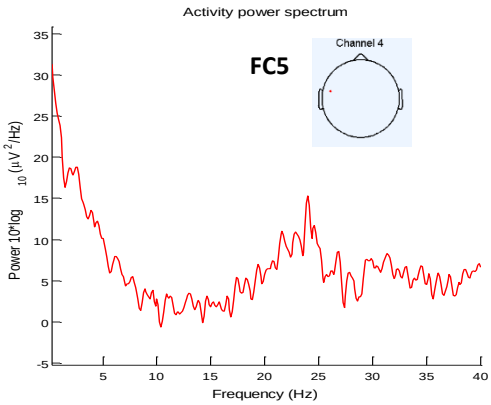

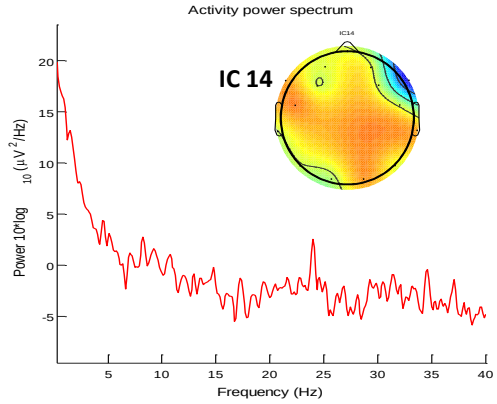

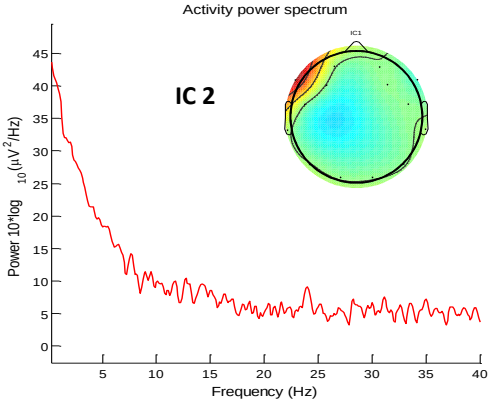

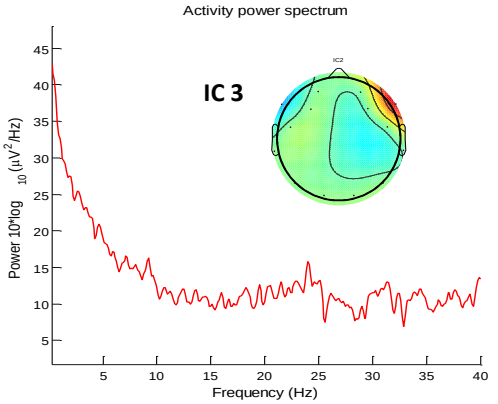

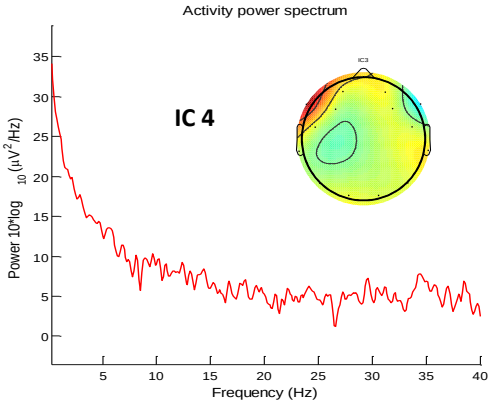

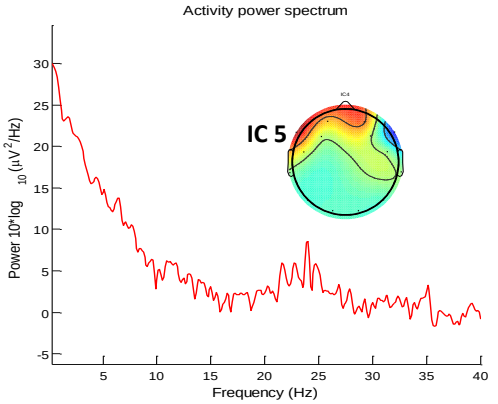

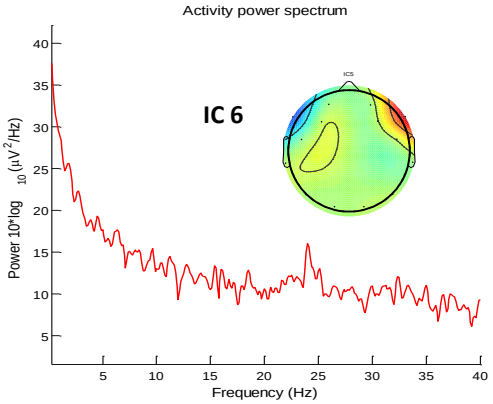

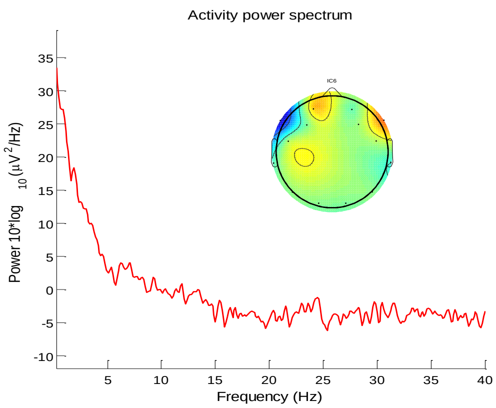
Activity power spectrum
Power $10*\log_{10}(\mu V^2/Hz)$
Frequency (Hz)

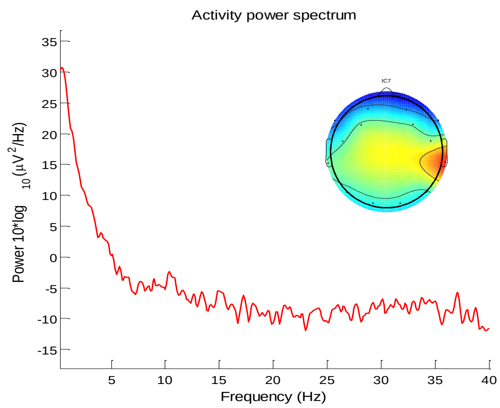
Activity power spectrum
Power $10*\log_{10}(\mu V^2/Hz)$
Frequency (Hz)

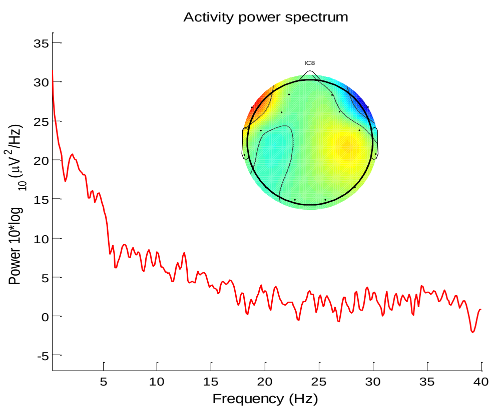
Activity power spectrum
Power $10*\log_{10}(\mu V^2/Hz)$
Frequency (Hz)

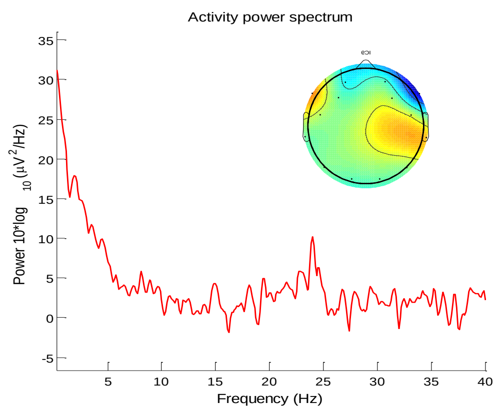
Activity power spectrum
Power $10*\log_{10}(\mu V^2/Hz)$
Frequency (Hz)

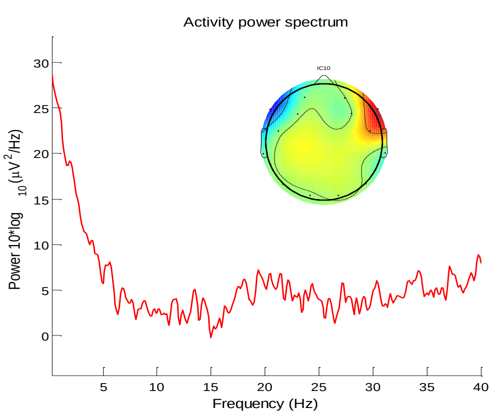
Activity power spectrum
Power $10*\log_{10}(\mu V^2/Hz)$
Frequency (Hz)

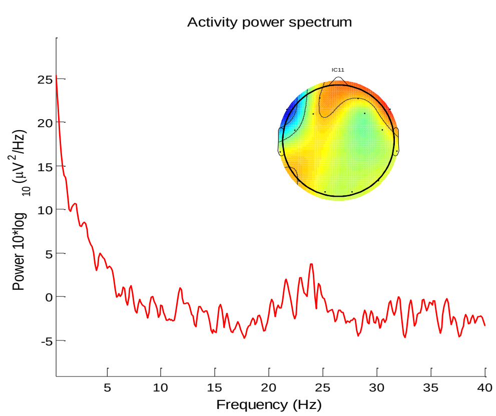
Activity power spectrum
Power $10*\log_{10}(\mu V^2/Hz)$
Frequency (Hz)

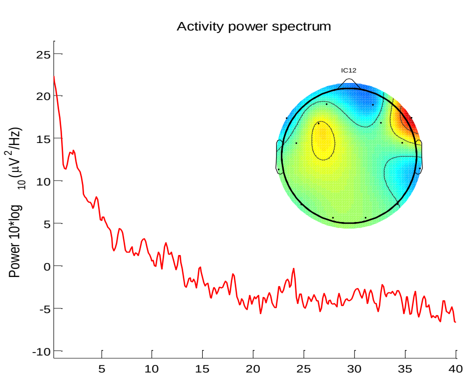
Activity power spectrum
Power $10*\log_{10}(\mu V^2/Hz)$
Frequency (Hz)

Contribution of IC 13 to other scalp channels at 25 Hz

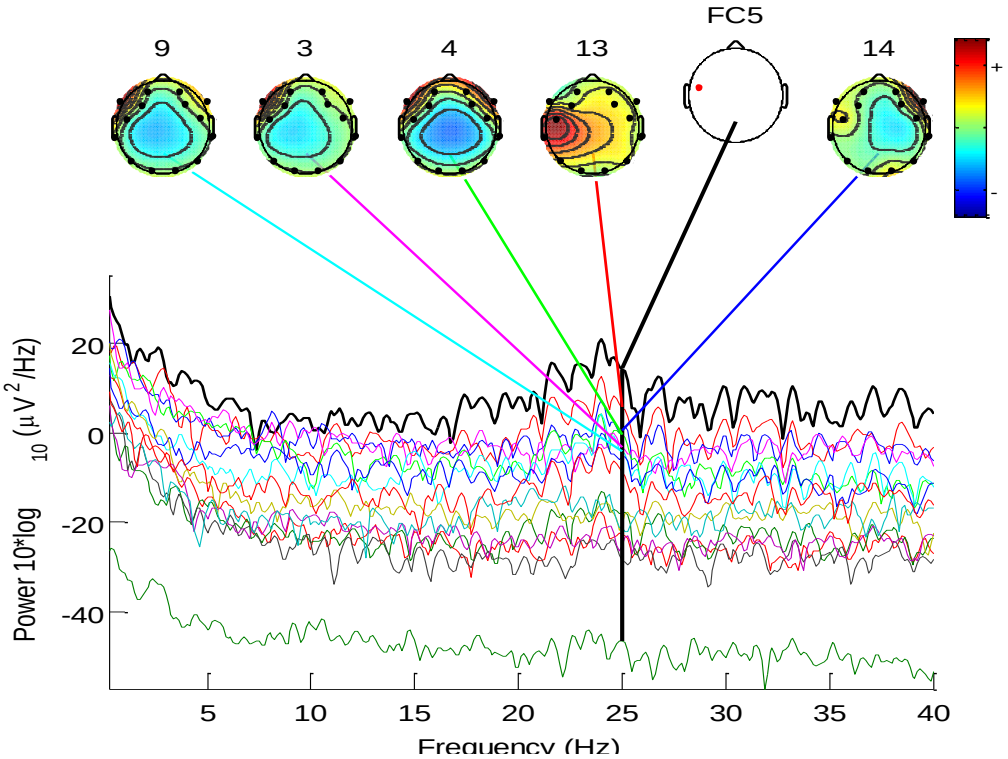

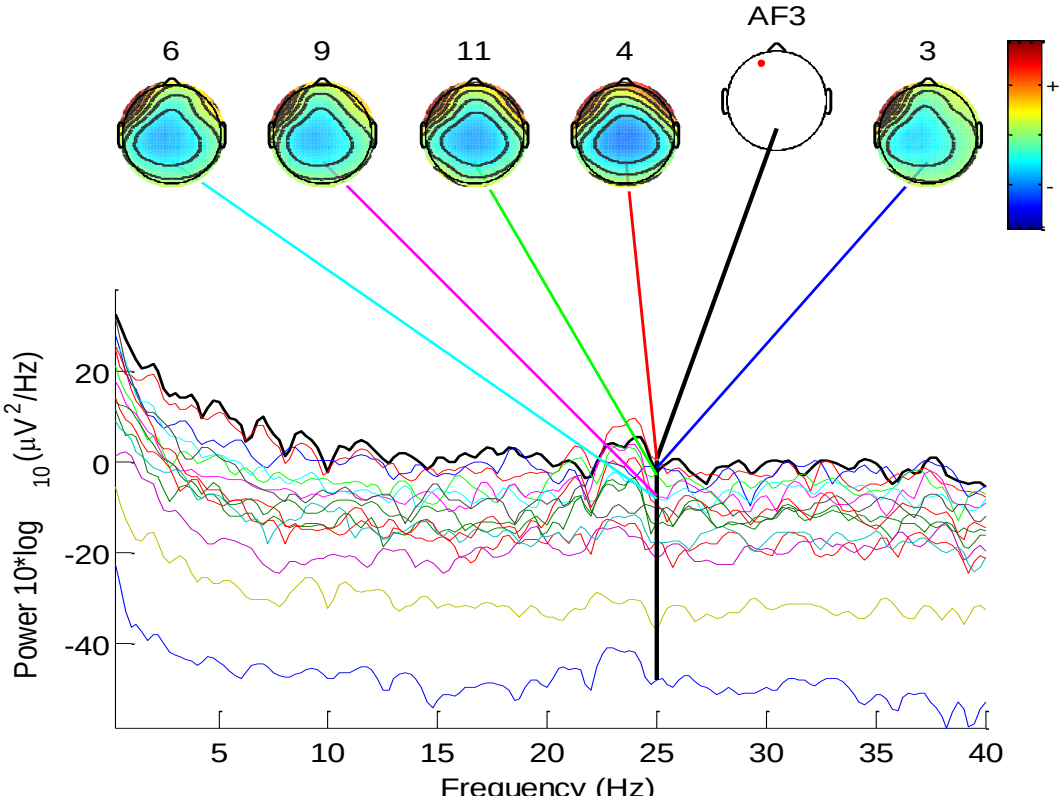

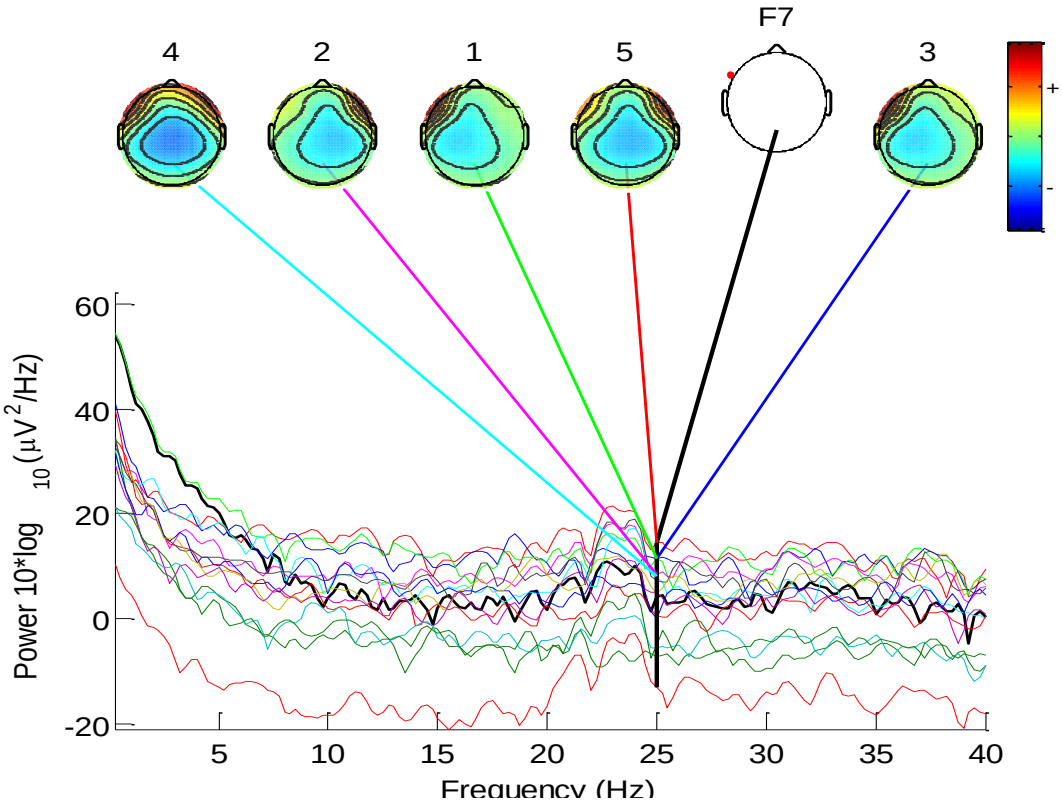
F7
4
2
1
5
3
+
-
60
40
20
0
-20
Power 10*log 10(μV2/Hz)
5
10
15
20
25
30
35
40
Frequency (Hz)

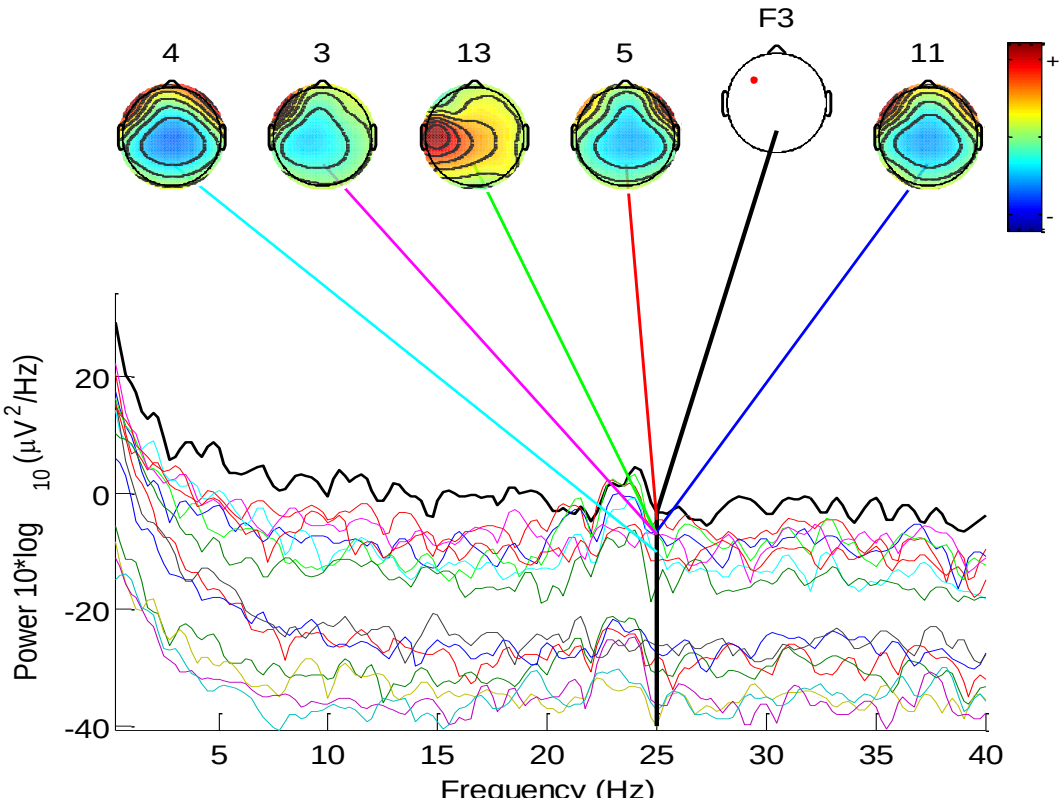
F3
4
3
13
5
11
+
-
20
0
-20
-40
Power 10*log 10(μV2/Hz)
5
10
15
20
25
30
35
40
Frequency (Hz)

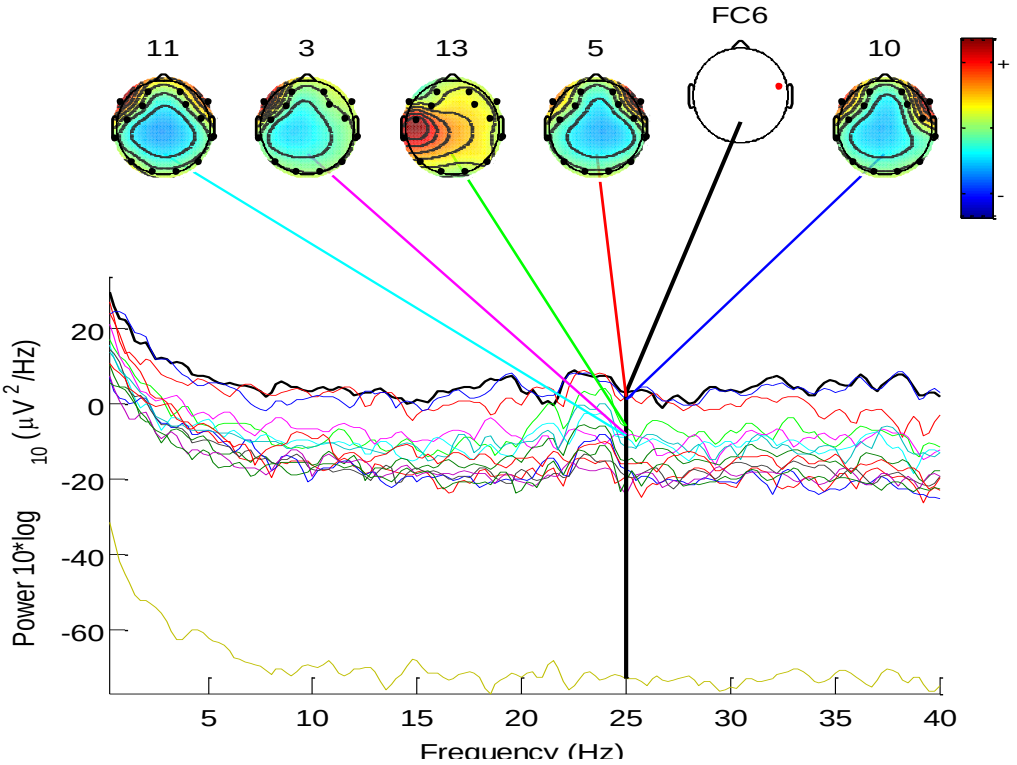
FC6
11
3
13
5
10
+
-
20
0
-20
-40
-60
Power 10*log10(μV2/Hz)
5
10
15
20
25
30
35
40
Frequency (Hz)

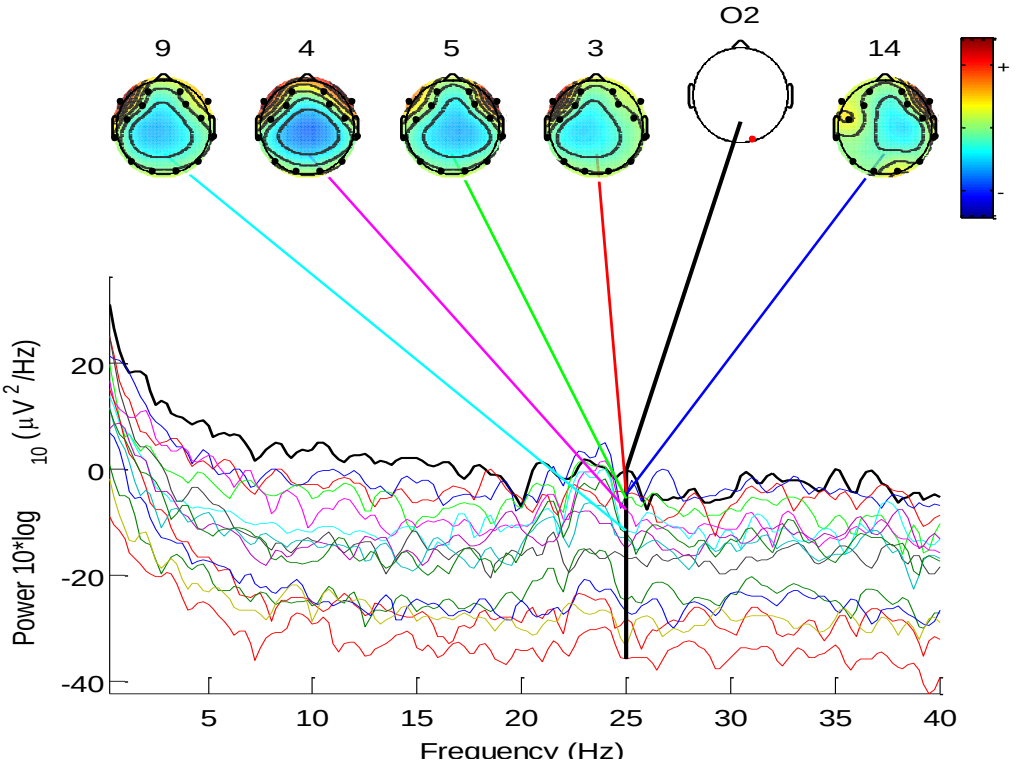
O2
9
4
5
3
14
+
-
20
0
-20
-40
Power 10*log10(μV2/Hz)
5
10
15
20
25
30
35
40
Frequency (Hz)

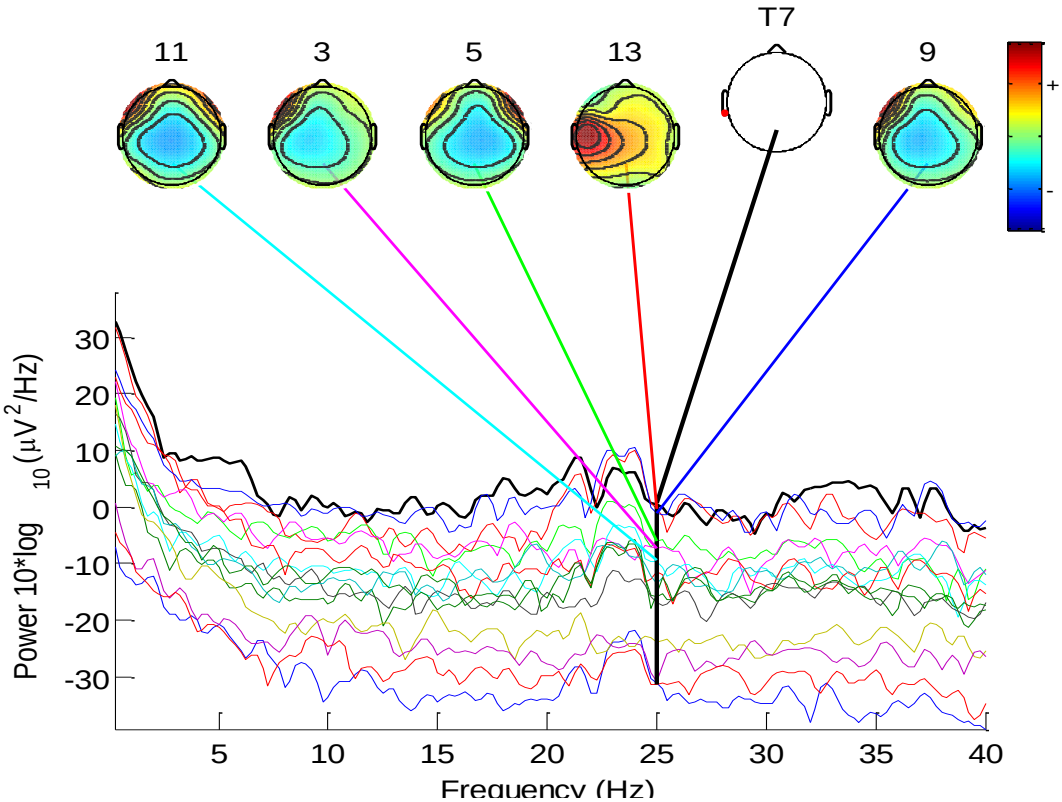
T7
11
3
5
13
9
+
-
30
20
10
0
-10
-20
-30
Power 10*log 10(μV2/Hz)
5
10
15
20
25
30
35
40
Frequency (Hz)

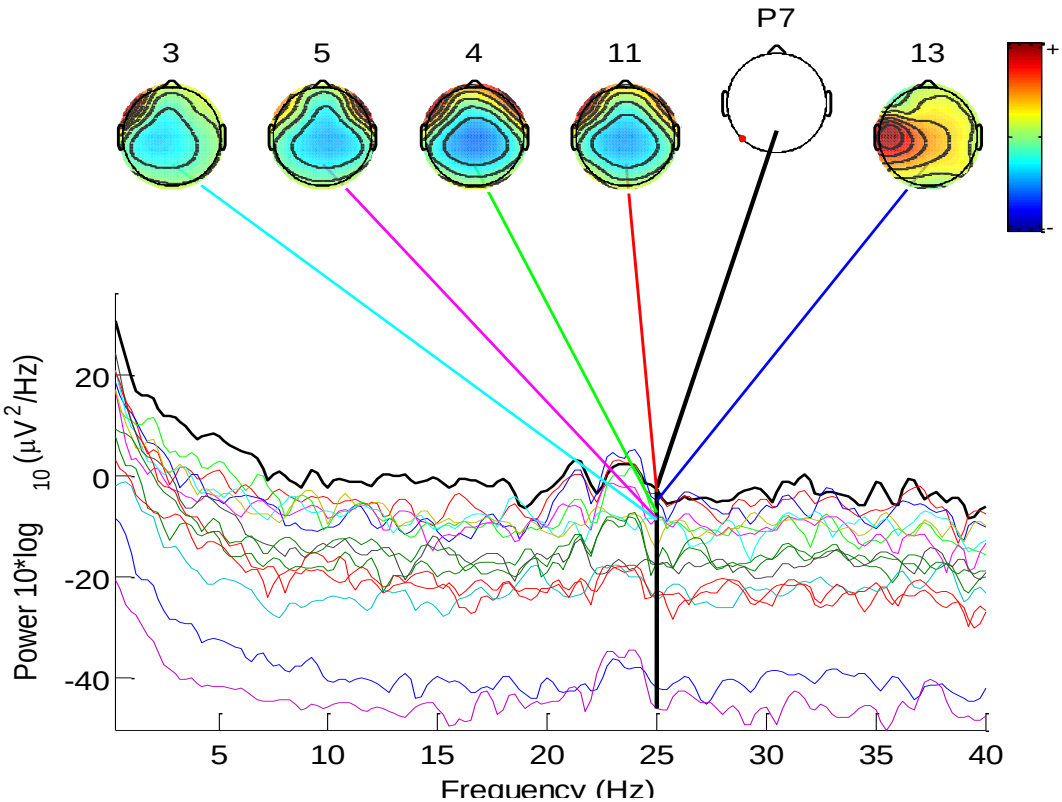
P7
3
5
4
11
13
+
-
20
0
-20
-40
Power 10*log 10(μV2/Hz)
5
10
15
20
25
30
35
40
Frequency (Hz)

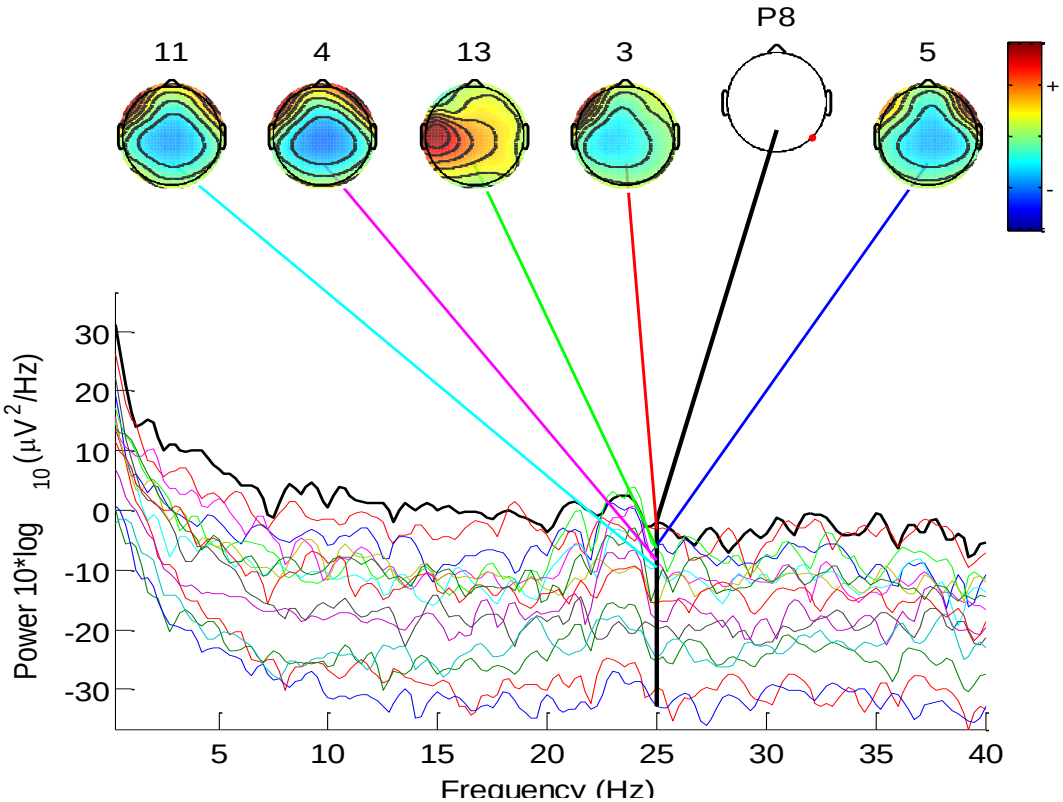
P8
11
4
13
3
5
+
-
30
20
10
0
-10
-20
-30
Power 10*log 10(μV2/Hz)
5
10
15
20
25
30
35
40
Frequency (Hz)

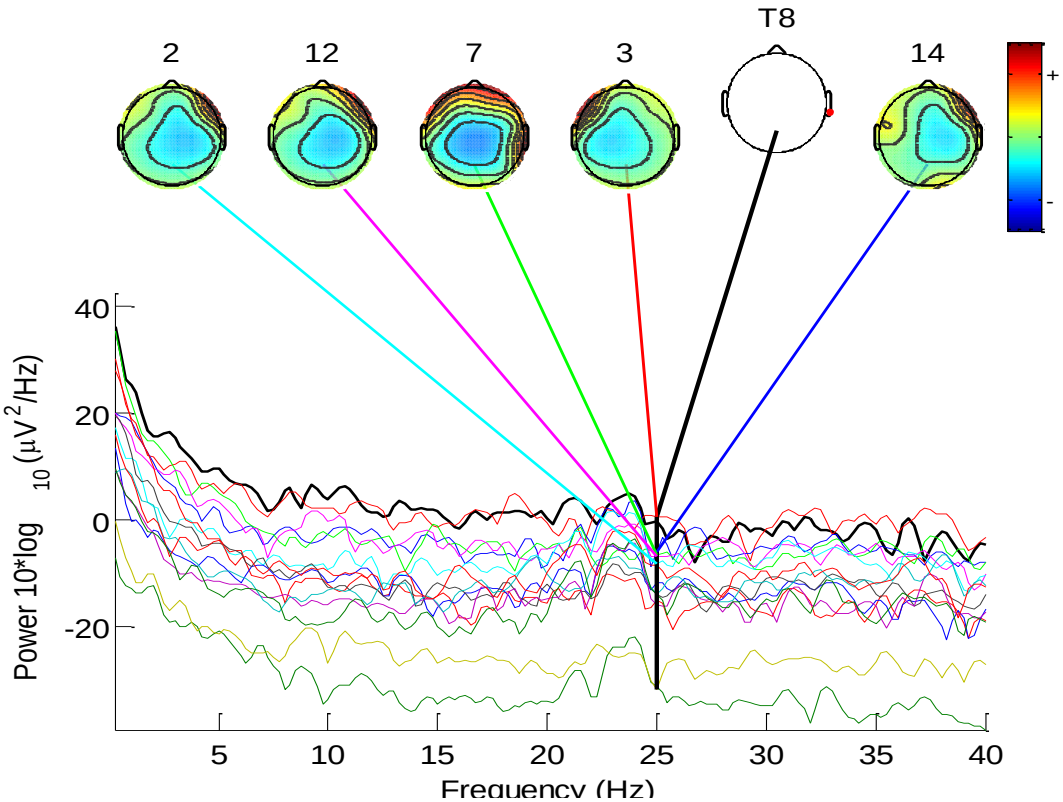
T8
2
12
7
3
14
+
-
40
20
0
-20
Power 10*log 10(μV2/Hz)
5
10
15
20
25
30
35
40
Frequency (Hz)

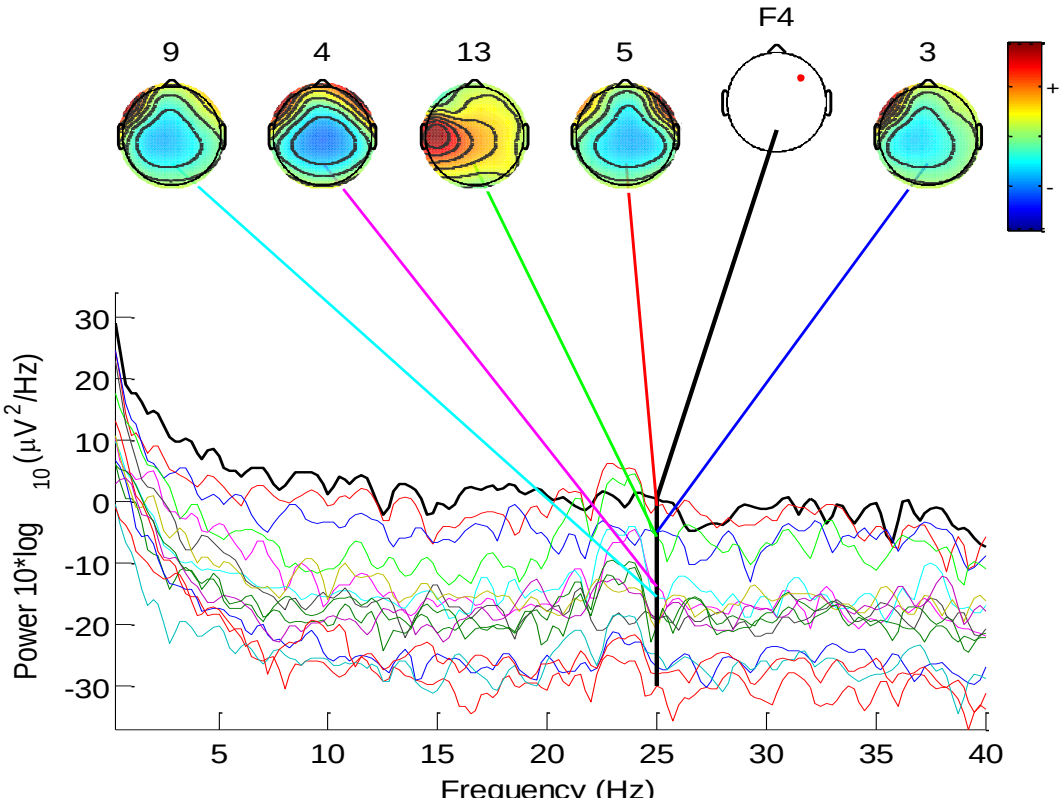
F4
9
4
13
5
3
+
-
30
20
10
0
-10
-20
-30
Power 10*log 10(μV2/Hz)
5
10
15
20
25
30
35
40
Frequency (Hz)

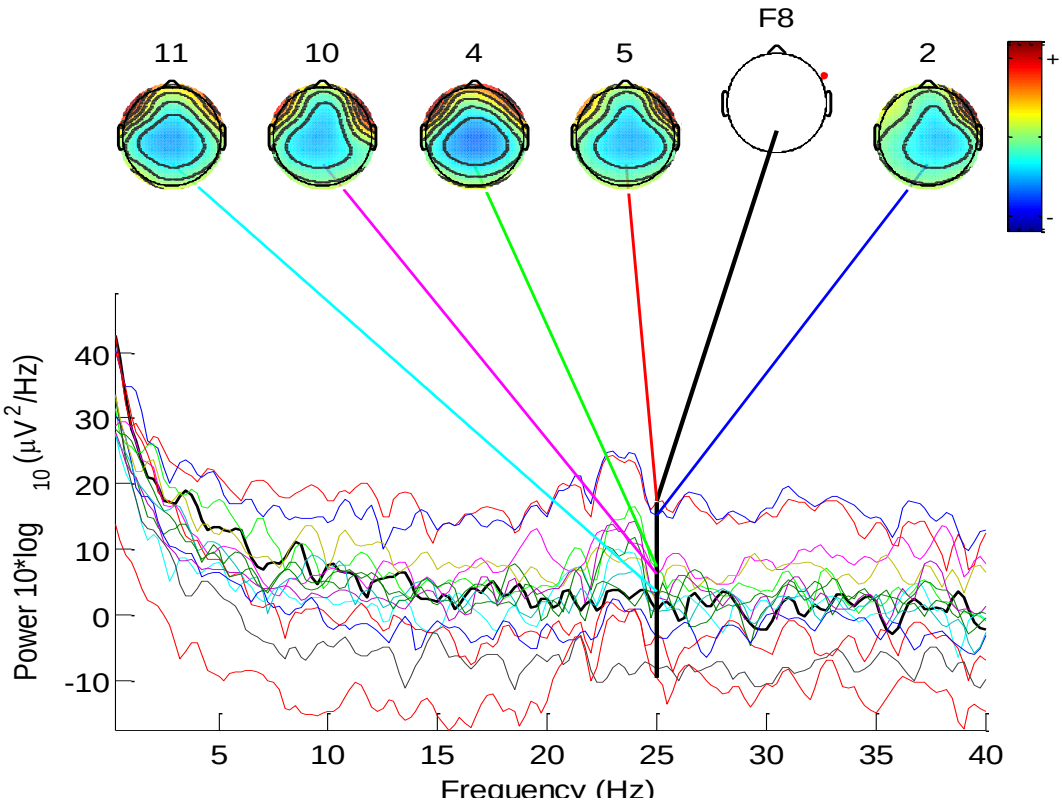
F8
11
10
4
5
2
+
-
40
30
20
10
0
-10
Power 10*log 10(μV2/Hz)
5
10
15
20
25
30
35
40
Frequency (Hz)

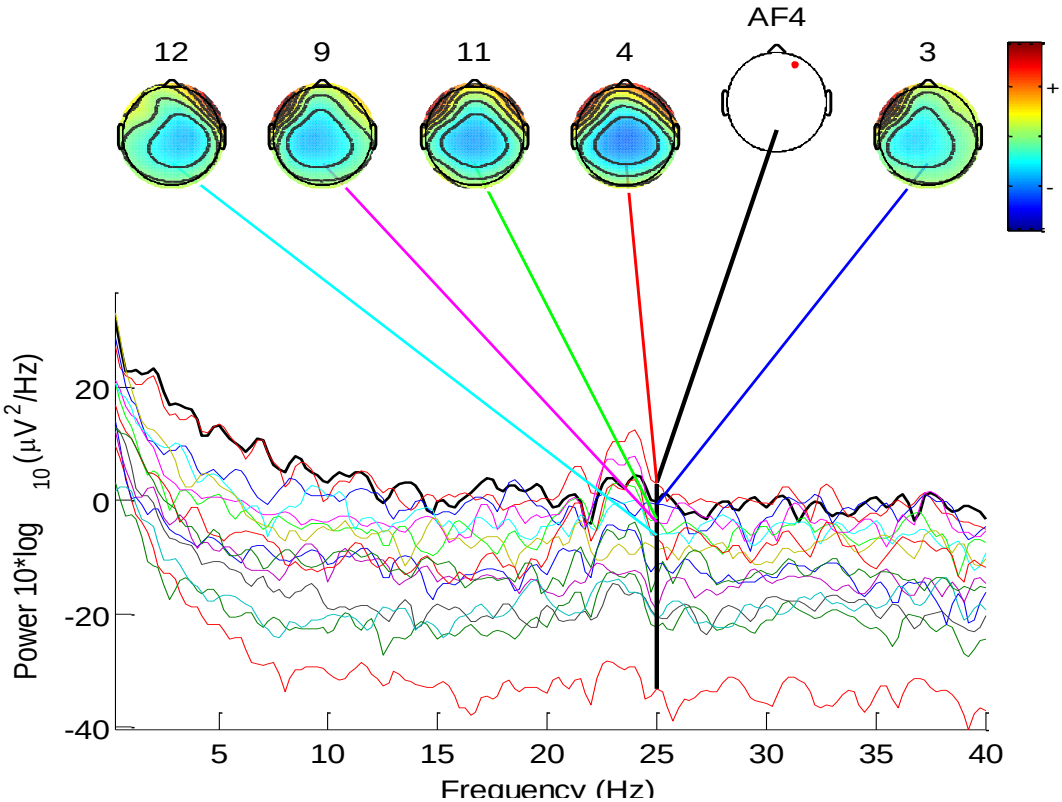
AF4
12
9
11
4
3
+
-
Power 10*log 10(μV2/Hz)
20
0
-20
-40
5
10
15
20
25
30
35
40
Frequency (Hz)

BIBLIOGRAPHY

[1] *Available: http://www.stat.ufl.edu/ winner/tables/wilcox_signrank.pdf*. 73

[2] Muhammad Kamil Abdullah, Khazaimatol S Subari, Justin Leo Cheang Loong, and Nurul Nadia Ahmad, *Analysis of the EEG signal for a practical biometric system*, World Academy of Science, Engineering and Technology 68 (2010), 1123–1127. 15

[3] National Highway Traffic Safety Administration et al., *Visual-manual nhtsa driver distraction guidelines for in-vehicle electronic devices*, Washington, DC: National Highway Traffic Safety Administration (NHTSA), Department of Transportation (DOT) (2012). 5, 51

[4] Charles W Anderson and M Kirby, *Classification of electroencephalogram (eeg) signals for brainmachine interfaces*, Computer Science Department, Colorado State University, USA (2003). 100

[5] Android, *Developers available: http://developer.android.com/index.html*. 108

[6] Jörn Anemüller, Terrence J Sejnowski, and Scott Makeig, *Complex independent component analysis of frequency-domain electroencephalographic data*, Neural Networks 16 (2003), no. 9, 1311–1323. 60

[7] Andrej Anokhin, Ortrud Steinlein, Christine Fischer, Yiping Mao, Peter Vogt, Edda Schalt, and Friedrich Vogel, *A genetic study of the human low-voltage electroencephalogram*, Human genetics 90 (1992), no. 1-2, 99–112. 15

[8] Garima Bajwa and Ram Dantu, *Cerebral autoregulation assessment using electroencephalograms*, Proceedings of the 8th International Conference on Body Area Networks, ICST (Institute for Computer Sciences, Social-Informatics and Telecommunications Engineering), 2013, pp. 327–330. 83

[9] ———, *Neurokey: Towards a new paradigm of cancelable biometrics-based key generation using electroencephalograms*, Computers & Security 62 (2016), 95–113, Online: http://dx.doi.org/10.1016/j.cose.2016.06.001. 11

[10] Garima Bajwa, Ram Dantu, Mohamed Fazeen Mohamed Issadeen, and Rajiv M Joseph,

Self-tracking via brain-mobile-cloud interface, 2013 AAAI Spring Symposium Series, 2013. 106

[11] Garima Bajwa, Ram Dantu, and R Joseph, *Self-tracking via brain-mobile-cloud interface*, AAAI Spring Symposium Series (2013). 78

[12] Garima Bajwa, Ram Dantu, and Arvind Nana, *Quantifying dynamic cerebral autoregulation using electroencephalograms*, Archives of Physical Medicine and Rehabilitation 96 (2015), no. 10, e69. 83

[13] Lucas Ballard, Seny Kamara, Fabian Monrose, and Michael K Reiter, *Towards practical biometric key generation with randomized biometric templates*, Proceedings of the 15th ACM conference on Computer and communications security, ACM, 2008, pp. 235–244. 17, 43

[14] Ruud M Bolle, Jonathan H Connell, and Nalini K Ratha, *Biometric perils and patches*, Pattern Recognition 35 (2002), no. 12, 2727–2738. 13

[15] Richard B. Buxton, Kamil Uludag, David J. Dubowitz, and Thomas T. Liu, *Modeling the hemodynamic response to brain activation*, NeuroImage 23, Supplement 1 (2004), no. 0, S220 – S233, Mathematics in Brain Imaging. 86

[16] Andrew Campbell, Tanzeem Choudhury, Shaohan Hu, Hong Lu, Matthew K Mukerjee, Mashfiqui Rabbi, and Rajeev DS Raizada, *Neurophone: brain-mobile phone interface using a wireless eeg headset*, Proceedings of the second ACM SIGCOMM workshop on Networking, systems, and applications on mobile handhelds, ACM, 2010, pp. 3–8. 47

[17] V. Chandrasekaran, R. Dantu, S. Jonnada, S. Thiyagaraja, and K.P. Subbu, *Cuffless differential blood pressure estimation using smart phones*, Biomedical Engineering, IEEE Transactions on 60 (2013), no. 4, 1080–1089. 89

[18] Yao-Jen Chang, Wende Zhang, and Tsuhan Chen, *Biometrics-based cryptographic key generation*, Multimedia and Expo, 2004. ICME'04. 2004 IEEE International Conference on, vol. 3, IEEE, 2004, pp. 2203–2206. ix, 15, 28, 30, 31, 39

[19] Haifeng Chen and Jungtae Lee, *The implementation of a wireless electroencephalogram in-*

formation system using wlan, IJCSNS International Journal of Computer Science and Network Security 8 (2008), no. 2, 166–172. 106

[20] King-Hong Cheung, Adams Kong, David Zhang, Mohamed Kamel, Jane Toby You, and Ho-Wang Lam, *An analysis on accuracy of cancelable biometrics based on bioHashing*, Knowledge-Based Intelligent Information and Engineering Systems, Springer, 2005, pp. 1168–1172. 13

[21] John Chuang, Hamilton Nguyen, Charles Wang, and Benjamin Johnson, *I think, therefore i am: Usability and security of authentication using brainwaves*, Financial Cryptography and Data Security, Springer, 2013, pp. 1–16. 15, 27

[22] Susan M Courtney, Laurent Petit, James V Haxby, and Leslie G Ungerleider, *The role of prefrontal cortex in working memory: examining the contents of consciousness*, Philosophical Transactions of the Royal Society of London B: Biological Sciences 353 (1998), no. 1377, 1819–1828. 102

[23] Bambi L DeLaRosa, Jeffrey S Spence, Scott KM Shakal, Michael A Motes, Clifford S Calley, Virginia I Calley, John Hart, and Michael A Kraut, *Electrophysiological spatiotemporal dynamics during implicit visual threat processing*, Brain and cognition 91 (2014), 54–61. 14, 40

[24] Arnaud Delorme and Scott Makeig, *Eeglab: an open source toolbox for analysis of single-trial eeg dynamics including independent component analysis*, Journal of neuroscience methods 134 (2004), no. 1, 9–21. 60

[25] Mamadou Diop, Kenneth M Tichauer, Jonathan T Elliott, Mark Migueis, Ting-Yim Lee, and Keith St Lawrence, *Time-resolved near-infrared technique for bedside monitoring of absolute cerebral blood flow*, Proc. SPIE, vol. 7555, 2010, p. 75550Z. 85

[26] Rohan Dixit, *Meditation training and neurofeedback using a personal eeg device*, AAAI Spring Symposium Series (2012). 47

[27] Yevgeniy Dodis, Leonid Reyzin, and Adam Smith, *Fuzzy extractors: How to generate strong keys from biometrics and other noisy data*, Advances in cryptology-Eurocrypt 2004, Springer, 2004, pp. 523–540. 13

[28] Yanchao Dong, Zhencheng Hu, Keiichi Uchimura, and Nobuki Murayama, *Driver inattention monitoring system for intelligent vehicles: A review*, Intelligent Transportation Systems, IEEE Transactions on 12 (2011), no. 2, 596–614. 48, 50

[29] Paul E Dux, Jason Ivanoff, Christopher L Asplund, and René Marois, *Isolation of a central bottleneck of information processing with time-resolved fmri*, Neuron 52 (2006), no. 6, 1109–1120. 74

[30] Emotiv, *Available: http://www.emotiv.com/*. 50, 53

[31] K. Ericson, S. Pallickara, and C.W. Anderson, *Analyzing electroencephalograms using cloud computing techniques*, Cloud Computing Technology and Science (CloudCom), 2010 IEEE Second International Conference on, 30 2010-dec. 3 2010, pp. 185 –192. 106

[32] Maryam Esmaeili, *Classifiers fusion for eeg signals processing in human-computer interface systems*, Proceedings of the 22nd national conference on Artificial intelligence-Volume 2, AAAI Press, 2007, pp. 1856–1857. 82

[33] DJ Ewing, JB Irving, F Kerr, JAW Wildsmith, and BF Clarke, *Cardiovascular responses to sustained handgrip in normal subjects and in patients with diabetes mellitus: a test of autonomic function*, Clinical Science 46 (1974), no. 3, 295–306. 90

[34] Xin-An Fan, Lu-Zheng Bi, and Zhi-Long Chen, *Using eeg to detect drivers emotion with bayesian networks*, Machine Learning and Cybernetics (ICMLC), 2010 International Conference on, vol. 3, july 2010, pp. 1177 –1181. 48

[35] A. Faro, D. Giordano, and C. Spampinato, *A multi-facets analysis of the driver status by eeg and fuzzy hardware processing*, Engineering in Medicine and Biology Society, 2006. EMBS 2006. 28th Annual International Conference of the IEEE, 30 2006-sept. 3 2006, pp. 6095 –6100. 48

[36] Sean Patrick Fitzgibbon, Kenneth J Pope, Lorraine Mackenzie, C Richard Clark, and John Osborne Willoughby, *Cognitive tasks augment gamma eeg power*, Clinical Neurophysiology 115 (2004), no. 8, 1802–1809. 99

[37] Brandon Foreman and Jan Claassen, *Quantitative eeg for the detection of brain ischemia*, Critical Care (2012), no. 2, 216. 95

[38] Ralph D. Freeman, B. N. Pasley, *Neurovascular coupling*, Scholarpedia 3 (2008), no. 3, 5340. xiii, 86, 87

[39] Samah H. Gad, *Cloud computing and mapreduce for reliability and scalability of ubiquitous learning systems*, Proceedings of the compilation of the co-located workshops on DSM'11, TMC'11, AGERE!'11, AOOPES'11, NEAT'11, & VMIL'11 (New York, NY, USA), SPLASH '11 Workshops, ACM, 2011, pp. 273–278. 106

[40] Erzhen Gao, William L. Young, John Pile-Spellman, Eugene Ornstein, and Qiyuan Ma, *Mathematical considerations for modeling cerebral blood flow autoregulation to systemic arterial pressure*, American Journal of Physiology - Heart and Circulatory Physiology 274 (1998), no. 3, H1023–H1031. 88

[41] GHSA, *Distracted driving: What research shows and what states can do*, Governors Highway Safety Association (GHSA) (2011). 5, 47

[42] Margaret Glick, *The instructional leader and the brain: Using neuroscience to inform practice*, Corwin Press, 2011. 7

[43] Camillo Golgi, *The neuron doctrine: theory and facts*, Nobel lecture 1921 (1906), 190–217. 1

[44] Lawrence O Gorman, *Comparing passwords, tokens, and biometrics for user authentication*, Proceedings of the IEEE 91 (2003), no. 12, 2021–2040. 43

[45] U K Government Biometrics Working Group (BWG), *Biometric security concerns*, [Online]. Available: http://docplayer.net/12457008-Biometric-security-concerns-v1-0-september-2003.html (Accessed April 1, 2016) (2003). 40

[46] Payas Gupta and Debin Gao, *Fighting coercion attacks in key generation using skin conductance.*, USENIX Security Symposium, 2010, pp. 469–484. 14

[47] L. F. Haas, *Hans berger (1873 to 1941), richard caton (1842 to 1926), and electroencephalography*, Journal of Neurology, Neurosurgery, and Psychiatry 74 (2003), no. 1, 9. 106

[48] Mark Hall, Eibe Frank, Geoffrey Holmes, Bernhard Pfahringer, Peter Reutemann, and

Ian H. Witten, *The weka data mining software: An update*, SIGKDD Explor. Newsl. 11 (2009), no. 1, 10–18. 67, 101

[49] Mark Hall, Eibe Frank, Geoffrey Holmes, Bernhard Pfahringer, Peter Reutemann, and Ian H Witten, *The WEKA data mining software: An update; SIGKDD explorations, volume 11, issue 1*, Available: http://www.cs.waikato.ac.nz/ml/weka (2009). 24

[50] Kenji Hamano, *The distribution of the spectrum for the discrete fourier transform test included in SP800-22*, IEICE TRANSACTIONS on Fundamentals of Electronics, Communications and Computer Sciences 88 (2005), no. 1, 67–73. 41

[51] Shihui Han, Yi Jiang, Glyn W Humphreys, Tiangang Zhou, and Peng Cai, *Distinct neural substrates for the perception of real and virtual visual worlds*, NeuroImage 24 (2005), no. 3, 928–935. 49

[52] Chen He, *Person authentication using EEG brainwave signals*, Master's thesis, University of British Columbia, 2009. 15

[53] Dandan Huang, Kai Qian, Ding-Yu Fei, Wenchuan Jia, Xuedong Chen, and Ou Bai, *Electroencephalography (EEG)-based brain–computer interface (BCI): A 2-d virtual wheelchair control based on event-related desynchronization/synchronization and state control*, Neural Systems and Rehabilitation Engineering, IEEE Transactions on 20 (2012), no. 3, 379–388. 44

[54] PW Humphreys and AR Lind, *The blood flow through active and inactive muscles of the forearm during sustained hand-grip contractions*, The Journal of physiology 166 (1963), no. 1, 120. 90

[55] L. Ingber, *EEG database, UCI machine learning repository, University of California, Irvine, School of Information and Computer Sciences*, `http://archive.ics.uci.edu/ml/datasets/EEG+Database`, 1997. 20

[56] Anil K Jain, Karthik Nandakumar, and Abhishek Nagar, *Biometric template security*, EURASIP Journal on Advances in Signal Processing 2008 (2008), 113. 12, 17, 43

[57] Anil K Jain, Arun Ross, and Salil Prabhakar, *An introduction to biometric recognition*,

Circuits and Systems for Video Technology, IEEE Transactions on 14 (2004), no. 1, 4–20. 12, 15

[58] Herbert Henri Jasper, *The ten twenty electrode system of the international federation*, Electroencephalography and clinical neurophysiology 10 (1958), 371–375. ix, 20, 89

[59] A. Teoh Beng Jin and L. Meng Hui, *Cancelable biometrics*, Scholarpedia 5 (2010), no. 1, 9201, revision - 91098. 13

[60] Liang Jingkun, Xu Guizhi, Ge Jianrong, Zhu Feng, and Feng Xiuyan, *Analysis of virtual simulation environment for driving behavior based on imaging movements*, Networking and Digital Society (ICNDS), 2010 2nd International Conference on, vol. 1, may 2010, pp. 246 –248. 48

[61] Zachary A Keirn, *Alternative modes of communication between man and machine*, Master's thesis, Purdue University, 1988. 18

[62] Zachary A Keirn and Jorge I Aunon, *A new mode of communication between man and his surroundings*, Biomedical Engineering, IEEE Transactions on 37 (1990), no. 12, 1209–1214. 18, 99

[63] JM Kilner, J Mattout, R Henson, and KJ Friston, *Hemodynamic correlates of eeg: a heuristic*, Neuroimage 28 (2005), no. 1, 280–286. 86

[64] Song-Ju Kim, Ken Umeno, and Akio Hasegawa, *Corrections of the NIST statistical test suite for randomness*, arXiv preprint nlin/0401040 (2004). 38

[65] Sheila G Klauer, Thomas A Dingus, Vicki L Neale, Jeremy D Sudweeks, David J Ramsey, et al., *The impact of driver inattention on near-crash/crash risk: An analysis using the 100-car naturalistic driving study data*, (2006). 51

[66] J. Klonovs, C.K. Petersen, H. Olesen, and A. Hammershoj, *ID proof on the go: Development of a mobile EEG-based biometric authentication system*, Vehicular Technology Magazine, IEEE 8 (2013), no. 1, 81–89. 15

[67] D. Kochhar, J. Auflick, J. Hogsett, L. Angell, L. Tijerina, P. A. Austria, S. Kiger, T. Diptiman, and W. Biever, *Driver workload metrics project, task 2 final report*, Final Research Report for National Highway Traffic Safety Administration (NHTSA) (2001-2005). 5, 47

[68] A Kramer and R Parasuraman, *Neuroergonomics–application of neuroscience to human factors*, Handbook of psychophysiology 2 (2007), 704–722. 74

[69] Brain Computer Interfaces Laboratory, *Keirn and aunon eeg dataset*, `http://www.cs.colostate.edu/eeg/main/data/1989_Keirn_and_Aunon`. 18

[70] Saroj KL Lal, Ashley Craig, Peter Boord, Les Kirkup, and Hung Nguyen, *Development of an algorithm for an eeg-based driver fatigue countermeasure*, Journal of Safety Research 34 (2003), no. 3, 321–328. 48

[71] N. Learner and S. Boyd, *On-road study of willingness to engage in distracting tasks*, Interim (Task2) Report for Highway Traffic Safety Administration (NHTSA) (2004). 47

[72] Mikhail A Lebedev and Miguel AL Nicolelis, *Brain–machine interfaces: past, present and future*, TRENDS in Neurosciences 29 (2006), no. 9, 536–546. 44

[73] Johnny Chung Lee and Desney S Tan, *Using a low-cost electroencephalograph for task classification in hci research*, Proceedings of the 19th annual ACM symposium on User interface software and technology, ACM, 2006, pp. 81–90. 99

[74] Sai-Cheung Lee, Jyi-Feng Chen, and Shih-Tseng Lee, *Continuous regional cerebral blood flow monitoring in the neurosurgical intensive care unit*, Journal of Clinical Neuroscience 12 (2005), no. 5, 520 – 523. 85

[75] S. Lei, S. Welke, and M. Roetting, *Drivers mental workload assessment using eeg data in a dual task paradigm*, Proceedings Of The 21st (Esv) International Technical Conference On The Enhanced Safety Of Vehicles, National highway traffic safety administration (2009). 48

[76] Albert B Levin, *A simple test of cardiac function based upon the heart rate changes induced by the valsalva maneuver*, The American journal of cardiology 18 (1966), no. 1, 90–99. 91

[77] Nan-Ying Liang, Paramasivan Saratchandran, Guang-Bin Huang, and Narasimhan Sundararajan, *Classification of mental tasks from eeg signals using extreme learning machine*, International Journal of Neural Systems 16 (2006), no. 01, 29–38. 100

[78] Mark H Libenson, *Practical approach to electroencephalography*, Elsevier Health Sciences, 2012. 7

[79] C-T Lin, L-W Ko, M-H Chang, J-R Duann, J-Y Chen, T-P Su, and T-P Jung, *Review of wire-*

less and wearable electroencephalogram systems and brain-computer interfaces–a mini-review, Gerontology 56 (2009), no. 1, 112–119. 47

[80] Chin-Teng Lin, Shi-An Chen, Tien-Ting Chiu, Hong-Zhang Lin, Li-Wei Ko, et al., *Spatial and temporal eeg dynamics of dual-task driving performance*, Journal of neuroengineering and rehabilitation 8 (2011), no. 1, 11–23. 48, 50

[81] Chin-Teng Lin, Shi-An Chen, Li-Wei Ko, and Yu-Kai Wang, *Eeg-based brain dynamics of driving distraction*, Neural Networks (IJCNN), The 2011 International Joint Conference on, 31 2011-aug. 5 2011, pp. 1497 –1500. 48

[82] Chin-Teng Lin, Sheng-Fu Liang, Yu-Chieh Chen, Yung-Chi Hsu, and Li-Wei Ko, *Driver's drowsiness estimation by combining eeg signal analysis and ica-based fuzzy neural networks*, Circuits and Systems, 2006. ISCAS 2006. Proceedings. 2006 IEEE International Symposium on, may 2006, pp. 4 pp. –2128. 49

[83] Chin-Teng Lin, Ruei-Cheng Wu, Tzyy-Ping Jung, Sheng-Fu Liang, and Teng-Yi Huang, *Estimating driving performance based on eeg spectrum analysis*, EURASIP Journal on Applied Signal Processing 2005 (2005), 3165–3174. 49

[84] AR Lind and GW McNicol, *Circulatory responses to sustained hand-grip contractions performed during other exercise, both rhythmic and static*, The Journal of physiology 192 (1967), no. 3, 595. 90

[85] Zhang Y Chen W Liu X, Zhu X-H, *Tightly coupled spontaneous eeg and cbf signals in the anesthetized rat brain*, Proceedings of the 16th Annual Meeting of ISMRM (Toronto, ON, CA), 2008, p. 755. 86

[86] G. Lokeshwari, S. Udaya, and G. Aparna, *A novel approach for data encryption using EEG, SPIHT and genetic algorithm for secured applications*, 5 (2013), 23–27. 16

[87] DT Lykken, A Tellegen, and K Thorkelson, *Genetic determination of EEG frequency spectra*, Biological Psychology 1 (1974), no. 4, 245–259. 15

[88] Lysesoft, *Andftp available: http://www.lysesoft.com/products/andftp/index.html*. 108

[89] Scott Makeig, Anthony J Bell, Tzyy-Ping Jung, Terrence J Sejnowski, et al., *Independent*

component analysis of electroencephalographic data, Advances in neural information processing systems (1996), 145–151. 60

[90] Davide Maltoni, Dario Maio, Anil Jain, and Salil Prabhakar, *Handbook of fingerprint recognition*, Springer Science & Business Media, 2009. 39

[91] S. Marcel and J.D.R. Millan, *Person authentication using brainwaves (EEG) and maximum a posteriori model adaptation*, Pattern Analysis and Machine Intelligence, IEEE Transactions on 29 (2007), no. 4, 743–752. 15

[92] Marius Marusteri and Vladimir Bacarea, *Comparing groups for statistical differences: How to choose the right statistical test?*, Biochemia medica 20 (2010), no. 1, 15–32. 73

[93] Fabian Monrose, Michael K Reiter, Qi Li, and Susanne Wetzel, *Cryptographic key generation from voice*, Security and Privacy, 2001. S&P 2001. Proceedings. 2001 IEEE Symposium on, IEEE, 2001, pp. 202–213. 28

[94] I. Nakanishi, S. Baba, and C. Miyamoto, *EEG based biometric authentication using new spectral features*, Intelligent Signal Processing and Communication Systems, 2009. ISPACS 2009. International Symposium on, 2009, pp. 651–654. 15

[95] Markus Näpflin, Marc Wildi, and Johannes Sarnthein, *Test–retest reliability of resting EEG spectra validates a statistical signature of persons*, Clinical Neurophysiology 118 (2007), no. 11, 2519–2524. 16

[96] Neurosky, *Available: http://www.neurosky.com/*. ix, 10, 50, 53, 78, 89, 100, 107

[97] NeuroskyDeveloper, *Available: http://store.neurosky.com/collections/developer-tools-3*. 78

[98] NeuroskyTools, *Available: http://support.neurosky.com/kb/technology/how-to-convert-raw-values-to-voltage*. 78

[99] Andrew Newberg and Eugene G d'Aquili, *Why god won't go away: Brain science and the biology of belief*, Ballantine Books, 2008. 1

[100] NHTSA, *New guidance lists unsafe driver distractions :*, Occupational Health and Safety (OHS) (2012). 47

[101] Anton Nijholt, *BCI for games: A 'State of the Art' survey*, Entertainment Computing-ICEC 2008, Springer, 2009, pp. 225–228. 44

[102] Arne Öhman, *The role of the amygdala in human fear: automatic detection of threat*, Psychoneuroendocrinology 30 (2005), no. 10, 953–958. 14

[103] Robert Oostenveld and Peter Praamstra, *The five percent electrode system for high-resolution EEG and ERP measurements*, Clinical neurophysiology 112 (2001), no. 4, 713–719. ix, x, 20, 49

[104] Self-Learning Packet, *Overview of adult traumatic brain injuries*, Orlando Regional Healthcare, Education & Development, Orlando, FL (2004). 5

[105] R Palaniappan and KVR Ravi, *A new method to identify individuals using signals from the brain*, Information, Communications and Signal Processing, 2003 and Fourth Pacific Rim Conference on Multimedia. Proceedings of the 2003 Joint Conference of the Fourth International Conference on, vol. 3, IEEE, 2003, pp. 1442–1445. 15

[106] Ramaswamy Palaniappan, *Brain computer interface design using band powers extracted during mental tasks*, Neural Engineering, 2005. Conference Proceedings. 2nd International IEEE EMBS Conference on, IEEE, 2005, pp. 321–324. 100

[107] Ramaswamy Palaniappan, Jenish Gosalia, Kenneth Revett, and Andrews Samraj, *PIN generation using single channel EEG biometric*, Advances in Computing and Communications, Springer, 2011, pp. 378–385. 16

[108] Ramaswamy Palaniappan and KVR Ravi, *Improving visual evoked potential feature classification for person recognition using PCA and normalization*, Pattern Recognition Letters 27 (2006), no. 7, 726–733. 15

[109] R. B. Panerai, R. P. White, H. S. Markus, and D. H. Evans, *Grading of cerebral dynamic autoregulation from spontaneous fluctuations in arterial blood pressure*, Stroke 29 (1998), no. 11, 2341–2346. 88

[110] RB Paranjape, J Mahovsky, L Benedicenti, and Z Koles, *The electroencephalogram as a biometric*, Electrical and Computer Engineering, 2001. Canadian Conference on, vol. 2, IEEE, 2001, pp. 1363–1366. 15

[111] Andrew S Patrick, *Fingerprint concerns: Performance, usability, and acceptance of fingerprint biometric systems*, National Research Council of Canada.[Online]. Avail-

able: http://www. andrewpatrick. ca/essays/fingerprint-concerns-performanceusability-and-acceptance-of-fingerprint-biometric-systems (Accessed April 1, 2016) (2008). 40

[112] A. Pauzie, *A method to assess the driver mental workload: The driving activity load index (dali)*, Intelligent Transport Systems, IET 2 (2008), no. 4, 315 –322. 48

[113] Daniela Perani, Ferruccio Fazio, Nunzio Alberto Borghese, Marco Tettamanti, Stefano Ferrari, Jean Decety, and Maria C Gilardi, *Different brain correlates for watching real and virtual hand actions*, Neuroimage 14 (2001), no. 3, 749–758. 49

[114] Fabien AP Petitcolas, *Kerckhoffs principle*, Encyclopedia of cryptography and security, Springer, 2011, pp. 675–675. 12

[115] M Poulos, M Rangoussi, N Alexandris, A Evangelou, et al., *Person identification from the EEG using nonlinear signal classification*, Methods of information in Medicine 41 (2002), no. 1, 64–75. 15

[116] M Poulos, M Rangoussi, V Chrissikopoulos, and A Evangelou, *Person identification based on parametric processing of the EEG*, Electronics, Circuits and Systems, 1999. Proceedings of ICECS'99. The 6th IEEE International Conference on, vol. 1, IEEE, 1999, pp. 283–286. 15

[117] T.A. Ranney, E. Mazzae, R. Garrot, and M.J. Goodman, *Nhtsa driver distraction research: Past, present and future*, 17th International Technical Conference on the Enhances Safety of Vehicles (2001). 5, 47, 51

[118] Nalini K. Ratha, Jonathan H. Connell, and Ruud M. Bolle, *Enhancing security and privacy in biometrics-based authentication systems*, IBM systems Journal 40 (2001), no. 3, 614–634. 13

[119] Christian Rathgeb and Andreas Uhl, *A survey on biometric cryptosystems and cancelable biometrics*, EURASIP Journal on Information Security 2011 (2011), no. 1, 1–25. 12

[120] Pascal Ravassard, Ashley Kees, Bernard Willers, David Ho, Daniel Aharoni, Jesse Cushman, Zahra M Aghajan, and Mayank R Mehta, *Multisensory control of hippocampal spatiotemporal selectivity*, Science 340 (2013), no. 6138, 1342–1346. 49

[121] K. Revett, F. Deravi, and K. Sirlantzis, *Biosignals for user authentication - towards cog-*

nitive biometrics?, Emerging Security Technologies (EST), 2010 International Conference on, 2010, pp. 71–76. 15

[122] Andrew Rukhin, Juan Soto, James Nechvatal, Miles Smid, and Elaine Barker, *A statistical test suite for random and pseudorandom number generators for cryptographic applications*, Tech. report, DTIC Document, 2001. 34

[123] Mark A Schier, *Changes in eeg alpha power during simulated driving: a demonstration*, International Journal of Psychophysiology 37 (2000), no. 2, 155–162. 48

[124] Tom A Schweizer, Karen Kan, Yuwen Hung, Fred Tam, Gary Naglie, and Simon J Graham, *Brain activity during driving with distraction: an immersive fmri study*, Frontiers in human neuroscience 7 (2013). 56

[125] Emily Shardlow and Alan Jackson, *Cerebral blood flow and intracranial pressure*, Anaesthesia and Intensive Care Medicine 12 (2011), no. 5, 220 – 223. xiii, 84

[126] Raymond Carl Smith, *Electroencephalograph based brain computer interfaces*, Ph.D. thesis, Citeseer, 2004. 99

[127] Joan G Snodgrass and Mary Vanderwart, *A standardized set of 260 pictures: norms for name agreement, image agreement, familiarity, and visual complexity.*, Journal of experimental psychology: Human learning and memory 6 (1980), no. 2, 174. 20

[128] Colin Soutar, Danny Roberge, Alex Stoianov, Rene Gilroy, and Bhagavatula Vijaya Kumar, *Biometric Encryption: enrollment and verification procedures*, Aerospace/Defense Sensing and Controls, International Society for Optics and Photonics, 1998, pp. 24–35. 16

[129] SPM, *Statistical parametric mapping available: http://www.fil.ion.ucl.ac.uk/spm/*. 86

[130] RL Sprangers, KH Wesseling, AL Imholz, BP Imholz, and W Wieling, *Initial blood pressure fall on stand up and exercise explained by changes in total peripheral resistance*, Journal of Applied Physiology 70 (1991), no. 2, 523–530. 90

[131] Kenyon Stamps and Yskandar Hamam, *Towards inexpensive BCI control for wheelchair navigation in the enabled environment–a hardware survey*, Brain Informatics, Springer, 2010, pp. 336–345. 44

[132] Robert Sylwester, *An educator's guide to the human brain*, Alexandria, VA: Association for Supervision and Curriculum Development (1995). 1

[133] William O Tatum IV, *Handbook of eeg interpretation*, Demos Medical Publishing, 2014. 7

[134] Michal Teplan, *Fundamentals of eeg measurement*, Measurement science review 2 (2002), no. 2, 1–11. 1, 7

[135] Julie Thorpe, Paul C van Oorschot, and Anil Somayaji, *Pass-thoughts: authenticating with our minds*, Proceedings of the 2005 workshop on New security paradigms, ACM, 2005, pp. 45–56. 14, 15

[136] Umut Uludag, Sharath Pankanti, Salil Prabhakar, and Anil K Jain, *Biometric cryptosystems: issues and challenges*, Proceedings of the IEEE 92 (2004), no. 6, 948–960. 12, 16

[137] Arenda HEA van Beek, Marcel GM Olde Rikkert, Jaco W Pasman, Maria TE Hopman, and Jurgen AHR Claassen, *Dynamic cerebral autoregulation in the old using a repeated sit-stand maneuver*, Ultrasound in medicine & biology 36 (2010), no. 2, 192–201. 89

[138] J J Vidal, *Toward direct brain-computer communication*, Annual Review of Biophysics and Bioengineering 2 (1973), no. 1, 157–180, PMID: 4583653. 47

[139] Friedrich Vogel, *The genetic basis of the normal human electroencephalogram (EEG)*, Humangenetik 10 (1970), no. 2, 91–114. 15

[140] Shouyi Wang, Yiqi Zhang, Changxu Wu, Felix Darvas, and Wanpracha Art Chaovalitwongse, *Online prediction of driver distraction based on brain activity patterns*, Intelligent Transportation Systems, IEEE Transactions on 16 (2015), no. 1, 136–150. 76

[141] YK Wang, TP Jung, and CT Lin, *Eeg-based attention tracking during distracted driving.*, IEEE transactions on neural systems and rehabilitation engineering: a publication of the IEEE Engineering in Medicine and Biology Society (2015). 50

[142] Yu-Kai Wang, Shi-An Chen, and Chin-Teng Lin, *An eeg-based brain–computer interface for dual task driving detection*, Neurocomputing 129 (2014), 85–93. 50

[143] Yu-Te Wang, Yijun Wang, and Tzyy-Ping Jung, *A cell-phone-based brain–computer interface for communication in daily life*, Journal of neural engineering 8 (2011), no. 2, 025018. 47

[144] Christopher D Wickens, *Multiple resources and mental workload*, Human Factors: The Journal of the Human Factors and Ergonomics Society 50 (2008), no. 3, 449–455. 74

[145] J.W. Williamson, J.H. Mitchell, H.L. Olesen, P.B. Raven, and N.H. Secher, *Reflex increase in blood pressure induced by leg compression in man.*, J Physiol 475 (1994), no. 2, 351–7. 88

[146] Jonathan R Wolpaw, Niels Birbaumer, Dennis J McFarland, Gert Pfurtscheller, and Theresa M Vaughan, *Brain–computer interfaces for communication and control*, Clinical neurophysiology 113 (2002), no. 6, 767–791. 47

[147] Seul-Ki Yeom, Heung-Il Suk, and Seong-Whan Lee, *Person authentication from neural activity of face-specific visual self-representation*, Pattern Recognition 46 (2013), no. 4, 1159–1169. 16

[148] Alois Zauner and J. Paul Muizelaar, *Head injury: Pathophysiology and management of severe closed injury; measuring cerebral blood flow and metabolism*, 1997. 6, 85

[149] _____, *Measuring cerebral blood flow and metabolism*, 1997. 85, 86

[150] Biao Zhang, Jianjun Wang, and Thomas Fuhlbrigge, *A review of the commercial brain-computer interface technology from perspective of industrial robotics*, Automation and Logistics (ICAL), 2010 IEEE International Conference on, IEEE, 2010, pp. 379–384. 44

[151] Xiao Lei Zhang, Henri Begleiter, Bernice Porjesz, Wenyu Wang, and Ann Litke, *Event related potentials during object recognition tasks*, Brain Research Bulletin 38 (1995), no. 6, 531–538. 20, 26, 39

[152] Qinglin Zhao, Hong Peng, Bin Hu, Quanying Liu, Li Liu, YanBing Qi, and Lanlan Li, *Improving individual identification in security check with an EEG based biometric solution*, Brain Informatics, Springer, 2010, pp. 145–155. 14

[153] Gang Zheng, Wanqing Li, and Ce Zhan, *Cryptographic key generation from biometric data using lattice mapping*, Pattern Recognition, 2006. ICPR 2006. 18th International Conference on, vol. 4, IEEE, 2006, pp. 513–516. 12